Development of an Acoustic Wave Based Biosensor for Vapor Phase Detection of Small Molecules

A Dissertation

Presented to

The Academic Faculty

by

Desmond Stubbs

In Partial Fulfillment

of the Requirements for the Degree

Doctor of Philosophy in Chemistry

Georgia Institute of Technology

December, 2005

Development of an Acoustic Wave Based Biosensor for Vapor Phase Detection of Small Molecules

Approved by:

Dr. William Hunt, Advisor
School of Electrical & Computer Engineering
Georgia Institute of Technology

Dr. Charles Liotta
School of Chemistry & Biochemistry
Georgia Institute of Technology

Dr. Larry Bottomley, Co-Advisor
School of Chemistry & Biochemistry
Georgia Institute of Technology

Dr. Jiri Janata
School of Chemistry & Biochemistry
Georgia Institute of Technology

Dr. Roger Wartell
School of Biology
Georgia Institute of Technology

Date Approved: October 31st, 2005

On this special occasion I would like to acknowledge my family for their unwavering support during my matriculation. In particular, I would like to thank my mother Susan Mortimer for having faith in me and my abilities. I would also like to acknowledge my family by name: Lesley, Laurie, Pamela, Donna, Paulette and last but not least my recently departed sister Wendy (- you are truly missed). Thank you all!

Last but certainly not least I would like to dedicate this work to my very supportive wife Mrs. Brandee Stubbs, words can not truly express the gratitude I owe to you for all your support. Thank you!

Acknowledgments

First I would like to thank my advisors Dr. William Hunt and Dr. Larry Bottomley for their support and the opportunity to work together. A special thank you in particular to Dr. Hunt for recruiting me on the basketball court during our lunch-break "pick-up games", it was very perceptive on your part to recognize my talent and I'm not talking ball skills. To the guys in the "Mag"lab Sang, Chris, Tony, Ryan, Eric thanks for your help along the way I wish you all the best with your careers. In particular Sang Lee for teaching everything I know about device fabrication thanks.

Very special thanks to Dr. Gloria Anderson an icon at my Alma Mater, Morris Brown College. Over the years your mentorship and friendship have inspired me to achieve beyond my wildest expectations!!!

Thanks to Steve Woodard and Jonafel Crowe of Georgia Tech's Institute for Bioengineering and Biosciences for training on the Zeiss LSM 510 and providing some input on the research. Further, I would also like to thank my collaborators James Cairney (School of Biology), Dr. Peter Edmonson (McMasters University, Toronto), Susan Hallowell (Transportation Security Administration), Terry Mills III, Mark D. Burns and Tina Wu at GBI Crime Lab for their support. Finally, I would like to thank Dave Hoglund of the U.S. Customs Service for his support of this research.

Table of Contents

List of Tables

List of Figures

List of Abbreviations

AWR	Acoustic Wave Resonators
SAW-R	Surface Acoustic Wave –Resonators
QCM	Quartz Crystal Microbalance
IDT	Interdigital transducer
CLSM	Zeiss Confocal Laser Scanning Microscope
TSM	Thickness shear Mode
FITC	Fluorescein Isothiocyanate
TAE	Tris-base /Acetate/EDTA buffer
dB	Decibel
Hz	Hertz
BZE	Benzoylecgonine
SAM	Self Assembled Monolayers
TE	Tris / EDTA
DNOP	Dinitrophenol
Q	Q-factor
IL	Insertion loss
Fab	Antigen binding fragment
Fc	Carboxylic terminal end fragment
Ab	Antibody
IgG	Immunoglobulin

Summary

For centuries scientific ingenuity and innovation have been influenced by Mother Nature's perfect design. One of her more elusive designs is that of the sensory olfactory system, an array of highly sensitive receptors responsible for chemical vapor recognition. In the animal kingdom this ability is magnified among canines where ppt (parts per trillion) sensitivity values have been reported. Today, detection dogs are considered an essential part of the US drug and explosives detection schemes. However, growing concerns about their susceptibility to extraneous odors have inspired the development of highly sensitive analytical detection tools and biosensors known as "electronic noses".

In general, biosensors are distinguished from chemical sensors in that they use an entity of biological origin (e.g. antibody, cell, enzyme) immobilized onto a surface as the chemically-sensitive film on the device. The established convention suggests that these sensors are limited to aqueous environments due to the very nature of the sensing mechanism. That is, virtually all biomolecular interactions, both in *vivo* and in *vitro* involve a **liquid assay**. This ensures that conformational changes and molecular specificity associated with these events occur without loss of biological activity. Our biosensor involves a label free detection mechanism that utilizes biomolecules, specifically IgG monoclonal antibodies entrapped in a semi-aqueous layer (hydrogel) to achieve molecular recognition of relatively small molecules in the **vapor phase** [1].

For immunoassay techniques, antibodies specific for a target antigen, are utilized as the chemically-specific receptor molecule. The production of these so-called monoclonal

antibodies by the hybridoma technique was first reported by Kohler and Milstein [2]. This technique made it possible to produce antibodies in large quantities using cultures of myeloma cells fused with lymphocytes raised against the target antigen. A culture of the resulting hybridoma cells synthesizes the antibody of the parent lymphocyte and has the immortality of the myeloma cancer cell. Antibodies have been generated for a wide variety of antigens and are commercially available from numerous industrial sources.

Acoustic sensors represent an approach for high precision sensing which has been highly successful and which has a long history of reduction to practice. Quartz Crystal Microbalances (QCM) were there at the dawn of the semiconductor industry, having been utilized since the 1950s monitor the thickness of metals being deposited on wafers in evaporation systems. In these early papers and in later papers it was pointed out that it was not just the mass which induced the change in the resonant frequency of the crystal but that there are other factors that affect the resonant frequency as well. In fact, in addition to mass, acoustic wave resonators (AWR's) are sensitive to viscosity, charge and the mechanical characteristics of the chemically-selective film immobilized on the device surface. Here, we will presume that a reference sensor is available and that it samples essentially the same volume as the active sensor. As such we will presuppose that the charge and viscosity effects during analyte sampling will be roughly identical on the two sensors so that the only difference between them will be the molecular recognition event is taking place on the active sensor and that this recognition event is not taking place on the referenced sensor. The difference in resonant frequencies between the two sensors will then be due strictly to the impact of the molecular recognition event which will be

both mass attachment and any induced changes in the mechanical characteristics of the chemically-sensitive film. Because we gather real-time data, we can monitor the resonant frequency changes in the AWR before, during and after the molecular recognition event. We will make the assumption that the additional mass on the sensor is due strictly to the analyte which has bound to its immobilized antibody. Further, we will make the somewhat radical conjecture that the changes in the mechanical properties of the film are due to biomolecular conformational changes in the biolayer.

The contents of this thesis represent a collection of work dividing topically into chapters. In chapter one, AWR devices and their physical properties are introduced. Chapter two describes a novel fluorescence assay we developed that serves as visual confirmation of vapor phase chemical detection. Chapters three and four describe experiments conducted with the purpose of detecting low vapor pressure molecules such as 2,4,6-trinitrotoluene (TNT) and cocaine. The results of these studies suggest that we were able to detect and distinguish unique chemical signatures associated with the analytes of record. In chapter five, we present evidence indicating that biomolecular conformational changes in the biolayer may result in a positive or negative shift in the resonance frequency. To address this issue we study a non-mass loading event, that is, the transition from B-DNA to A-DNA. Finally, in chapter six, we examine the utility of this research as it pertains to public policy.

The work presented is a summary of over **two thousand** experiments conducted both on the campus of Georgia Institute of Technology and off campus laboratories such as the

Georgia Bureau of Investigation's Chemical Analysis Labs (Decatur, GA) and the Transportation Security Administration's Explosives Detection Labs located in Atlantic City, NJ. The experiments required the fabrication of thousands of SAW devices with a significant portion to be used as a reference device to characterize any non-specific interactions. All experiments were repeated for reproducibility and many control devices were designed to elucidate the observed data. The results of this research have been published in seven peer reviewed journals and five conference proceedings (see Appendix B).

Chapter 1: Introduction

Over the past decade there has been a large flux in sensing technology due to need for more precise analytical measuring tools. The ability to detect and quantify various chemical and biological species emerged as an important factor in this technology boom. As the sensing world expands the need for a standardized criteria for characterizing these devices become more well defined. Table 1.1 lists a variety of parameters that may define the basic characteristics of a "good" biosensor. Two essential features of a typical biosensor are sensitivity and selectivity. Sensor sensitivity is defined as a measure of the magnitude of the output signal produced in response to an input quantity; sensor selectivity is degree to which the device can distinguish one input quantity from another; limit of detection (LOD) is minimum change of input quantity that can be measured [3].

What makes a "good" sensor?

Table 1.1 A description of biosensor characteristics.

Sensor Characteristic	Biosensors
Size	**Micro-nano**
Speed	**Real-time**
Cost	**$$ (cost derived from Biolayer)**
Selectivity	**Bio-receptors are very selective**
Detection Limit	**Very low detection limits**

Table 1.1 Continued

Stability	**Tend to be very stable**
Versatility	**Versatility determined by stringency of the biolayer**
Precision	**Very precise**

In the case of an acoustic biosensor discussed here, obtaining adequate sensitivity and selectivity for the measurement of a given analyte requires a biochemical interface, referred to herein as the "biolayer". The coating is bound *via* physi- and/or chemisorption to the surface of the sensing platform. The biolayer interacts with the analyte mainly *via* hydrogen bonding and charge-charge interactions. These interactions serve to immobilize the analyte and in turn perturb the SAW surface. The perturbations caused by "mass loading" forms the basis for detection and quantification. Mass loading perturbs the propagating surface acoustic wave velocity without producing attenuation effects. In addition, it is now clear that other factors such as changes in the mechanical and electrical properties of the sensing layer can affect the sensor response.

Surface mass changes can result from the sorptive interactions (adsorption and absorption) or chemical interactions between analyte and biolayer, and can be used for sensing applications *in both liquid and gas phases*. Although the absolute mass sensitivity (see table 1.2) of an uncoated sensor depends on the nature of the piezoelectric substrate, device dimensions, frequency of operation, and the acoustic mode that is being utilized, a linear dependence is predicted in all cases. This allows a very

general description of the working relationship between mass-loading and frequency shift for surface acoustic wave devices to be written [4,5,6]:

$$\Delta f_m = -kS_m \Delta m_A \qquad (1.1)$$

where Δf_m is the change in frequency due to mass changes, S_m is a device constant that depends on the factors mentioned above, k is the geometry factor for the fraction of the active device area being perturbed and Δm_A is the change in mass/area on the device surface.

Thus the mass sensitivity can be defined as:

$$S_m = \frac{1}{\Delta m}\left(\frac{\Delta v_p}{v_p}\right) \qquad (1.2)$$

where Δv_p = change of acoustic wave velocity from its unperturbed value v_p,which is produced by adding a mass per unit area, Δm, onto the surface of the device. In our case, the Δm_A, causes a frequency shift, Δf , from the unperturbed resonance frequency f , one can show that (Δf / f) = ($\Delta v/v$), thus:

$$S_m = \frac{1}{\Delta m}\left(\frac{\Delta f}{f}\right) \qquad (1.3)$$

Table 1.2. Typical Mass Sensitivities of Uncoated Surface Acoustic Wave Devices [7,8,9,10,11,]

Device Description	Theoretical Mass Sensitivity(S_m) ($Hz \bullet cm^2 / \mu g$)	Freq. Range (MHz)	Frequency (MHz)	Substrate Thickness (mm)	S_m ($Hz - cm^2 / \mu g$)
AT-cut quartz TSM resonator	$2.3 \bullet f_o^2$	5 – 30	6	0.26	84
X-propagating SAW delay lines ST-cut quartz	$1.32 \bullet f_o^2$	900 – 1000	97	N/A	12,200
ST-quartz SAW resonator	$1.26 \bullet f_o^2$	25 –500	200	N/A	50,400
ST-quartz	$80 / t^2$	25 –200	104	0.20	2,000

1.1 Device Selectivity: Biolayer Immobilization

Immobilizing biomolecules on various solid-phase materials has been featured in an extensive array of applications ranging from protein purification to common immunoassays. Here, we describe two primary methods namely: alkanethiol and protein A, for immobilizing antibodies and DNA. In both cases, biolayer immobilization involves a random process that relies on the self-assembly properties of the adherent layer.

1.1.1 Alkanthiol Immobilization (Self -assembled Monolayers, SAMs)

When comparing both methods of immobilization, self-assembled monolayers (SAMs) can potentially provide a reproducible and robust immobilizaton method while maintaing

orientation control of the bio-receptor. Aided by the affinity of thiols for metal surface (such as gold electrodes), SAMs layers provide an ideal methodolgy for antibody immobilization on AWR such as QCM.

Alkanethiols chemisorb spontaneously from solution onto the surface of gold, silver and platinum via a thiolate bond [12,13,14,15]. Attractive Van der Waals forces between the alkyl chain enhance the stability and order of the SAM. Thus the fidelity of the order of the SAMs depends on the chain length and surface roughness. The saturated alkane chains are all tilted slightly from the normal of the surface by ~20^0-30^0 (Figure 1.1) forming a densely packed, highly ordered monolayer. SAMs layers are rigid in nature and have been shown to be stable to potentials between approximately +0.8 and -1.4V. Outside of this range the thiols can be oxidatively or reductively desorbed [16].

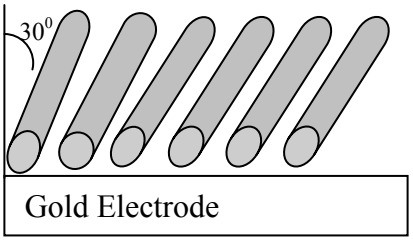

Figure 1.1 Showing self-assembled a monolayer of alkanethiols on gold electrodes.

1.1.2 Protein A Immobilization

When antibodies are covalently attached to solid supports, their binding capacity (valency) is usually less than that of soluble antibodies. One of the main reasons for this reduction is attributed to the random orientation of the antibodies on the support surface, in this case the gold electrode. The asymmetric macro molecule immunoglobulin G (IgG) is composed of the Fab' domains (two) and a third domain called the Fc domain. The antigen binding site is positioned at the amino end of each Fab'fragment. In normal coupling schemes, coupling does not discriminate between possible attachment points near or removed from the specific binding site (or sites), which results in spatial orientation of antibodies on the electrode that may not provide the optimum conditions for forming antigen-antibody complex. Thus the presence of lysine groups on the surface of an antibody signals possible attachment point. Consequently, this can result in different orientations of the antibody (Figure 1.2) on the electrode depending on the location of the lysine group severely impairing its ability to bind the antigen.

In addressing the orientation issue, Gersten and Marchalons showed that linking an antibody with protein A, a protein found in the cell wall of *Staphylococcus aureus*, they were able to improve the antibody's binding capacity [17]. Protein A is an Fc receptor that binds to the Fc portion of IgG subclass antibody leaving its antigen binding sites free. Wild type protein A comprises of five homologous extracellular domains each capable of binding an IgG molecule. However, steric interference between IgG molecules may block some receptors on the surface and ultimately affect the binding capacity on the electrode [18,19].

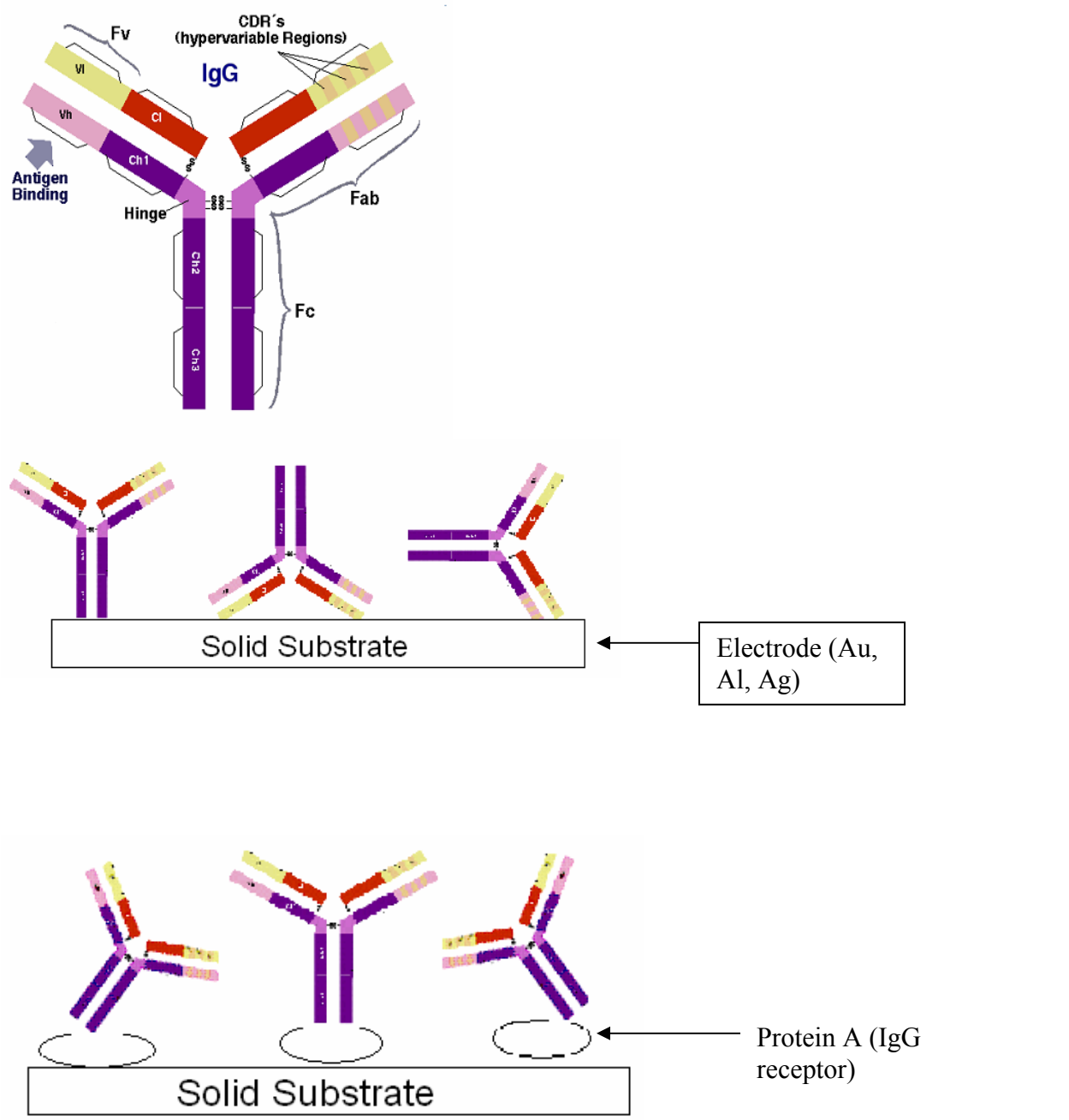

Figure 1.2 Random Immobilization of IgG on Solid Substrates [20].

1.1.3 Gel Entrapment

It is well understood [21,22] that for antibodies or other biomolecules to maintain their tertiary structure and hence their prescribed functionality, they must be in an aqueous environment. This knowledge has led to the accepted convention for the use of bioreceptors for chemical sensing purposes, that is, detection assays must **occur** in liquid phase. If biomolecules can be utilized for the detection of specific analytes in the vapor phase, a powerful sensor can be developed capable of molecular recognition of air-borne analytes of interest.

To provide a semi-aqueous environment for the immobilized biolayer a thin layer of agarose (0.5% w/v (1xTAE)) is applied to the sensor surface [23]. The gel itself is a porous matrix commonly used in separation methods such as electrophoresis and size exclusion chromatography. The gel is considered as a network of overlapping or cross-linked chains in which "pore size" or "mesh size" is a defining parameter of the system. Currently there are three established models for predicting pore size; Ogston Model, Brinkman Model and the Renkin Model [24,25,26,]. In an attempt to estimate the diffusivity of agarose gel to various macromolecules (BSA, Ovalbumin, Lactalbumin) Pluen et. al., [27] calculated pore size values for agarose using all three models. Diffusion measurements were performed in free solutions of 2% agarose gels using an image based FRAP (Fluorescence Recovery After Photobleaching). Agarose pore size was estimated using diffusion co-efficient data obtained from the three Models. For example, the diffusion coefficient D_s, of BSA (molecular radius of ~3.93 nm) in 2% agarose was ~6.4 x 10^{-7} cm^2 s^{-1} and the calculated pore size ranged from ~146 - 206 nm depending on the

model used for the calculation. The targets investigated in our study such as cocaine, TNT, and its nitrobenzene analogs are all on the order of Angstroms in terms of molecular radius. Thus for our purposes (small molecule detection or) the diffusivity of agarose layer should not present a mass transport issue. In fact, when comparing the relative size of the molecules detected in this study to that presented in Pluen et al the diffusivity rate should increase by a magnitude of three.

1.2 Equivalent Circuit Modeling

The device sensitivity is also derived from the sensing platform for our biosensor i.e. surface acoustic wave resonator. When a SAW resonator is excited by an electrical signal it produces a mechanical resonance that can be measured. The device itself along with its' electrical characteristics can be represented using an equivalence circuit model (Figure 1.3) [28]. One such model, named the Butterworth Van-Dyke model after its author, provides some identification of elements with physical properties of the device however these parameters are not easily obtained (Table 1.3).

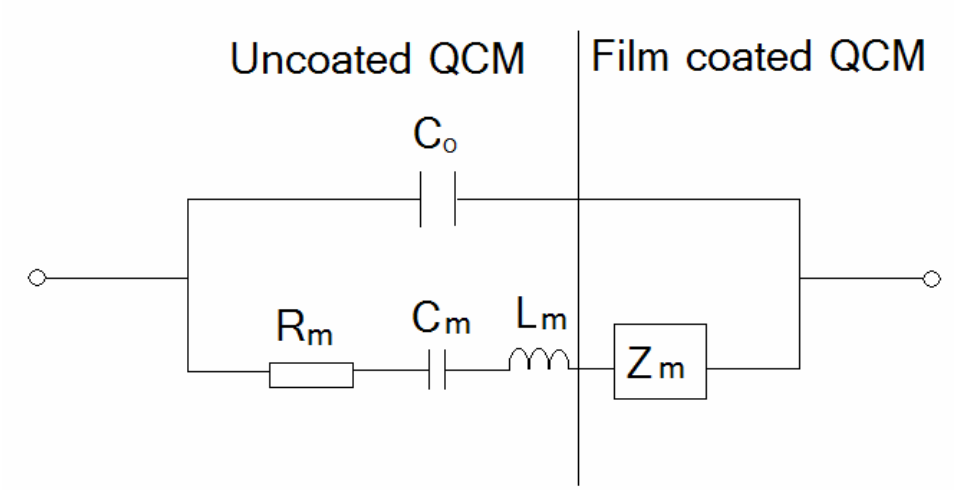

Figure 1.3 Pictured below is a lumped-element model called the Butterworth Van-Dyke (BVD) model.

where
C_0 is the static capacitance inherent in QCM design
Cm is the motional capacitance
Rm is the motional resistance
Lm is the motional inductance

Zm is the motional impedance
$Z_m = (R_m + R_2) + j\omega (L_m + L_2) + 1/j\omega C_m$
R2 and L2 are components of the film's mechanical impedance

Table 1.3. Advantages and Disadvantages to using an Equivalence Circuit Model

Advantages	Disadvantages
Can be connected in any configuration	Each device requires a different model
Allows some identification of elements with physical properties of the device	Parameters cannot easily be obtained
Will work over a wide range of frequencies	Most models are linear

This thesis will feature two types of acoustic wave based devices; quartz crystal microbalance and the Rayleigh wave based (sometimes called SAW) electronic.

1.3 Quartz Crystal Microbalance

QCM, the predominate term found in the literature is also referred to by the more descriptive thickness-shear mode (TSM) resonator. These devices typically consist of a thin disk of AT-cut quartz with circular electrodes patterned on both sides (Figure 1.5). Due to the electrical properties and crystalline orientation of the quartz, the application of

voltage between the electrodes results in a shear deformation of the crystal. These devices possess very high Q-factors (ratio conserved to energy dissipated over a cycle) between 10^4 -10^6 which is important for a biosensor application. The application of a biolayer attenuates the device Q-factor and results in higher insertion losses to the device due to the change in boundary conditions.

The sensing mechanism of QCM is based on perturbation of the sensor surface when the detection occurs that leads to the change of the resonant frequency. The perturbation arises from a mass attached on the sensor surface or changes of physical properties of the contacting medium, or both. In 1959 Sauerbrey [29] published the following equation describing the linear relationship of frequency change (Δf) and mass loading (Δm) on a QCM surface.

$$\Delta f = -K f_0^{\,2} \frac{\Delta m}{A} \qquad (1.4)$$

where f_0 is the resonance frequency, K is a constant, and A is the sensing area. This is a fundamental equation for the QCM based sensors but it can only be used for a rigid film with negligible thickness and in vacuum environment.

In 1985, Kanazawa and Gordon [30] derived a similar relationship of QCM in contact with liquid.

$$\Delta f = -f_0^{3/2} (\eta\rho / \pi\mu_q\rho_q)^{1/2} \bullet \Delta m \qquad (1.5)$$

where f_0 is again the resonance frequency, η and ρ are the viscosity and absolute density of the solution, respectively, and μ_q and ρ_q are the shear stiffness and density of the quartz crystal, respectively. This equation introduces another term, the viscosity of the medium, in addition to the mass.

As the coating layer becomes complex, however, additional physical factors need to be involved to describe the characteristic of sensor responses. Figure 1.4 represents a side cross-sectional view of a QCM in thickness shear mode and with a selective layer, an antibody film here, attached on it. h_q and h_f are the thickness of the quartz plate and the film respectively. In case of a QCM immunosensor coated with antibody layer and/or other biomolecules, the profile of the sensor response does not always follow the equation (1.4) or (1.5). To examine more detailed behavior of the frequency responses in this particular situation, we review the partial differential equation for the frequency shift of QCM based sensors developed by Hunt *et al.* (1.6) from the complex reciprocity relation and time-dependent perturbation theory.

$$t\frac{\partial \Delta\omega}{\partial t} + \Delta\omega = \frac{\omega_u h_f}{\pi\sqrt{\rho_q \mu_q}}\left\{-\omega_u\left[\Delta\rho - \frac{\Delta\mu}{V_s^2}\right] + j\left[\frac{\partial \Delta\rho}{\partial t} - \frac{1}{V_s^2}\cdot\frac{\partial \Delta\mu}{\partial t}\right]\right\} \qquad (1.6)$$

where V_s is the acoustic velocity across the thickness; ρ is the density of the film; μ is the stiffness (N/m^2) of the film; Δ is the difference between perturbed and unperturbed (denoted by subscript u) quantities.

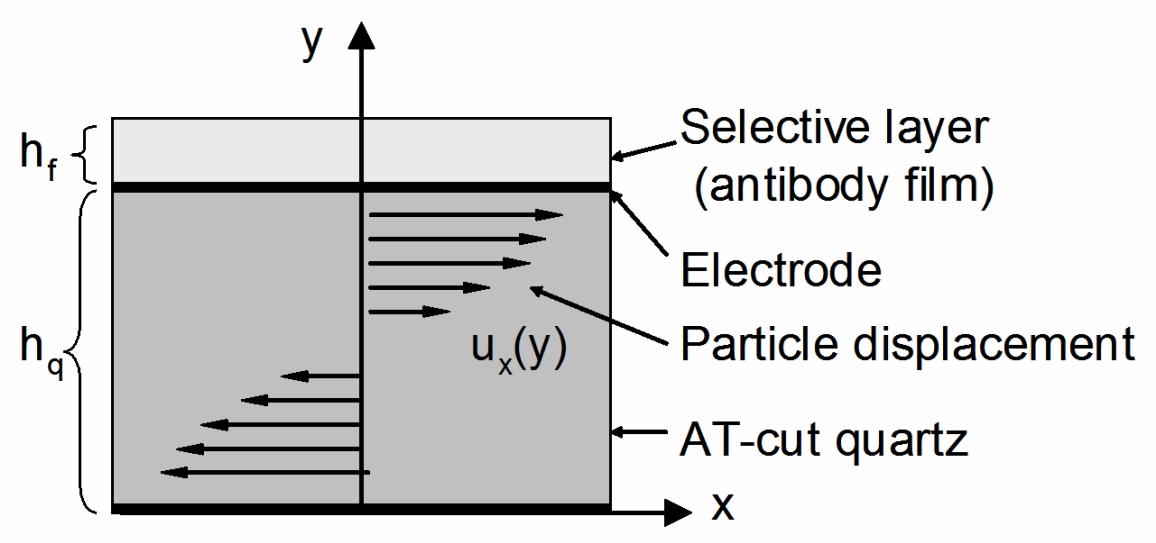

Figure 1.4 Side cross-sectional diagram of a QCM with biofilm coated (Not drawn to scale)

Assuming that neither $\Delta\omega$, $\Delta\rho$ or $\Delta\mu$ changes with time, we get

$$\Delta f = -\frac{2f_u^2 h_f}{\sqrt{\rho_q \mu_q}}\left[\Delta\rho - \frac{\Delta\mu}{V_s^2}\right] \qquad (1.7)$$

Noting that μ_q and ρ_q are constants and the mass loading can be expressed as $\Delta m = \Delta\rho A h_f$, (1.7) is essentially the Sauerbrey equation (1.4) with an additional term describing changes in the mechanical stiffness of the film. This equation predicts that mass loading will lower the frequency but increase in stiffness will incur a positive frequency shift. Note that neither (1.4) nor (1.5) can explain a positive frequency shift. If $\Delta\rho$ and $\Delta\mu$ were known as function of time, the solution of (1.6) would be

$$\Delta\omega(t) = \frac{1}{t}\left(\int_t \frac{\omega_u h_f}{\pi\sqrt{\rho_q \mu_q}}\left\{-\omega_u\left[\Delta\rho(\tau) - \frac{\Delta\mu(\tau)}{V_s^2}\right]\right\} d\tau + j\left[\Delta\rho(t) - \frac{\Delta\mu(t)}{V_s^2}\right] + C\right) \qquad (1.8)$$

Though $\Delta\rho$ can be extracted from kinetic approximations, $\Delta\mu$ is a complete unknown. This equation represents a mathematical tool for extract conformational change data from real-time QCM measurements by recording $\Delta\omega(t)$ [1].

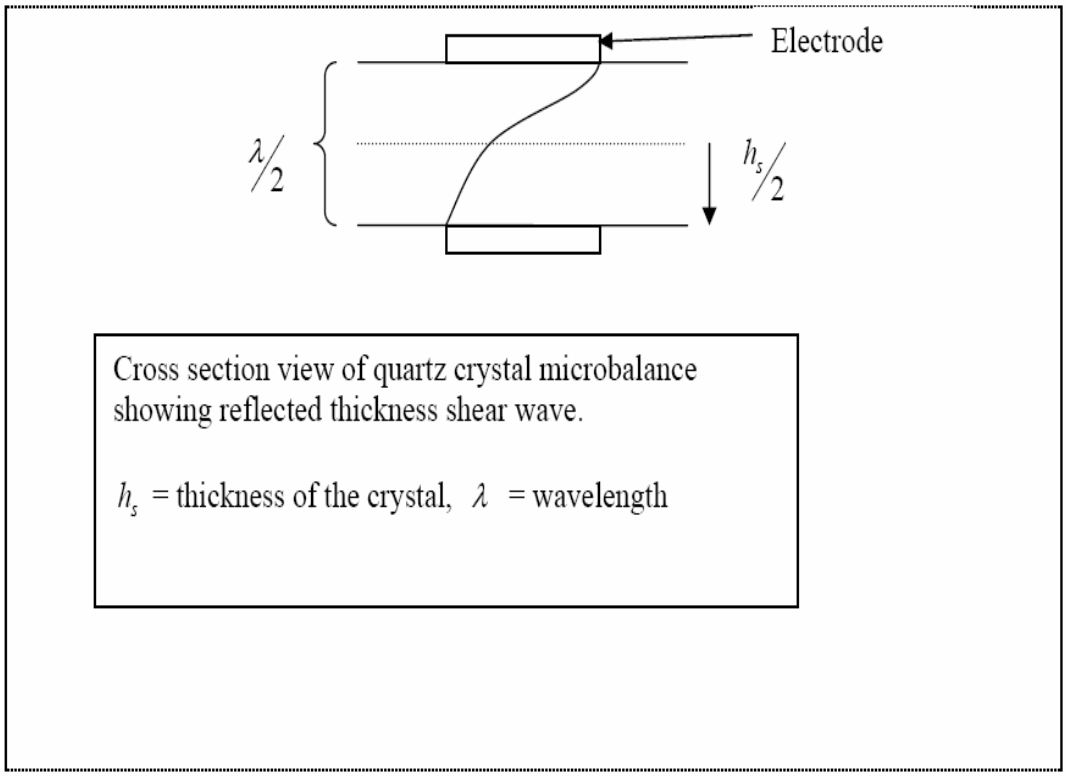

Figure 1.5 Showing Quartz Crystal Microbalance design [3].

1.4 Solving Sauerbrey

Sauerbrey relates changes in frequency with respect to the resonant frequency to changes in surface mass with respect to device mass density:

$$\frac{\Delta f}{f_0} = \frac{\Delta \rho_s}{\left(h_s \bullet \rho_q\right)} \qquad (1.9)$$

$$h_s = \lambda/2$$

$$\Delta f = \frac{2 f_0^2 \rho_s}{V_A \rho_q} \qquad \lambda = \frac{V_A}{f_0}$$

$$h_s = \frac{V_A}{2 f_0}$$

$$\Delta f = \frac{2 f_0^2 \rho_s}{\left(\mu_q \bullet \rho_q\right)^{1/2}} \qquad V_A = \left(\frac{\mu_q}{\rho_q}\right)^{1/2}$$

1.5 Differential mode QCM experimental Set-up

The quartz crystal microbalance (QCM) experimental setup consisted of a Maxtek TM-400 plating monitor, two crystal controlled oscillators, a flow cell, two AT-cut 10 MHz crystals (Figure 1.6), and a personal computer. The oscillators and crystals were supplied by International Crystal Manufacturing (ICM) while the flow cell was custom built in-house. The surfaces of the crystals were affixed with gold electrodes to facilitate electrical connection to the oscillator circuits. The area of these attached electrodes was 0.205 cm^2. The crystals chosen for the testing were polished by the manufacturer prior to delivery. These polished surfaces allowed for maximum hydrophobicity in the liquid test medium.

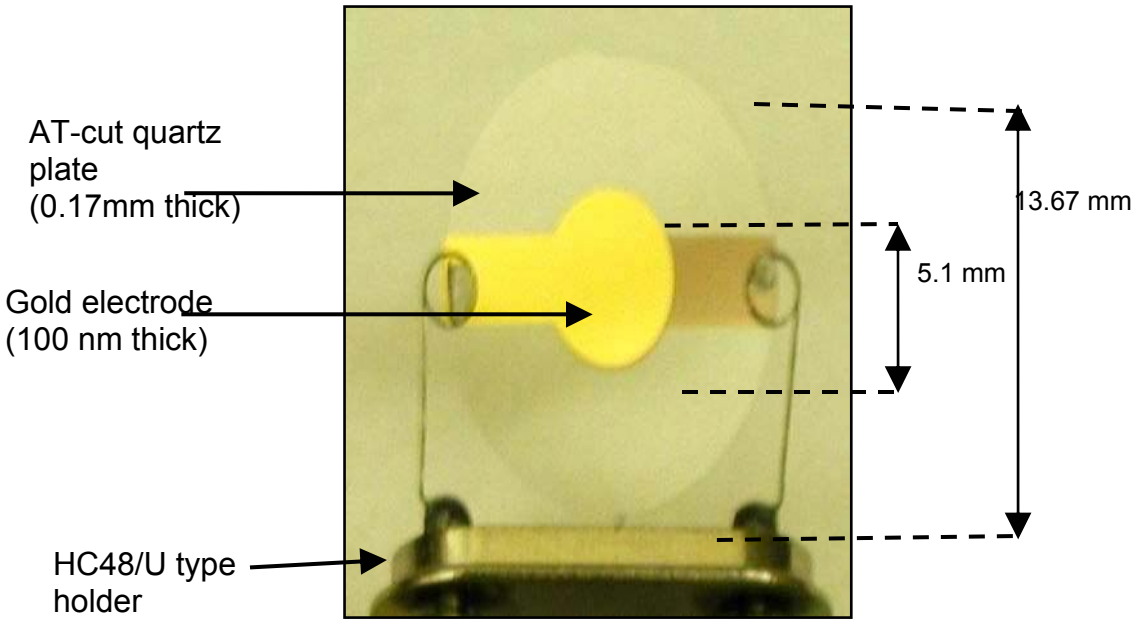

Figure 1.6 A diagram depicting a 10 MHz Quartz Crystal Microbalance.

1.5.1 Alkanethiol Immobilization on QCM

The gold surfaces of the QCM crystal were cleaned using Piranha solution (3 parts of 30% H_2O_2 in 7 parts H_2SO_4). The crystals were air-dried. 3,3'- Dithiopropionic acid (0.0234g) was dissolved in 100% ethyl alcohol to make a 0.01M alcoholic solution. The solution was applied to the QCM gold electrodes and allowed to incubate overnight. Surface was washed 95% ethanol then aliquots of deionized water before allowing to air-dry. 1-Ethyl-3-(3-Dimethylamino-propyl) carbodiimide (EDC) (0.0133mg) was dissolved in 0.1ml of 1x TAE buffer. N-hydroxysuccinimide) (0.0135g) (NHS) was dissolved in 0.1ml of buffer and mixed with EDC solution and the resulting mixture was incubated with the QCM surface for 30 min (Figure 1.7). The surface was washed with deionized water and allowed to dry. Mouse monoclonal antibody IgG1 (20ul of 100ul/0.1ml) was incubated with the QCM gold electrodes for 6 hrs. The crystal was washed with 1 X TAE buffer and allowed to dry. Ethanolamine (0.5M) was titrated with HCl to pH 8.0 before being applied to the quartz crystal. The surface was washed with deionized water and allowed to air dry [31].

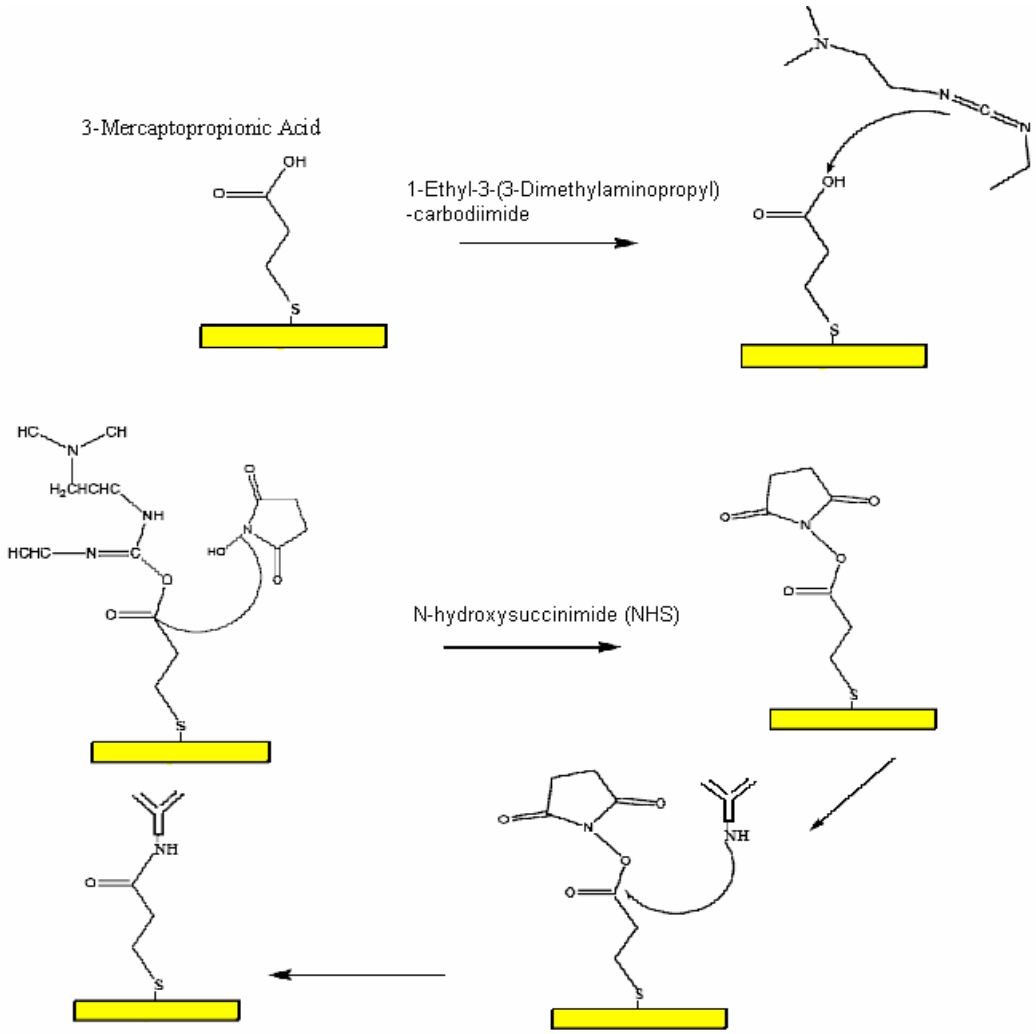

Figure 1.7 Showing typical immobilization protocol on QCM [13,14,15]

Figure not drawn to scale.

The AT-cut crystals operate in thickness shear mode (TSM) which is most advantageous in liquid phase tests where the density and mass of the test liquid can cause motion normal to the crystal surface to be muted.

The crystals were connected to the oscillator and mounted in the acrylic flow cell. The flow cell was used to secure the crystals in place while physically and electrically isolating opposite sides of each device. This allowed the introduction of liquid to one surface of each crystal while keeping the other side of each exposed only to air. The flow cell used was designed to facilitate the securing of the crystals in the cell so that the exposed sides of each crystal were in contact with the same test liquid. Figure 1.8 shows a block diagram and the general orientation of the crystals mounted in the flow cell.

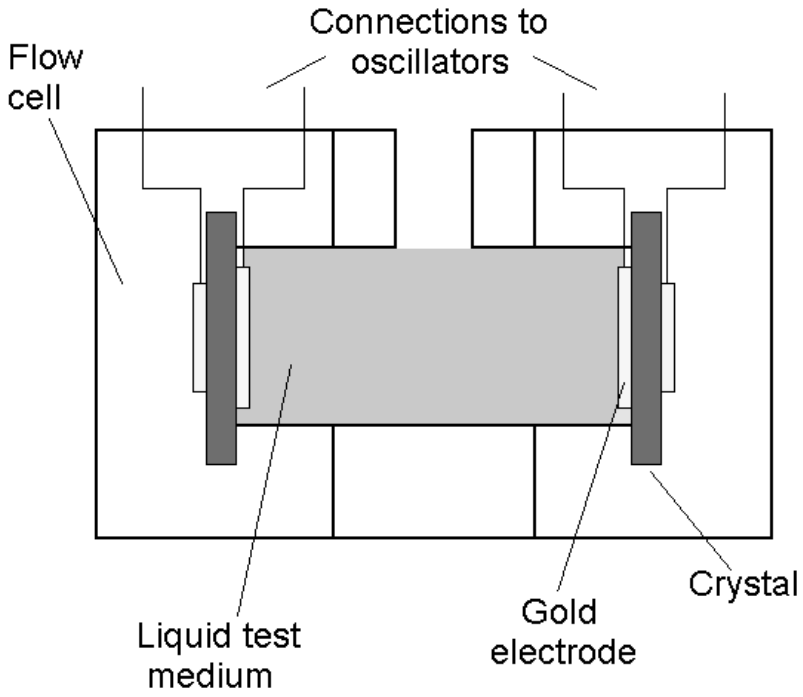

Figure 1.8 Showing QCM flow cell Designs for Differential Medium Monitoring .

1.6 Rayleigh Wave based Resonators (SAW)

Lord Rayleigh first discovered in 1887 that a stress free boundary imposed by the surface of a crystal gave rise to a unique acoustic mode of propagation. This mode of propagation in which acoustic energy is confined to very near the surface of an isotropic solid is known now as the Rayleigh wave. These waves are of interest to seismologists because earthquakes propagate using the same mode. The utility of Rayleigh waves in sensor applications is also due to the surface confinement of energy allowing them to be excited by surface electrodes and also making the wave extremely sensitive to surface perturbations.

R.M. White [32] discovered a technique that could be used to excite surface acoustic waves using lithography to pattern interdigital electrode geometry on piezoelectric crystals. These devices have since been used as filters, delay lines and resonators. In a SAW-R application the voltage between alternately connecting electrodes cause a periodic electric field (Figure 1.7) to be imposed on the crystal resulting in a standing wave. The interdigital transducers,(IDT) formed by patterning electrodes on the surface of quartz (piezoelectric material) for exciting surface acoustic waves, operates most efficiently when the SAW wavelength, λ, matches the transducer periodicity, d (Figure 1.8).

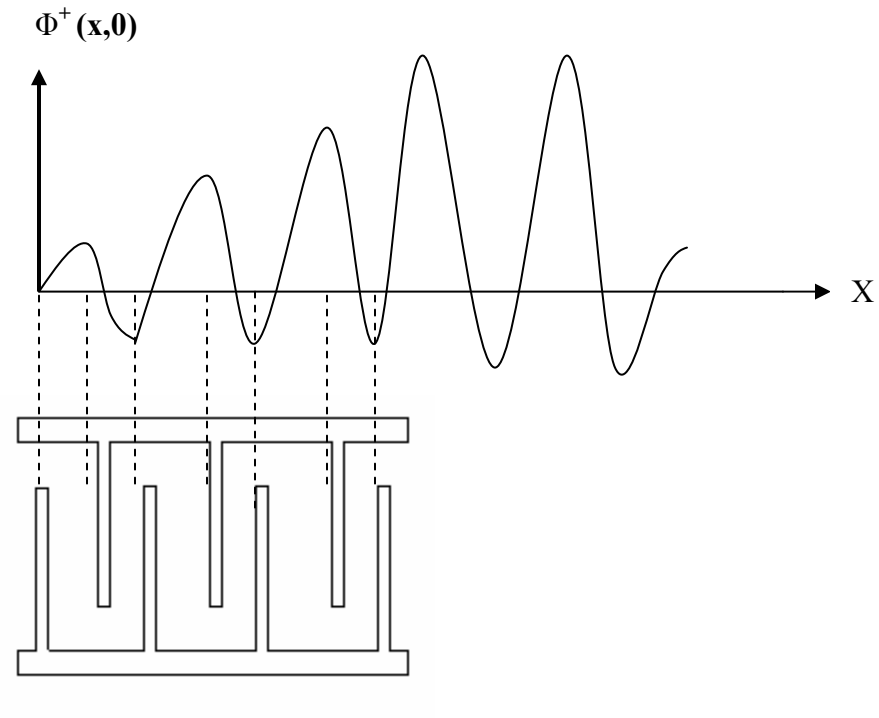

Figure 1.9 SAW Electrical Potential through an Interdigital Transducer [3].

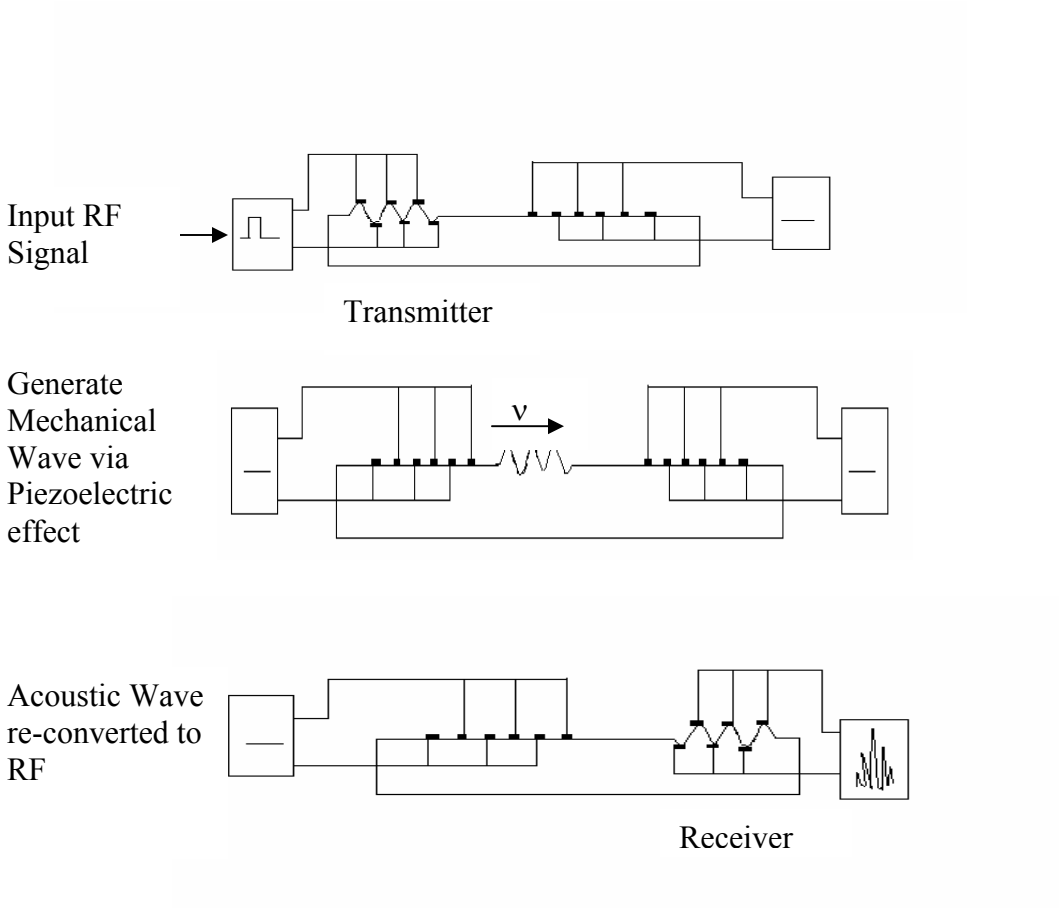

Figure 1.10 Generation of Surface Waves due to Patterning of IDT's on Piezoelectric Substrate [33].

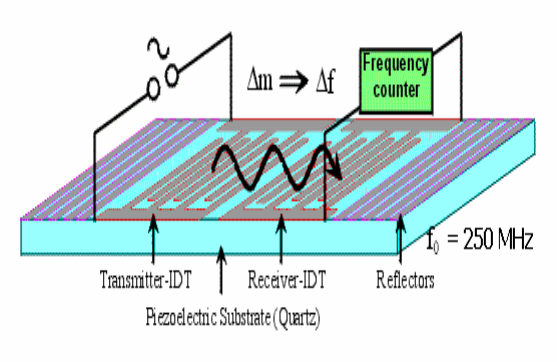

Figure 1.11, showing the simplified diagram of a typical two-port SAW resonator.

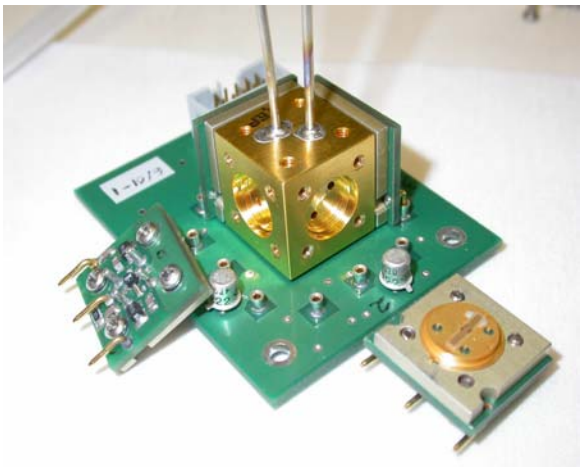

Figure 1.12 showing the packaged resonators in circuit oscillator and flow system. Sensor head holds and facilitates the simultaneous sampling of four sensors.

1.7 Data Analysis

In constructing a biosensor, there should be a practical scheme to quantify and qualify the response data. The mass sensing modality of SAW sensors provides the necessary parameters for high throughput data analysis. The Sauerbrey equation is classical method for interpreting the electrical output data of a SAW sensor by establishing a linear relationship between a known measurable quantity (frequency, impedance, phase) and an unknown (mass, binding kinetics). Further analysis of the biolayer and its' interface with the introduced analyte has yielded vast body of kinetic modeling data for antibody-analyte interactions.

1.7.1 Reaction Kinetics and the Mass Transport Paradigm

At this time, we would like to address the issue of modeling antibody – analyte reactions using basic kinetic principle. Kinetic studies have become a growing trend among the current biosensor literature [34]. This data is borne out of the fact that SAW sensors are continuous, real-time detectors. Unfortunately, many of these publications fail to account for the inherent mass transport issue as well as other affects other than antibody – analyte binding. That is, in evaluating a response one must consider the rate of flow of the bulk solution, the flow of analyte in the bulk and the diffusion to the surface of the device.

In this thesis, we use monoclonal antibodies as our sensing agent. These molecules typically possess affinity constants of 10^6 $M^{-1}s^{-1}$ or better (anti-FITC Ka = 10^9 M^{-1} s^{-1}) [35]. Interactions between the immobilized antibody [Ab] and the molecule in the bulk solution [A] are usually treated as a first order kinetic reaction. Therefore, in our

sampling practices, the binding kinetics would be attributed more to rate of introduction of a target into the flow cell rather than the reaction rate itself. In a study done by Skladal et al, [36] kinetic equations were developed for calculating binding constants using piezoelectric crystals.

$$[A]+[Ab] \Leftrightarrow A \bullet Ab \qquad (1.10)$$

$$\frac{d[A \bullet Ab]}{dt} = K_a[A][Ab] - K_d[Ab] \qquad (1.11)$$

where K_a is the association rate constant and K_d is the dissociation rate constant.

Factor in some reaction time (t),

$$[Ab] = [Ab]_0 - [A \bullet Ab] \qquad (1.12)$$

$$\frac{d[A \bullet Ab]}{dt} = K_a[A][Ab_0 - [A \bullet Ab] - K_d[A \bullet Ab] \qquad (1.13)$$

where Ab_0 is the concentration of B at t = 0.

Assuming the Sauerbray equation describes the mass –frequency relationship (i.e. increase in mass leads to a decrease in frequency, Δf) and using Δf_m as the frequency change after a complete saturation of the surface of the crystal with A, the concentration of the free Ab is proportional to (Δf_m -Δf), and the concentration of the complex ($A \bullet Ab$) to Δf.

Thus the relationship can be expressed as:

$$\frac{d(\Delta f)}{dt} = K_a \times (\Delta f_m - \Delta f) \times C - K_d \times \Delta f \qquad (1.14)$$

$$\frac{d(\Delta f)}{dt} = -(K_a \times C \times K_d) \times \Delta f + K_a \times \Delta f_m \times C \qquad (1.15)$$

where C is concentration of the free A, hold constant in a continuously flowing solution. For the determination of the constants K_a and K_d from the experimental f versus t curves, the derivatives d(Δf)/dt must be plotted versus the corresponding frequency change Δf. A straight line characterized by a slope, sl and intercept, int, should be obtained according Equation 14. The parameters sl and int are related to the kinetic constants:

$$sl = -(K_a \times C + K_d) \qquad (1.16)$$

$$\text{int} = K_a \times \Delta f_m \times C \qquad (1.17)$$

By measuring the binding curves (f-t) determined for several concentration, C, all of the desired parameters k_a, k_b, and Δf_m could be obtained.

It is the opinion of this author that many of the assumptions used in Skladal's study would lead to unrepeatable and inconsistent data. For instance, Skladal used the term f_m to define the frequency change after device saturation. The problems lie in the fact that the method of immobilization was random and nature which suggests a high relative

standard deviation value (>10%). This immediately questions the repeatability and reproducibility of the experiments and the binding kinetics values obtained.

Chapter 2: Background

To date there has been a limited amount of work reported on vapor phase biosensors. In a series of papers Guilbault and fellow researchers [37-39] reported the use of films of biomolecules such as enzymes and antibodies on Quartz Crystal Microbalance (QCM) devices for vapor phase detection of formaldehyde and organophosphorous pesticides such as parathion. Subsequent studies by others were unable to confirm the specificity reported by Guilbault. Rajakovic *et al* [40] found that sensors coated with anti-parathion antibodies showed sensitivities to malathion, parathion and disulfoton that were not markedly different from the response of sensors coated with proteins (valproic acid antiserum, bovine serum albumin and human IgG) containing no specific binding sites for these analytes. In addition, one could also conclude that the anti-parathion QCM immunoassay sensor of Ngeh-Ngwainbi, *et al.* [37] does not indicate antigen-antibody binding activity. When an antigen/antibody binding event occurs, the antigen becomes tightly bound to the antibody and one would expect a shift in the baseline frequency of an acoustic-based oscillator. There was no such baseline shift was reported by Ngeh-Ngwainbi *et al*. One explanation for the nonspecific binding [3] was that in the absence of an aqueous environment, the binding sites on the antibodies will lose their prescribed structure required for molecular recognition.

2.1 Proof of Concept

SAW Resonator Device Description. The experiments described herein were conducted using two port SAW resonators fabricated in the laboratories of the Microelectronic Acoustics Group at Georgia Tech. These devices have a center frequency of nominally 250 MHz two port resonators with Al electrode metallization on ST-X quartz substrates. ST-X quartz is a particular cut of quartz for which interdigital transducer (IDT) structures generate more or less a Rayleigh wave in the substrate material. More importantly for sensor applications, the ST-X cut of quartz is known to provide very high temperature stability near room temperature [41] which minimizes the need for precise temperature control. In Figure 2.5, we present a diagram of a typical two port SAW resonator. The gratings on either side of the IDTs form a resonant acoustic cavity. One IDT acts as an input transducer which converts the driving RF signal into an acoustic standing wave within the cavity. The output IDT converts the acoustic wave back into an RF signal which is fed back into the attendant oscillator circuitry. Two important parameters in the design of the SAW resonator are d_g and d_m, the distance between grating and IDT and the distance between two IDTs respectively. To maintain the standing waves in the cavity region, d_g and d_m should be respectively:

$$d_g = \lambda/8 + n\lambda/2 \text{ , } (n=0,1,2,3\ldots) \quad (2.1)$$

$$d_m = \lambda/4 + n\lambda/2 \text{ , } (n=0,1,2,3\ldots) \quad (2.2)$$

Since our protocol for antibody immobilization is expected to ensure that the antibodies attach to the metal electrodes (fingers) but not to the quartz surface, we designed our resonators to minimize the amount of bare quartz in the cavity region. This would also help us to achieve a uniform distribution of biomolecules in the SAW resonators' most sensitive region. Selecting the minimum possible value for d_m can aid in the achievement of this goal. For our SAW resonators, there are 500 fingers in each of the gratings and these ideally have widths of $\lambda/4$ where λ is the acoustic wavelength at the center frequency of the resonator. Generally, the IDT finger width is same as that of gratings. In our design, however, split-finger IDTs are used so as to reduce SAW reflections from the IDTs within the resonant cavity. Hence, the size of the IDT finger widths and the spacing between IDT fingers is 1.5 μm. This is the minimum feature size of our devices and it is one that, with care, can be achieved in our facilities. Each IDT in this design has 200 metal fingers. The main features of the SAW resonators used in this experiment are summarized in Table 2.1.

Table 2.1: SAW Resonator Device Parameters

Wafer material	ST-X Quartz
Acoustic aperture (W)	850 μm
IDT-grating gap(dg)	7.8 μm
IDT-IDT gap (dm)	3.1 μm
IDT pitch (λ/2)	6.2 μm
IDT finger width	1.5 μm
Grating pitch (λ/2)	6.2 μm
Grating finger width (λ/4)	3.1
Metal film thickness	1500 Å
Diced chip size	8100x1980 μm

Briefly, our fabrication procedures are as follows. After proper surface cleaning and treatment, Shipley S1805 positive photoresist was spun at 3200 rpm for 20 secs and the device pattern was exposed to UV light for 10 secs at the intensity of 8mW/cm^2 (Figure 2.1). Developing was done with the Microposit MF351 5:1 solution for 15 to 20 secs.

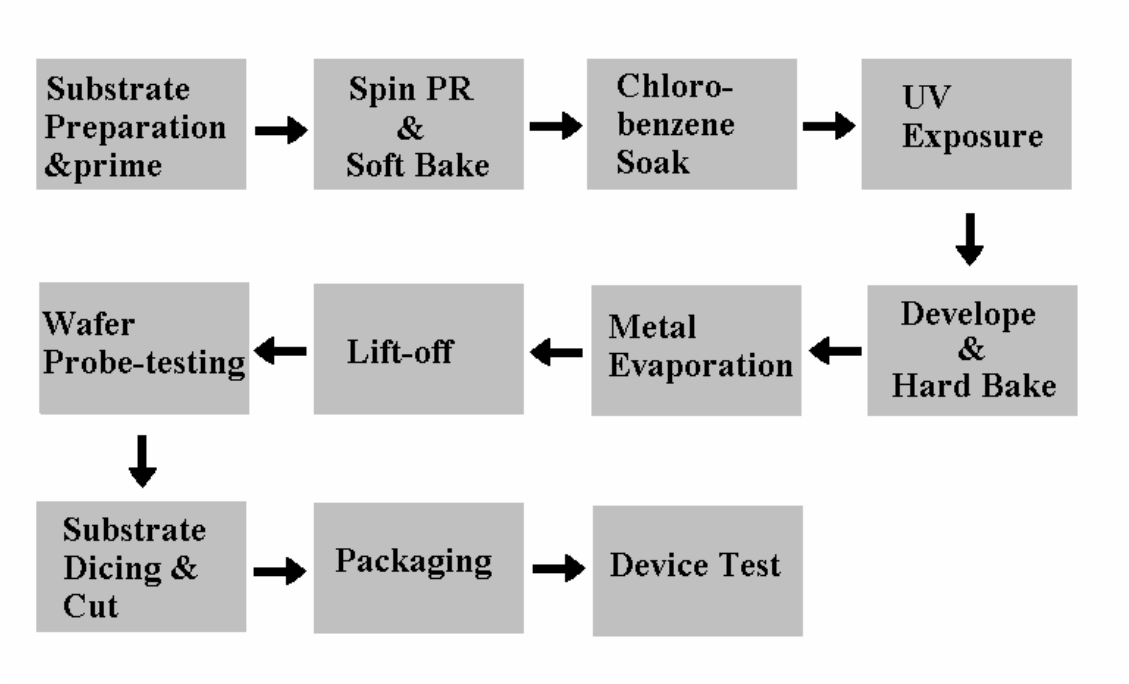

Figure 2.1 Showing SAW Fabrication Using Photolithography

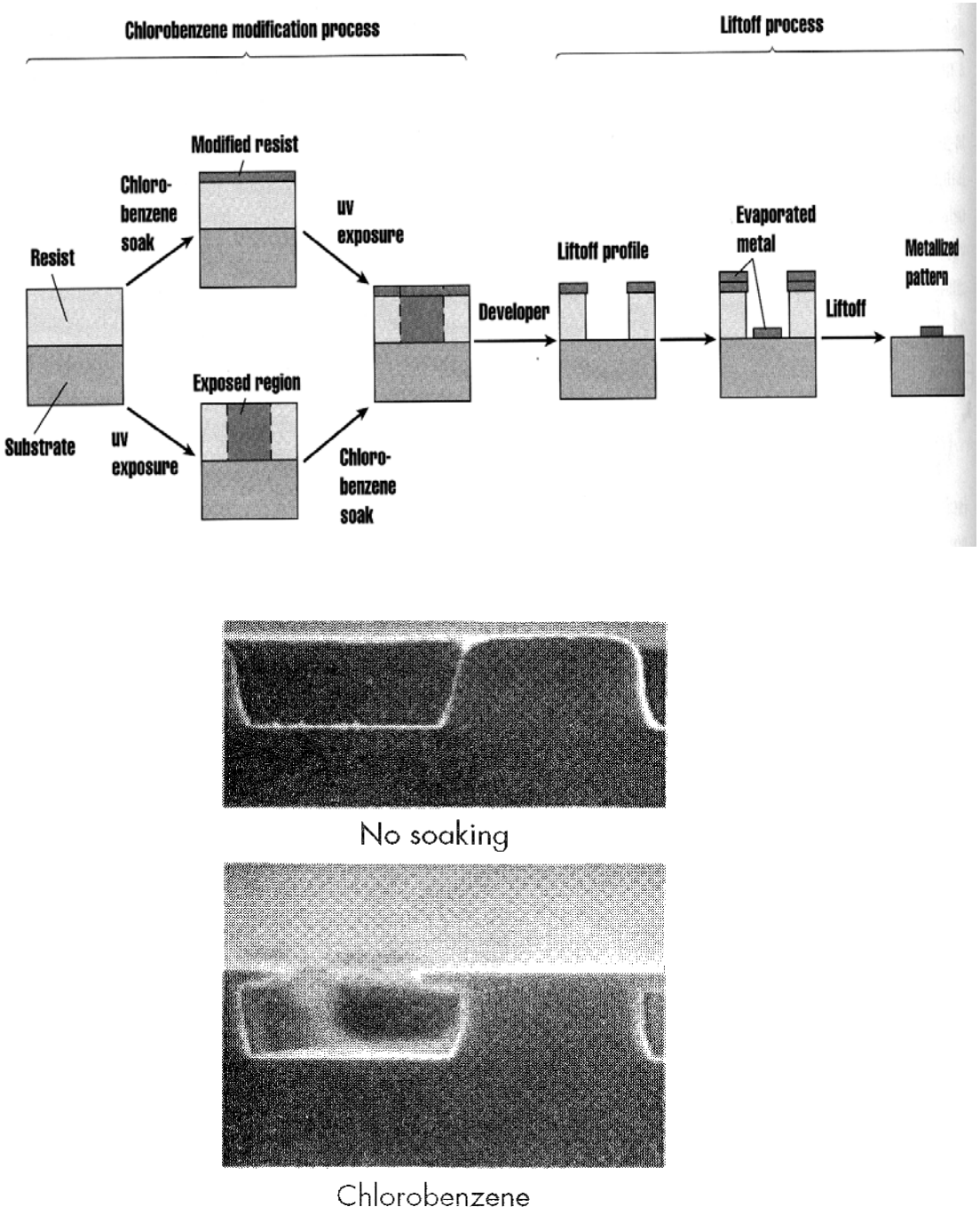

Figure 2.1 Showing SAW Fabrication Using Photolithography [42].

Two different metal layers were deposited using a CVC electron beam evaporator. An adhesion layer of 300Å of Cr was deposited as a first layer followed by 1200Å of Al. For the devices in these experiments where gold electrodes are used, an additional 300Å of Au was deposited on top of the Al layer. After a lift-off process using acetone, the wafer was diced with a 3 mil-thick, diamond-coated high speed rotating blade. Then, each die was coated with the proper biofilm and mounted on a TO-8 header, which has a 12.7mm (0.5") diameter.

2.1.1 Methodology

Our approach is to construct a vapor phase biosensor by immobilizing a monolayer of antibodies onto the surface of a Surface Acoustic Wave (SAW) device [43-45]. The antibodies are immobilized using protein A and process ends with the application of a thin hydrogel layer that we suggests helps maintain a semi-aqueous environment for the biomolecules attached to the device surface. For illustration purposes we show a simple version of this device structure for a SAW delay line in Figure 2.5. In general, the device is then connected into an oscillator circuit and the frequency of oscillation can then be precisely measured. When the antigen binds to the antibody, the acoustic velocity is decreased and the oscillator frequency shifts to a lower value.

2.1.2 Antibody Immobilization

The antibody immobilization technique first requires polarizing the gold surface. This was accomplished by immersing the SAW chip in 5ml of 1.2M HCl for 5 min then washing with deionized water, followed by 5ml of 1.2M NaOH for 5 min. The SAW chip

was washed again with deionized water before it was immersed in 3ml of 1.2M HCl for 2 min. The chip was washed twice with deionized water followed by buffer solution and was allowed to air dry. Protein A (0.2mg) was dissolved in 100µl of buffer solution at physiological pH. Then 10µl of antibody (0.023mg/ml) was mixed with the buffered protein-A solution and the mixture was placed in a 4^{o}C refrigerator for 2 hrs. It is important to mention here that the antibody concentration used was determined by insertion loss analysis in SAW-R's coated with varying concentrations of the protein (Figure 2.2). Three microliters of the cross-linker-antibody solution was used to coat the device. The chip was allowed to air dry for hour and the remaining solution was spun off for 30 sec at 5000rpm. A thin layer of hydrogel (3µl) was then applied by spinning the chip on a silicon wafer for 50 sec at 5000 rpm. We obtained both the mouse monoclonal anti-FITC antibodies and Protein A – soluble (extracellular) from Sigma Chemical Co. St. Louis, Mo. Uranine was obtained from Fluka Chemika, Paris, France.

Network Analysis of SAW-R's coated with varying concentrations of anti-FITC antibodies was processed using a Network Analyzer (Figure2.2).

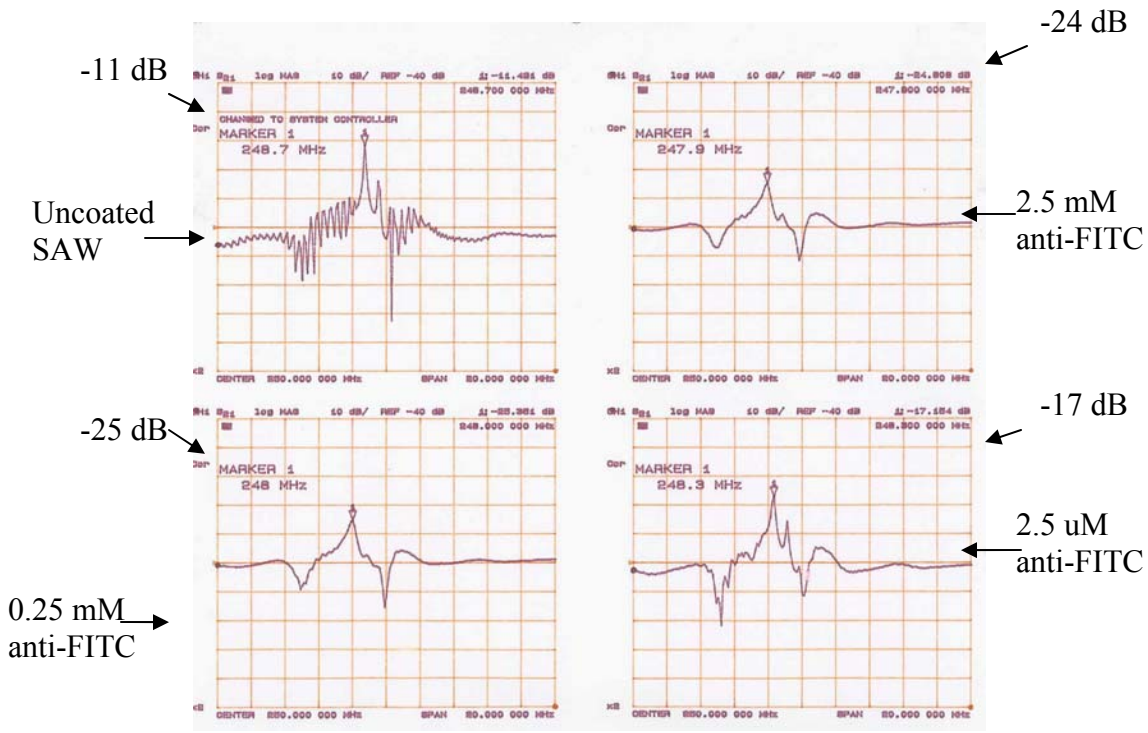

Figure 2.2 Plot Showing S_{21} Transmission Spectrum of a 250 MHZ SAW device with Various Antibody Concentrations.

2.1.3 Fluorescent Assay

It is clear that the experimental protocol for gas phase biosensors should include at least at the early stages of sensor development, an independent assessment of the predicted molecular recognition event. To verify vapor phase analyte binding events, we developed a novel fluorescence antibody/analyte assay. This was to provide a method, independent of the SAW device response, to detect the occurrence of molecular recognition. Further to ensure hydration of the biomolecule, we have developed a method for applying a hydrogel layer over the immobilized antibodies. SAW devices with and without anti-FITC antibody films were tested against two different fluorescent analytes: uranine and Alexa Fluor®. The latter will hereafter referred to as Alexa. Our protocol consisted of presenting the analyte to the SAW resonator devices by bubbling nitrogen at 0.5 standard liters per minute (SLPM) through a 1nM aqueous solution of the analyte compound. After brief, 15 sec, exposure to the analyte vapor in the SAW Pro 250 system the TO-8 packaged devices (Figure 1.12) were pulled from the system, washed with buffer to remove unbound analyte, and then viewed using a Zeiss LSM510 confocal fluorescent microscope (CLSM). The approximate time between exposure to the analyte and observation with the CLSM was 30 min. If fluorescence was observed in the CLSM image, this was taken as evidence of tightly bound fluorescent analyte. As you will see, in the results to be presented, we observed good binding affinity of the uranine molecule to the anti-FITC antibody that, among other things, indicates that the epitope on FITC does not include the isothiocyanate group.

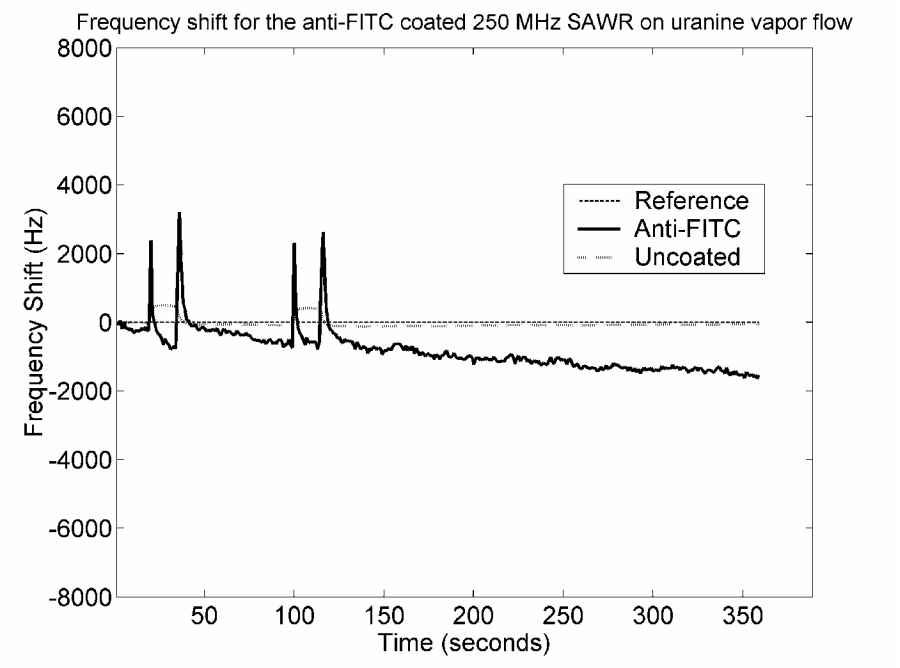

Figure 2.3 Anti-FITC coated SAW response to uranine(soluble FITC salt) vapor flow. For analyte presentation, N_2 (g) was bubbled through a 1nM solution of the uranine at a flow rate of 0.5 slpm (standard liters per minute). N_2 (g) flow was continuous during the experiment as analyte vapor samples were pulsed into the stream for two different 15 sec periods (20 to 35secs and 100 to 115 secs).

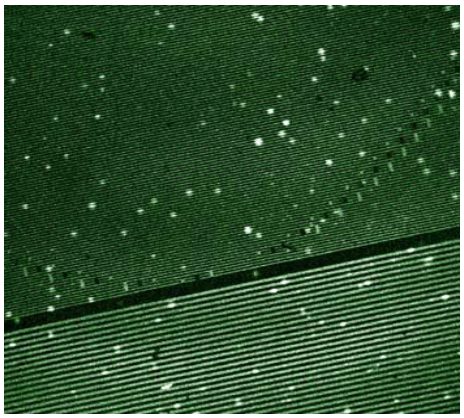

Figure 2.4 CLSM Image of SAW device. The response from the reference sensor has automatically been subtracted from the response of the other two sensors so that ideally temperature, humidity and pressure effects will be cancelled out so that the response which remains is indicative of only the antibody-antigen interaction.

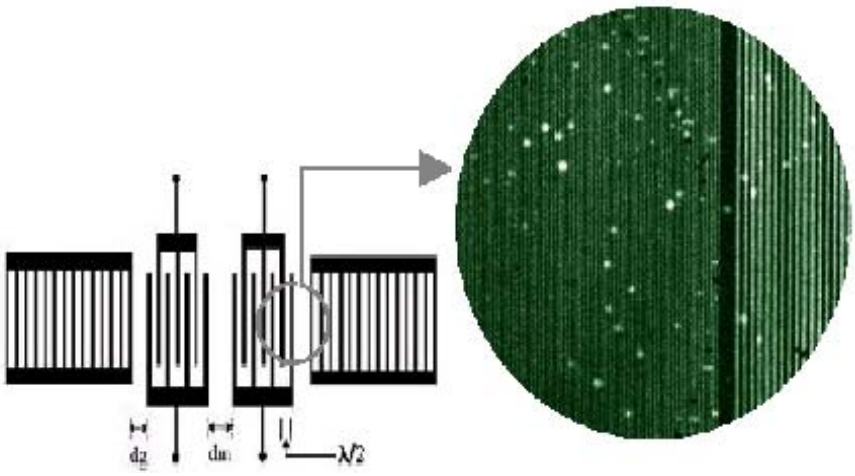

Figure 2.5 Image of a typical two-port SAW resonator along with CLSM image of uranine attached to the SAW electrodes. The image represents the IDT (interdigital transducer) and gratings portion of electrode geometry. Fluorescent molecules are observed on the metal electrode (green due to reflection) and not the quartz (black due to light absorption) as dictated by the immobilization procedure.

As in any immunoassay technique, it is important to test the device against an analyte which is dissimilar in substantive, but not radical, ways from the antigen. For this we have chosen Alexa, the structural formula for which is shown in Figure 2.6 (c), as the negative control. This compound is similar to FITC in that it has four linked phenyl groups, but the introduction of charged groups attached to the outer portion of the molecule prevents recognition by the anti-FITC antibody.
The data presented in the next section were generated from three SAW resonator sensors. The SAW devices differed only in the nature of the film coated onto the surface of the device. The anti-FITC device was coated with FITC antibody and the hydrogel layer. The uncoated device had just the hydrogel layer. Uncoated here refers to the absence of antibodies. The reference device had no coatings at all. In every other way, the SAW devices were identical.

Our approach was to construct a vapor phase biosensor by immobilizing a monolayer of antibodies onto the surface of a 250-MHz SAW device fabricated on ST-Quartz. For the particular cut and propagation direction, the interdigitated transducer on the device generates a Rayleigh wave which has particle polarization in the saggital plane that is retrograde (opposite to the normal universal convention) and decays within roughly one acoustic wavelength from the surface. With our SAW devices, we have obtained sensitivities of approximately 20 Hz/pg with a detection limit on the order of a few picograms. To illustrate the sensing mechanism, we show a simple version of this device structure, a SAW delay line, in Figure 2.5. The device is connected into an oscillator circuit, and the frequency of oscillation can be measured with great precision. When the

antigen binds to the antibody, the acoustic velocity is decreased, and the oscillator frequency shifts to a lower value. The situation is much more complicated, however, when SAW resonators are used. Because a binding event might take place in either the reflector gratings or the transducer sections of the device, the frequency can increase or decrease in the presence of a binding event. To add to the confusion for SAW resonator signatures, stiffness changes in the biofilm would increase the resonant frequency of a delay line SAW sensor but could either increase or decrease the frequency of a SAW resonator.

Once we immobilized the anti-FITC onto a SAW resonator under test using protein-A, brief pulses of analyte vapor were flowed past the devices. The response of a reference device and oscillator circuit taken simultaneously with the response from the coated SAW resonators has already been subtracted from the recorded responses presented. The reference device is subjected to the same temperature environment as the sensor under test, but is not exposed to the analyte stream.

The sensor data in the Figures have already had the reference variation subtracted out; this resultant frequency shift was measured and recorded. Over numerous trials with coated and uncoated devices, a consistent picture began to emerge. In short, antigen–antibody binding occurred quickly and with a response far more dramatic than what was observed when the device was not coated with antibodies. For devices without antibodies, there was not a dramatic response and no baseline frequency shift. Two characteristic responses are presented in Figures 2.3 and 2.7. As mentioned previously, for analyte

presentation, N_2 gas was bubbled through a 1 nM solution of the analyte at a flow rate of 0.5 standard liters per minute (SLPM). The flow was continuous during the experiment. Vapor samples were extracted from the stream for two different 15s periods (20–35 s and 100–115 s). In Figure 2.3, we present the response of an anti-FITC coated device and an uncoated device to uranine vapor. As seen, the uncoated device shows a frequency shift during the sampling periods of a few hundred hertz and then returns to the baseline. This is a typical response for an uncoated device, and the return to baseline indicates that little of the analyte has permanently attached itself to the surface of the SAW device. For the anti-FITC coated device, the device shows a more radical frequency response and a fairly substantial shift in the baseline frequency. We believe that the more or less permanent shift in the baseline frequency represents direct evidence of molecular recognition in the vapor phase. One should keep in mind that the response shown is the raw data from the system and represents the frequency of the SAW resonator in the oscillator circuit. The oscillation frequency is determined by adequate loop gain and a phase matching condition. Unfortunately, this does not always translate into a smooth, continuous curve, particularly if the phase of the resonator is near a discontinuous part of its transfer function response. Further it should be noted that the anti-FITC coated device had a substantially increased insertion loss (signal attenuation) over the uncoated device and hence, in this oscillator circuit, exhibits greater frequency noise. The steady decrease in the absence of the uranine pulse could be due to the fact that we continuously have uranine vapor flowing through a tube from which the vapor is extracted. We have not eliminated the possibility of diffusion of the analyte into the sensor chamber. The response of the uncoated sensor indicates a change in pressure associated with the

introduction of the uranine analyte stream. Again, as stated previously, it is the magnitude and time course of the frequency deviation which is relevant, since the complex nature of the SAW resonator makes it difficult to extract any pertinent information from the positive or negative direction of the frequency variation.

In Figure 2.7, we show the response of an anti-FITC coated SAW resonator and an uncoated SAW resonator to the Alexa vapor. Neither of the devices shows a dramatic response to the analyte, and both the uncoated device and the anti-FITC coated device show no evidence of a marked baseline shift. This would indicate there is no binding of the Alexa to either of the device surfaces.

As indicated previously, in order to verify vapor phase analyte binding events, we developed a fluorescent antibody/analyte assay. After brief vapor phase exposure to the fluorescent analytes uranine and Alexa, the TO-8 packaged devices were pulled from the system, washed with buffer to remove unbound analyte and then viewed using a Zeiss LSM510 confocal fluorescent microscope (CLSM) located in the Institute for Bioengineering and Biosciences on Georgia Tech's campus. There were approximately 30 min between the presentation of the analyte and the capture of the CLSM image. If fluorescence was observed in the CLSM image, this was taken of evidence of tightly bound fluorescent analyte.
Many measurements have been taken, but only a small sampling of these will be presented here. Though it is not shown here, in the CLSM image for a hydrogel-coated SAW device exposed to uranine vapor, there was no evidence of fluorescence. In Figure

2.4, we show CLSM images of an anti-FITC coated SAW chip after exposure to uranine. In this image, the bright spots are the fluorescent areas, indicating that over this relatively brief exposure to the uranine vapor, binding did indeed occur. It should also be noted that fluorescent spots, as seen at the higher magnification, are predominantly located on the electrodes and not on the quartz. This observation supports the established notion that, using the conventional, previously presented protocol, the complex of antibody/protein-A molecules will be immobilized onto the gold electrodes.

Because we observed the uptake of uranine by the anti-FITC coating, we were compelled to prove, whether, we were observing molecular recognition, i.e., highly specific binding, by the antibodies. To accomplish this, an aqueous solution of Alexa was used, which has a similar chemical structure (i.e., fluorescein moeity), but in theory should not bind to anti-FITC with the same affinity. In Alexa, the presence of negatively charged sulfite groups significantly changes the binding characteristics of the molecule. In Figure we show the CLSM image for the anti-FITC devices after exposure to Alexa and subsequent washing to remove unbound analyte. There is no evidence of fluorescence in these images, indicating that the Alexa did not bind to anti-FITC.
These results suggest that real-time binding events were observed as a change in the fundamental frequency. The characteristic response observed in both experiments, was determined not only by device design but also by molecular interactions. That is, the initial transient observed we believe is due to mass loading and some changes in the stiffness of the biolayer. An alternative explanation would suggest that the difference of vapor pressure alone could result in the observed results.

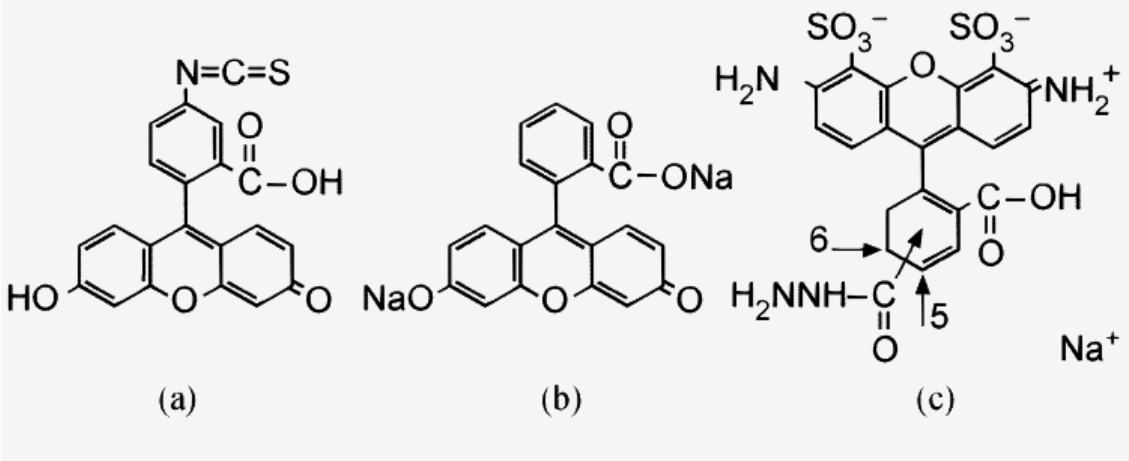

Figure 2.6 Showing structures of fluorescence analytes a) fluorescein isothiocyanate, b) uranine (soluble FITC), c) Alexa Fluora

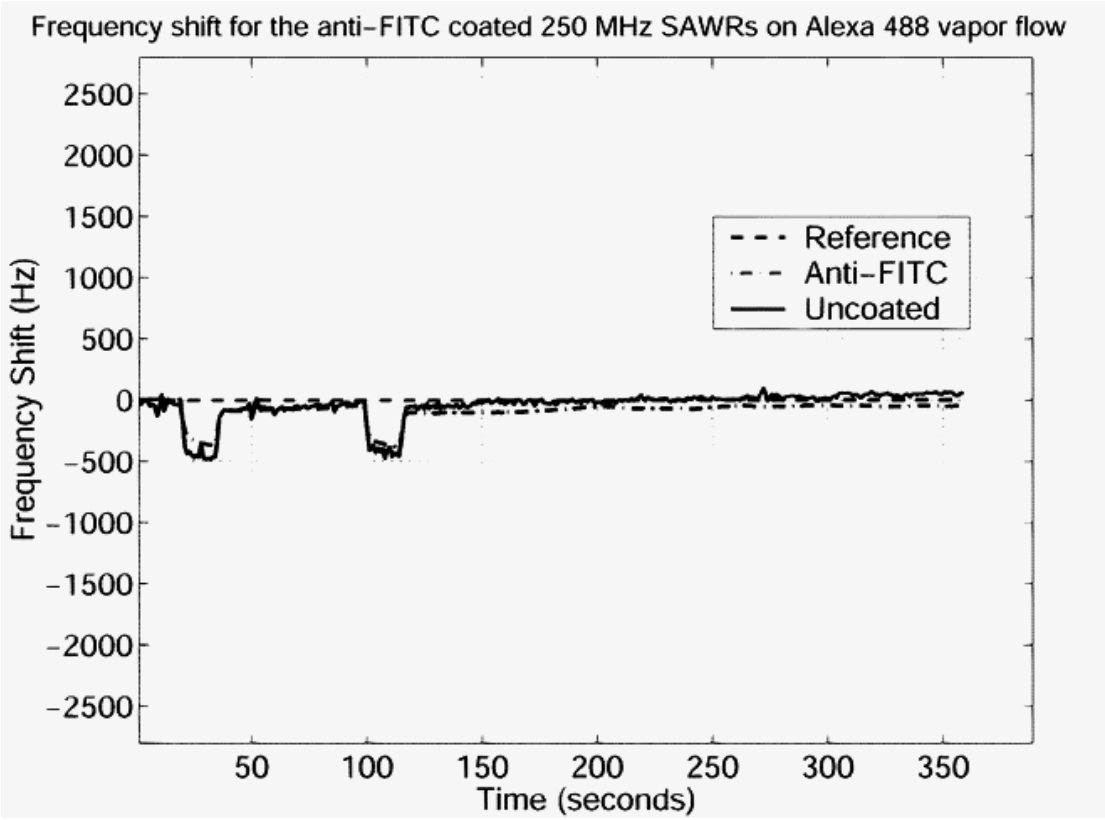

Figure 2.7 Response of anti-FITC coated SAW-R to Alexa Fuora (synthetic fluorescent dye).

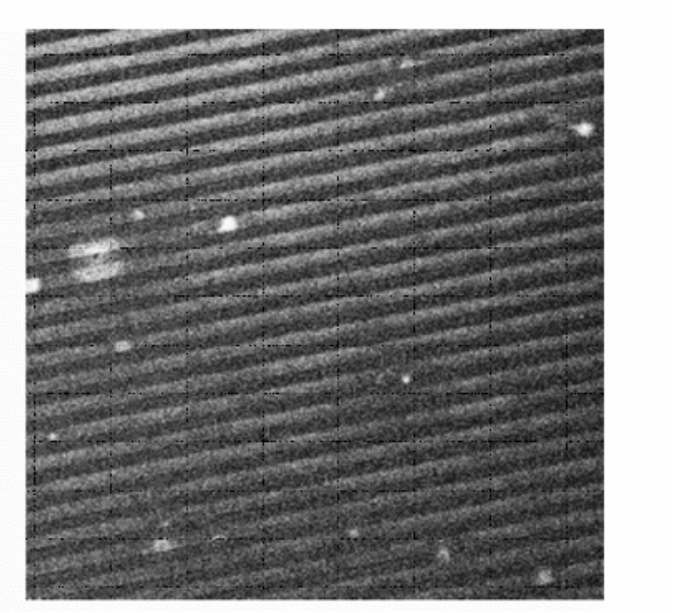

Figure 2.8 CLSM Image of SAW device after exposure to Uranine vapors

Chapter 3: Vapor Phase Detection of Cocaine using Surface Acoustic Wave Immunoassay Sensors

There have been numerous laboratory studies designed to determine the mechanism by which odor-sensing dogs identify a specific chemical target [46-51]. These studies indicate that under normal laboratory conditions there is a high degree of accuracy among the dogs with detection limits in the sub-parts per billion range. Unfortunately, under field conditions the problem become increasingly more complex due to the presence of extraneous odors created by the purveyors of these illicit materials in an attempt to thwart detection. With the introduction of these extraneous odors the dog's ability to detect a target odor was considerably hampered due to its inability to differentiate one odor over another in a complex chemical vapor. The highly specific and complex nature of olfactory sensing systems has lead to the development of vapor phase chemical detection systems that go by the name of "electronic nose". These systems usually consist of some chemical or biological sensing component attached to a transducer. Through-out the current literature surface acoustic wave devices have increasingly been incorporated into these sensing systems. SAW based devices have been used for various applications ranging from communications to its more recent function as a biosensor. In a series of papers Guilbault and fellow researchers [37-40] reported the use of films of biomolecules such as enzymes and antibodies on Quartz Crystal Microbalance (QCM) devices for vapor phase detection of formaldehyde and organophosphorous pesticides such as parathion. Subsequent studies by others were unable to confirm the specificity reported by Guilbault.

The two main features of a functional vapor-sensing device are sensitivity, and specificity. The sensitivity is prescribed by the sensor modality and design and the degree of specificity is dependent on the detailed nature of the chemically sensitive film on the surface of the device. These devices and systems are currently being used in biotechnology, food industry, medicine, environment and most recently law enforcement applications. Interdiction efforts continue in the search for technologies which can provide an inexpensive alternative to dogs as detectors of narcotics and explosives. One of the principle motivations for development of electronic noses for these applications is the expense associated with of the handlers and training and care for the dogs. Further, it is still unclear as to what chemically the dogs are actually detecting and this may vary from dog to dog. Consequently, all dogs do not respond to the same cocaine sample. Although, the dogs have proved to be a highly useful tool in detecting illicit materials, as a tool for analytical chemistry they leave one wanting. One would never accept data from an instrument without having a solid idea of the physical mechanism behind a detection event.

Herein, we used anti-BZE (antibodies to benzoylecgonine) as our sensing layer for the detection of cocaine molecules contained in a vapor stream. The molecular structures of cocaine and benzoylecgonine are shown in Figures 4A and 4B respectively. They differ only by a methyl group that forms a methyl ester with C'12 in cocaine that is cleaved when hydrolyzed to form the acid derivative in benzoylecgonine. Researchers have analyzed the headspace vapor of various cocaine samples and have found it to contain a concentration dependent upon the vapor pressure, temperature and nature of the sample

(Lawrence 1997) [52]. However, the complete vapor composition has not been revealed and cannot consistently be agreed upon. In our work we report the detection of cocaine vapors both in our lab using an Idaho National Engineering Laboratory (INEL) vapor generator loaded with pure cocaine sample and in the GBI (Georgia Bureau of Investigation) using seized "crack" cocaine samples.

For our sensor modality, we have selected surface acoustic wave (SAW) quartz resonator devices that are designed for vapor phase detection. The mode of acoustic propagation is determined by electrode geometry and by the particular cut of crystal used. Both the acoustic velocity and attenuation are affected by the selective medium.

3.1 **Methodology**

Our approach is to construct a vapor phase biosensor by immobilizing a monolayer of antibodies onto the surface of a SAW device as is shown schematically in Figure 3.1. The device is then connected into an oscillator circuit, as shown in Figure 3.2, and frequency changes can then be precisely measured. When the antigen binds to the antibody, the acoustic velocity is altered and the oscillator frequency shifts to different value. As a control we used both anti-FITC coated and hydrogel-coated devices and compared the responses. The reason being both anti-BZE and anti-FITC monoclonal antibodies are specific for small molecules which have molecular weights in the range of 300 Daltons. In addition, the two molecules, cocaine and FITC, may possess a hydrophobic epitope. Further, to overcome the problem of dehydration of the biomolecular film we have developed a method for applying a thin hydrogel layer over

the immobilized antibodies. For our devices we have obtained sensitivities of approximately 20Hz/pg with a detection limit on the order of a few picograms

3.1.1 Antibody Immobilization

The antibody immobilization technique first requires polarizing the electrode surface. This was accomplished by immersing the SAW chip in 5ml of 1.2M HCl for 5 min then washing with deionized water, followed by 5ml of 1.2M NaOH for 5 min (according to the method developed by Davis and Leary [42]). The SAW chip was washed again with deionized water before it was immersed in 3ml of 1.2M HCl for 2 min. The chip was washed twice with deionized water followed by buffer solution and was allowed to air dry. Protein A (0.2mg) was dissolved in 100µl of buffer solution at physiological pH. Then 10µl of antibody (0.023mg/ml) was mixed with the buffered protein-A solution and the mixture was placed in a 4^{o}C refrigerator for 2 hrs. Three microliters of the cross-linker-antibody solution was used to coat the device. The chip was allowed to air dry for hour and the remaining solution was spun off for 30 sec at 5000rpm. A thin layer of hydrogel (3µl) was then applied by spinning the chip on a silicon wafer for 50 sec at 5000 rpm. We obtained both the mouse monoclonal anti-FITC antibodies and Protein A – soluble (extracellular) from Sigma Chemical Co. St. Louis, Mo. Uranine was obtained from Fluka Chemika. Mouse anti-Benzoylecgonine was purchased from Research Diagnostics INC, Flanders, NJ. This lot of antibody was found to cross-react to benzoylecgonine and cocaine. Benzoylecgonine is the major metabolite of cocaine found in the blood stream.

3.2 **Results**

As indicated previously, in order to verify vapor phase analyte binding events, we developed a fluorescent antibody/analyte assay. This was to provide a method, independent of the SAW device response, to detect the occurrence of a molecular binding event. SAW devices with and without antibody films were tested. After brief exposure to the analyte vapor, the TO-8 packaged device was pulled from the system, washed with buffer to remove unbound analyte and then viewed using a Zeiss LSM510 confocal fluorescent microscope (CLSM) located in the Institute for Bioengineering and Biosciences on Georgia Tech's campus. If fluorescence was observed in the CLSM image, this is evidence of bound fluorescent analyte (as seen in Chapter 2).

3.2.1 Device "Field" Test

Under the supervision of the Georgia Bureau of Investigations chemical analysis scientist, we investigated the headspace of a seized sample being processed using the SAW Pro as the mode of presenting the vapor to the sensor head. The sample was believed to be cocaine free-base commonly called "crack". Vapor signature analysis revealed the characteristic device response commonly encountered under laboratory conditions. As a control we used non-specific anti-FITC antibodies and observed no such response (Figure 3.3). In addition, the response was only observed when held above the sample headspace indicative of the very low vapor pressure cocaine.

3.2.2 Vapor Presentation

The INEL vapor generator is calibrated to release a specific amount of cocaine when a particular temperature, flow rate and pulse time is entered (Data available at Houston's Research Labs). Cocaine pellets housed within a separate compartment are heated at a constant temperature that corresponds to a known amount of cocaine molecules that can be manually or automatically pulsed into the clean air flow. In this case, the automated vapor-generator was programmed to deliver ~1ng of cocaine vapor to a flow cell containing four surface acoustic wave resonators in oscillating circuits. The experiments begin with a flow of clean air (180 ccm) through the flow cell while monitoring the resonant frequency of the SAW devices in their respective oscillator circuits. This allowed us to account for any response to temperature and pressure changes during presentation of the analyte gas. A five-sec pulse of cocaine is injected into air-stream and presented to the flow cell.

The important variables are flow rate (180 ± 0.3 ccm), temperature and pressure, these values are held constant regardless of the pulse. In other words, the addition of cocaine molecules to the air stream during the pulses does not modulate the flow rate or cause a significant variance in temperature and pressure values. Therefore, any frequency shift after the initial onset of airflow cannot be attributed to changes in aerial quality but is solely due to the perturbation of the device surface by the cocaine molecules mixed in the airflow, whether the shift is from the specific binding events or not. The results (shown in Figure 3.4) were compared to the data published in previous work done by Stubbs *et al*.,

[43-45] where anti-uranine antibodies were immobilized on SAW devices for the detection uranine molecules in an air stream (Figure 3.5).

3.3 Discussion

Currently, the narcotic sniffing dog remains the most accurate, reliable and widely used sensing technology in the war on drugs. However recent studies done at the Institute for Biological Detection Systems at Auburn University have shown that in the presence of extraneous odors (non-target odors) these animals show a higher propensity for so-called false alarms. For this reason there have been an increasing demand for a portable, highly specific vapor sensing device capable of distinguishing a target vapor signature in a complex odor. Here, we present the results of a series of experiments demonstrating real-time vapor phase detection of cocaine molecules. A distinctive response or signature was observed under laboratory conditions, where the cocaine vapors were presented using an INEL vapor generator and under "field" conditions facilitated by the Georgia Bureau of Investigation (GBI) Crime Lab. For these experiments the sensor component was an ST-X quartz resonator with a center frequency of approximately 250MHz. Anti-benzoylecgonine (anti-BZE) antibodies are attached to the electrodes on the device surface via a protein-A cross linker. Vapor signature analysis revealed the characteristic device response commonly encountered under laboratory conditions. As a control we used non-specific anti-FITC antibodies and observed no such response. In addition, the response was only observed when held above the sample headspace indicative of the very low vapor pressure cocaine. The characteristic response we believe is determined not only by device design but also by molecular recognition events. That is, the initial

transient observed we believe is due to mass loading and some changes in the spring constant of the biolayer. This explanation however does not explain the differences in the magnitude of response; we believe that this difference may be a function of the technique used to deliver the vapors to the sensor head. For instance, the large response was observed when we had constant air flow and cocaine was pulsed into the air stream. The constant airflow (180ccm) may have a drying effect on the gel-coating and exaggerate the mass loading effect which translate into a larger than normal transient. Evidence for this is contained in the anti-FITC response that showed a 20 fold decrease in magnitude. The gel-coated device showed a similar response to the anti-FITC-gel coated device.

We observed a large transient frequency shift accompanied by baseline shift with the anti-BZE coated sensor when sampling "crack" cocaine. After repeated experiments and the use of numerous controls we believe that we have achieved real time molecular recognition of cocaine molecules.

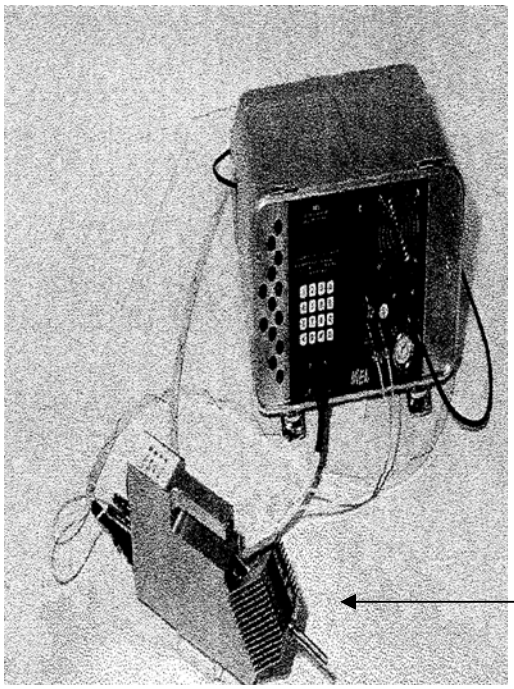

Figure 3.1 INEEL Vapor Generator for Sensor Research

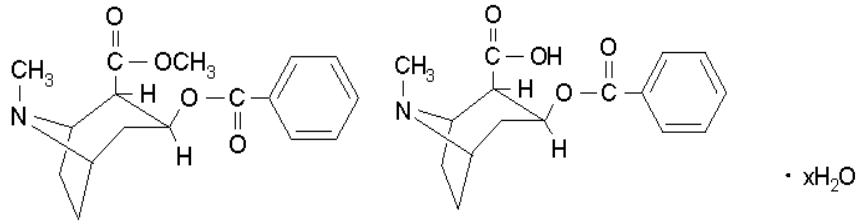

A B

Figure 3.2 (A) The structure of a cocaine molecule, (B) the structure of a benzoylecgonine molecule.

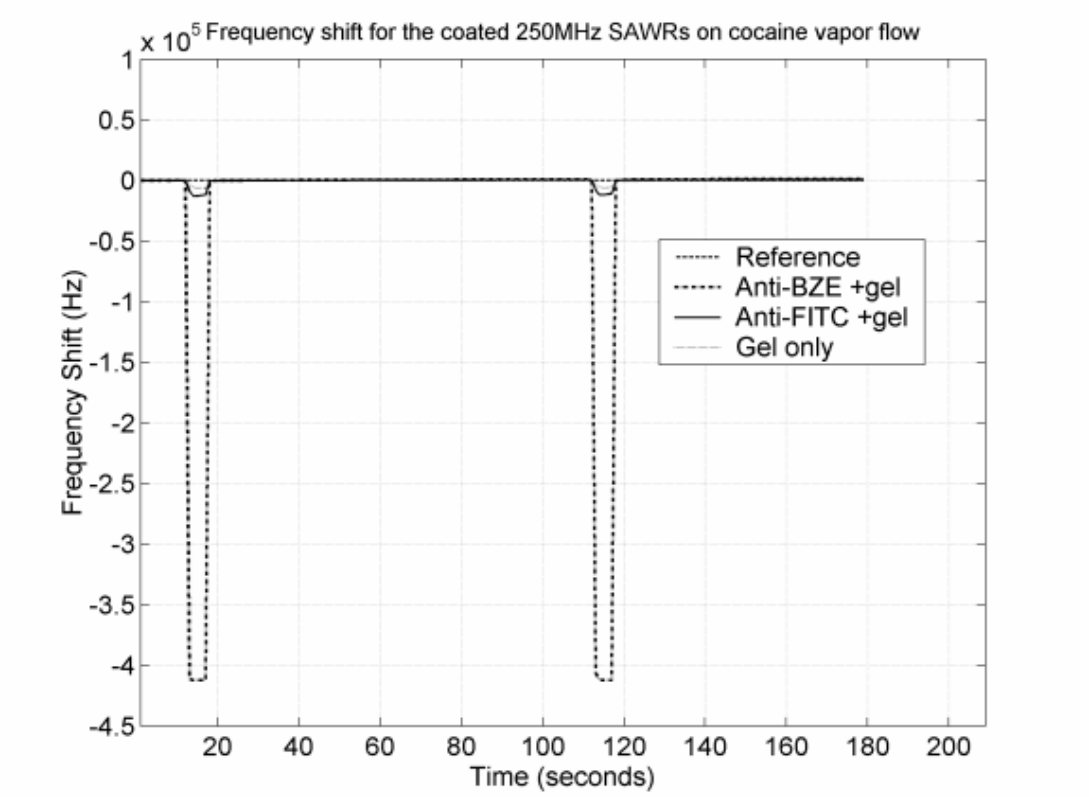

Figure 3.4 Antibody-coated and gel-coated device response to INEL cocaine vapor generator. Using a cocaine vapor generator specifically designed to release a precise amount of cocaine at a calibrated temperature and flow rate, two 5 sec pulses of a 1ng cocaine sample was presented over a 100 sec interval to the sensor head. The pulse was injected into a constant flow of 180ccm to minimize the impact associated with a sudden pressure differential. The oscillating circuit housed an anti-FITC/gel coated device, a gel only coated device, an anti-BZE/gel coated device and a reference device. As observed the response of the anti-BZE/gel coated device was far more dramatic (~40-fold differential) than the response of the other devices and that there was little or no difference between the gel-only coated device and the anti-FITC/gel coated device.

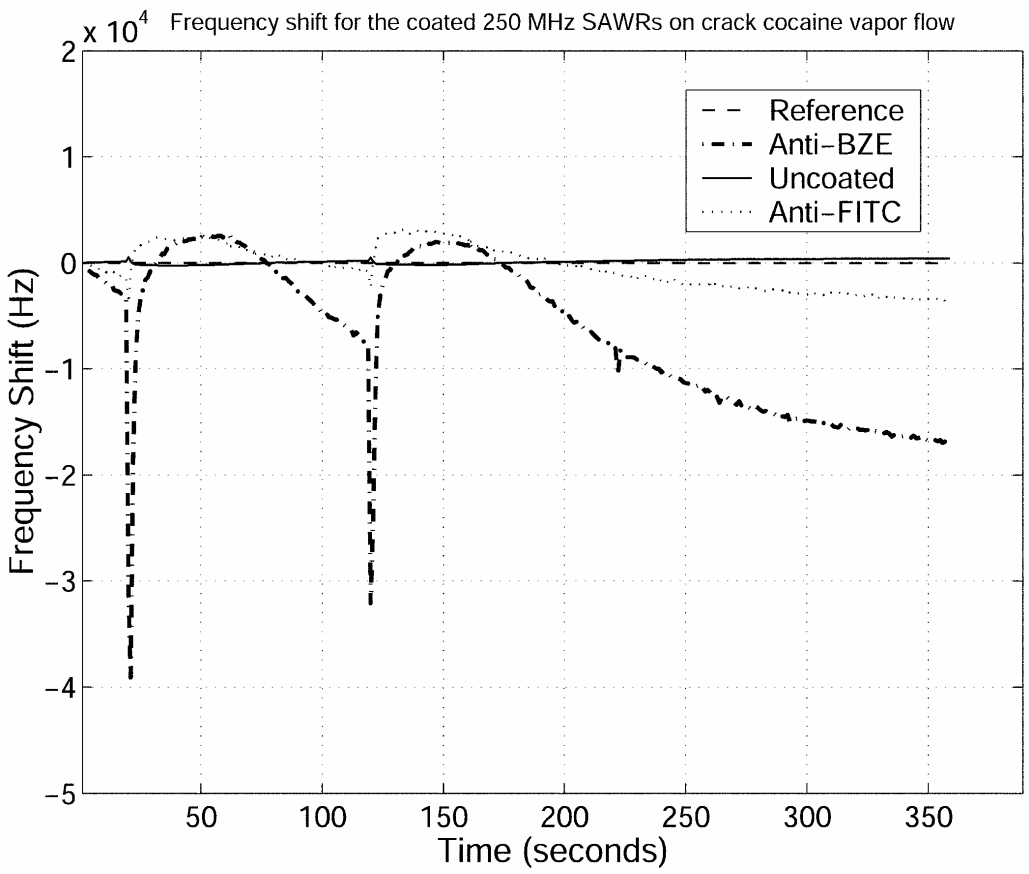

Figure 3.5. Response of anti-BZE/gel coated device during the sampling of seized "crack" cocaine at the GBI. Here the anti-BZE/gel coated device recovers to shifted baseline (~20 kHz) due to the mass loading effect. In this experiment an anti-FITC/gel coated resonator and an uncoated device were used as negative controls and displayed a relatively minimal response to the presentation of cocaine vapors. A reference device (uncoated) which was subjected to the same temperature and pressure environment as the other three resonators, was used to subtract out the effect of these fluctuation to the overall response.

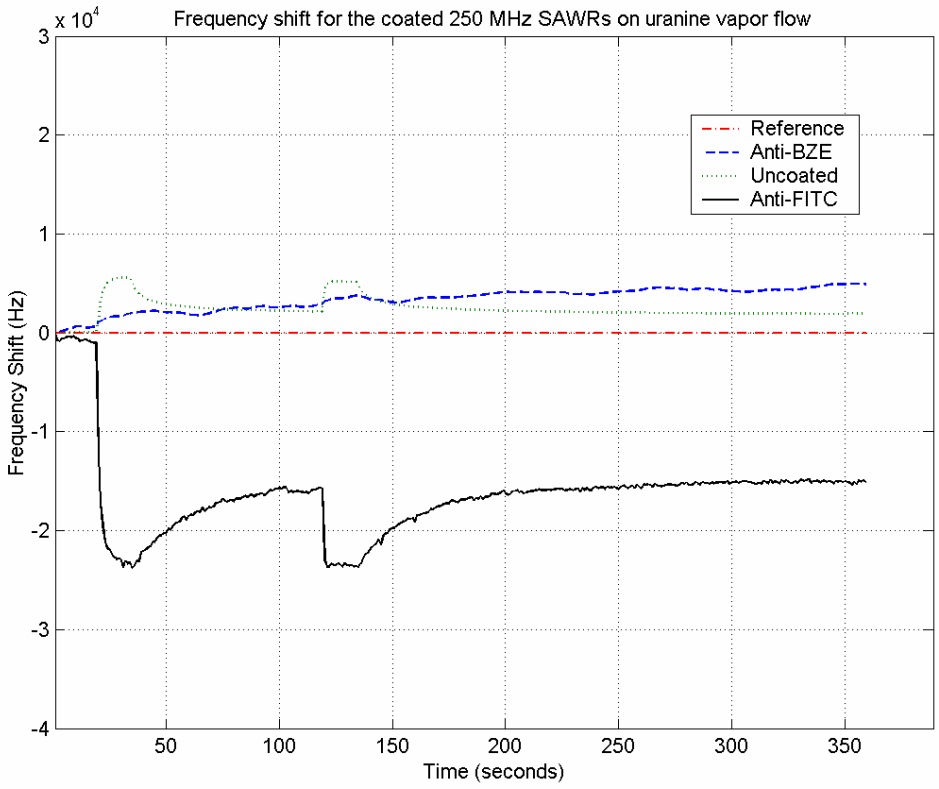

Figure 3.6 Shows the effect of uranine vapor flow on anti-BZE, anti-FITC and an uncoated device arranged in a SAW sensing array. Again for analyte presentation, N_2 (g) was bubbled through a 1nM solution of the uranine at a flow rate of 0.5 slpm (standard liters per minute). N_2 (g) flow was continuous during the experiment as analyte vapor samples were pulsed into the stream for two different 15 sec periods (25-40 sec and 125 to 140 sec)

Chapter 4: Detection of 2,4,6-Trinitrotoluene (TNT)

In previous publications, we have demonstrated the ability to detect and differentiate among analogous molecules using an acoustic immuno-assay vapor sensor appropriately called "dog-on-a-chip" [53]. This analytical tool was limited only by the availability of an antibody toward a specific small molecule; however, this issue can be addressed by exploiting the intrinsic promiscuity unique to all antibodies. The theory of antibody-antigen binding specificity was first introduced by Behring, a physicist who along with his long-time colleague Kitasato [54] won the Nobel Prize in 1901. Later that century another Nobel laureate, Karl Landsteiner [55] published the structure and mechanisms involved in antibody-antigen interactions. These works formed a classical collection of antibody-antigen binding convention, that is, the proposed precise fit model. This model has been subsequently revised following ground breaking work by Cameron and Erlanger [56] who introduced the cross reactivity phenomenon between antibodies, antigens and their structural homologues. The mechanism is said to comprise of both electrostatic and hydrophobic interactions due the preponderance of hydrophobic residues in the antigen binding site. In addition, some promiscuous antibodies can cross-react specifically with antigens that are not structural homologues through hydrogen bonding. James and Tawfik et. al. [57] concluded that promiscuous nature of antibodies suggests that each protein may have its own unique pattern of multispecificity and each activity stands alone and may be highly specific [58]. We define this pattern of promiscuous activity as a molecular signature that is unique and quantifiable. Here, we report evidence of multispecificity in an anti-TNT clone when exposed to vapors of 2,4,6-trinitrotoluene

(TNT) and Royal Demolition Explosives (RDX, hexahydro-1,3,5-trinitro-1,3,5-triazine) by introducing a novel method for the treatment of the data using communications theory to unveil the real-time dynamics of antibody/antigen interactions.

4.1 Explosives Detection

The proliferation of explosives and other warfare material during wars of the 20th century are still major sources of soil and water contamination [59]. Areas of former demolition sites, ammunition plants and artillery storage sites have long been identified as possible contamination sites due to the improper handling of explosive material [60-63]. The presence of 2,4,6-Trinitrotoluene (TNT) the main component of these products serves as an early indication of possible environmental contamination with nitroaromatic compounds. Thus the development of a rapid, inexpensive, reliable and sensitive tool to detect TNT and its explosive structural nitroaromatic analogs (Table 4.1) is of necessity.

Table 4.1 List of explosive chemical analogs detected along with their vapor pressures and chemical structures. Vapor pressure data obtained from a variety of sources including Environmental Protection Agency (EPA) Spectrum labs.

Name of Compound	Structure	Vapor Pressure (mm Hg)
1,3,5-Trinitrotoluene (TNT)	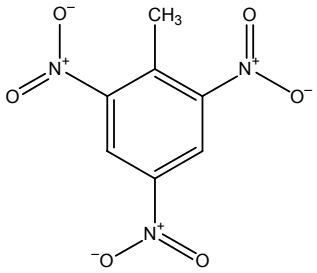	7.1×10^{-6}
(RDX- Royal Demolition eXplosive)	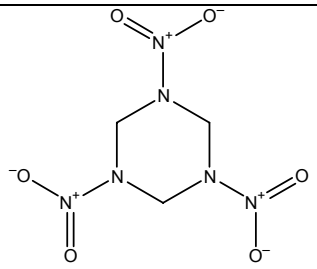	4.6×10^{-9}
4,6-Dinitro-o-cresol	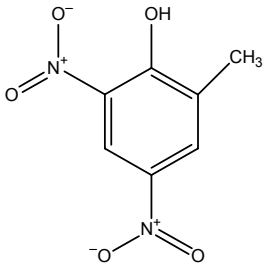	1.05×10^{-4}

Table 4.1 Cont'd

3-Nitrophenol	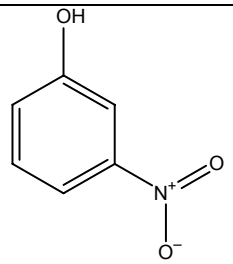	0.007
2,3-Dinitrophenol	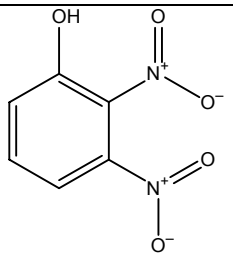	No data
2,6-Dinitrophenol	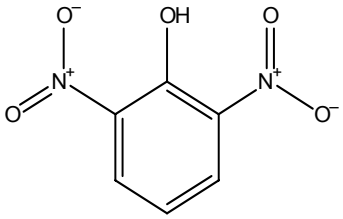	1 X 10^{-7}
3,4-Dinitrophenol	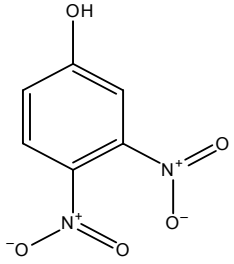	No data

Table 4.1 Cont'd

2,4-Dinitrophenol	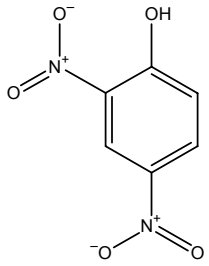	1.42 X 10^{-7}
Ammonium Nitrate	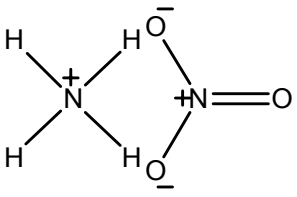	11.25
Musk Xylene (Data obtained from OSPAR Commission)	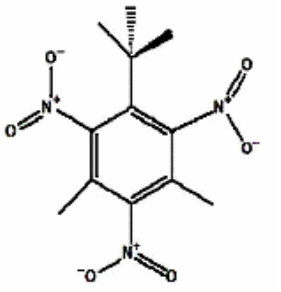	2.25 X 10^{-7}

4.2 Experiments conducted at the Transportation Security Administration Labs (Atlantic City, NJ).

Vapor sensing of explosive samples were conducted at the TSA Explosives Detection Labs. As illustrated in Figure 4.1, the targets were presented to the sensor array by use of a vapor generator and by simply sampling the headspace of an immobilized target. SAW immunosensors were prepared using protein A / antibody immobilization protocol. SAW sensors coated with anti-RDX and anti-TNT antibodies were configured in the sensing array. The results suggested that each SAW immunosensor had a unique response / signature in the presence of each chemical vapor. This behavior suggested that multi-specific nature of antibodies may be used to yield useful information about both a specific and non-specific analyte. In an attempt to elucidate this relationship we used a popular data mining technique called clustering. Clustering is a very popular and useful technique in data analysis / data mining. The analytical goal is to find clusters of samples such that observations within a cluster are more similar to each other than they are to observations in different clusters.

Here we described an array system consisting of two orthogonal bio-receptors; anti-TNT and anti-RDX. The linear relationship obtained from the frequency-time curves were plotted as a two dimensional map defined by anti-TNT (x) and anti-RDX (y). The results revealed a unique binding signature for each chemical analog. To further explore this we introduced another antibody (z) to our sensing array. This antibody, anti-dinitrophenol (anti-DNP) is believed to have some multispecific activity toward the chemical analogs. The result is a three dimensional map further defining the characteristic signature of each of the chemical analogs.

Table 4.2 Describing Data Clustering Map and Implications on Vapor Chemical Signatures

Parameters	Immunosensing Systems
Map	Frequency response data showing defining individual analyte chemical signature
Axes of the map	Three orthogonal or semi-orthogonal antibodies. Frequency information dependent on analyte binding
Data Clusters	Chemical data transformed via specificity into distinct groups of frequency change
Separation between data clusters	Degree of chemical similarity between analytes
Magnitude of data clusters within map	Dependent upon analyte characteristics such as concentration and/or vapor pressure
Antibody Selectivity	Distance between clusters. Dependent on the antibodies ability to distinguish antigenic differences (serotypes) to reject similar analytes
Antibody Sensitivity	Tight packing within clusters. Defines the ability of the system to respond to low concentrations (measured in parts per billion or trillion)
	Concentration of analyte and Δf characteristics
Cluster Overlapping	Cross-reactivity of antibodies to analytes
Binding Kinetics	Sensor's bound antigen concentration to total antibody concentration (r) to the concentration of free antigen ratio (c) ratio, r/c (Scatchard equation), dependent on analyte concentration, vapor pressure and antibody capacity.

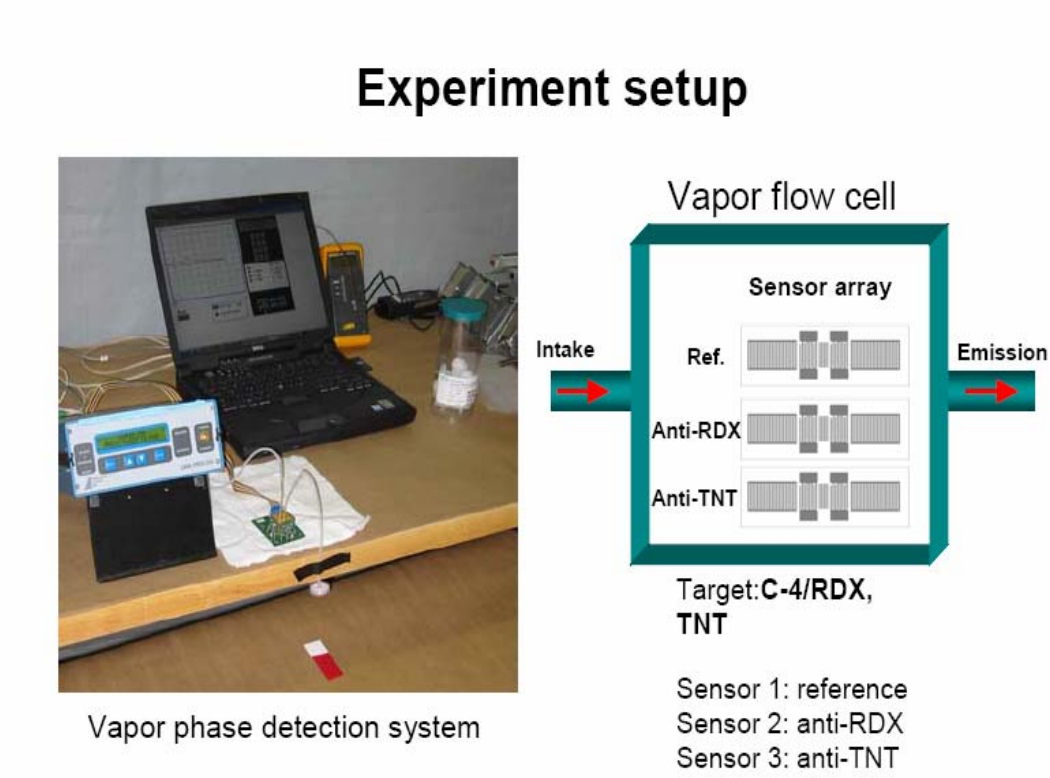

Figure 4.1 Showing Experimental Set-up and Method of Analyte Delivery.

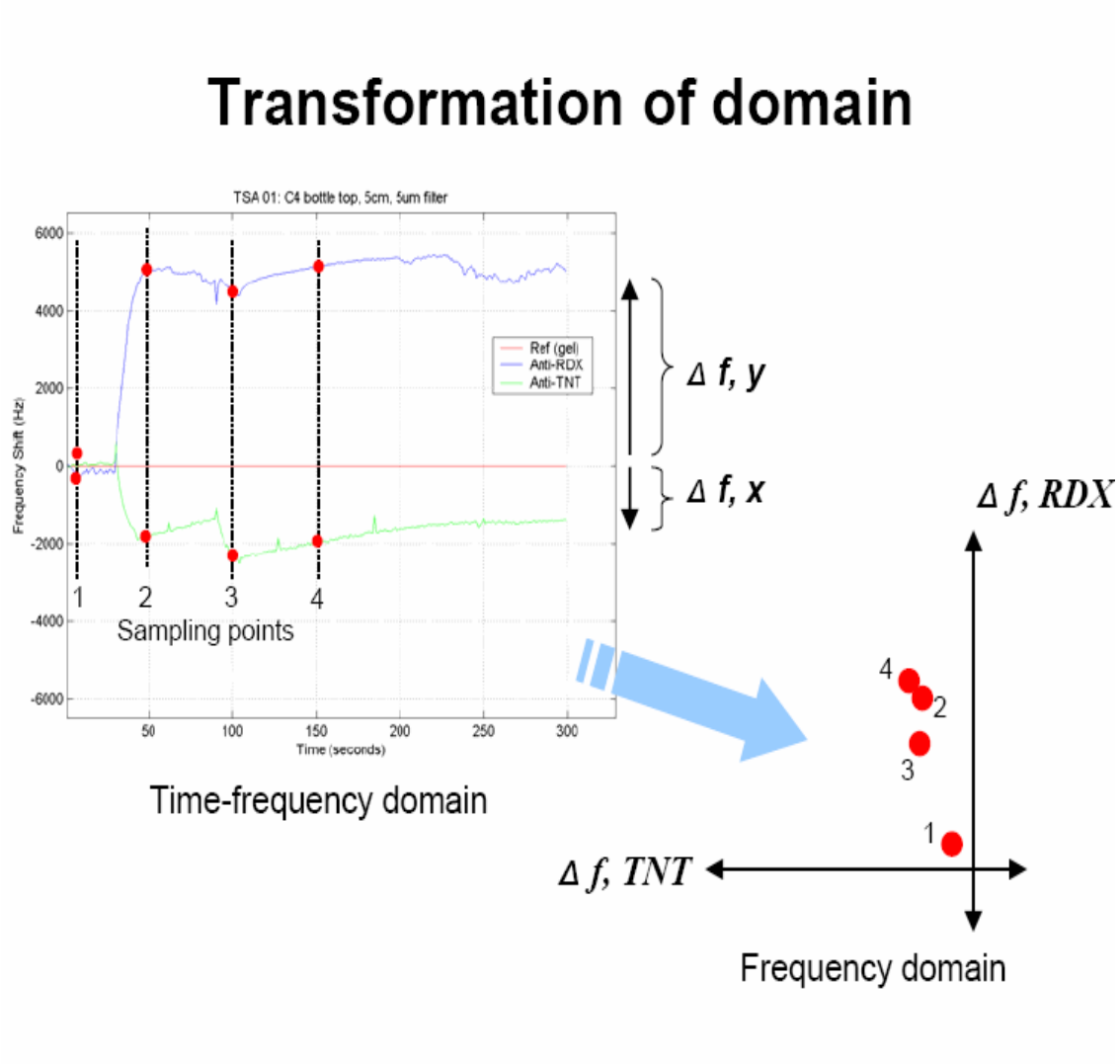

Figure 4.2 Showing How Data form F vs T Plot is Transformed into Clustering Plot

Experiments performed at the Transportation Security Administration (TSA) Atlantic City, NJ. ISO 9001:2000

Table 4.3 INEEL (VG) – Idaho National Engineering and Environmental Labs –Vapor Generator (US Government Property- (8004-85505700-00139725)

Experiment #	Chemical	Mode of Analyte Presentation
TSA 44	RDX	INEEL (VG) (50.3 pg, 3s pulse, 53 ^{0} C, 150 ccm).
TSA 43	RDX	INEEL (VG) (50.3 pg, 3s pulse, 53 ^{0} C, 150 ccm).
TSA 42	TNT	INEEL (VG) (50 pg, 0.3s pulse, 13 ^{0} C, 150 ccm).
TSA 41	Ammonium Nitrate	Head space 12’’from strip
TSA 40	Ammonium Nitrate	Head space 12’’ from strip
TSA 39	Ammonium Nitrate	Head space 12’’ from strip
TSA 01	C-4 (90% RDX, 10% Plasticized)	Head space 12’’ from strip
TSA 09	TNT	Head space 14.5’’ from strip

TSA Experiments: Nitro Group Cross-Activity

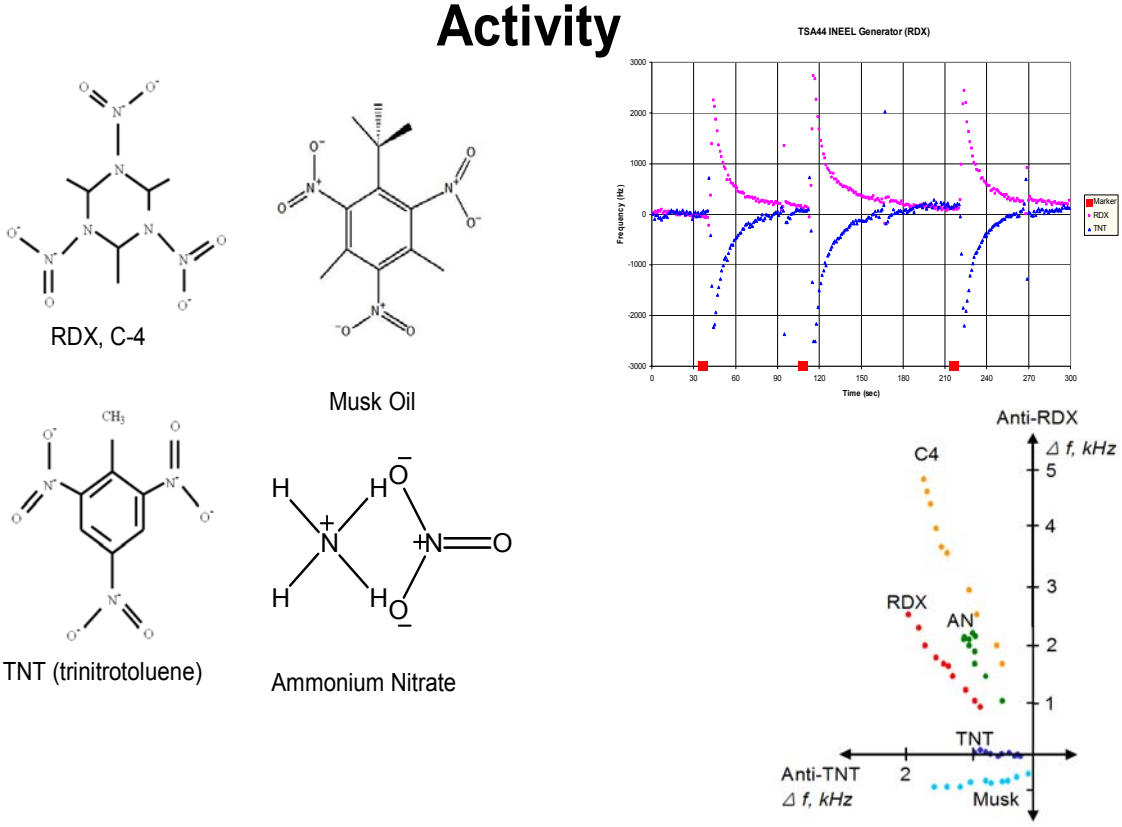

Figure 4.3 Transforming Multiple Vapor Sensing Experiments to Cluster Map

Chemometrics on TSA DATA

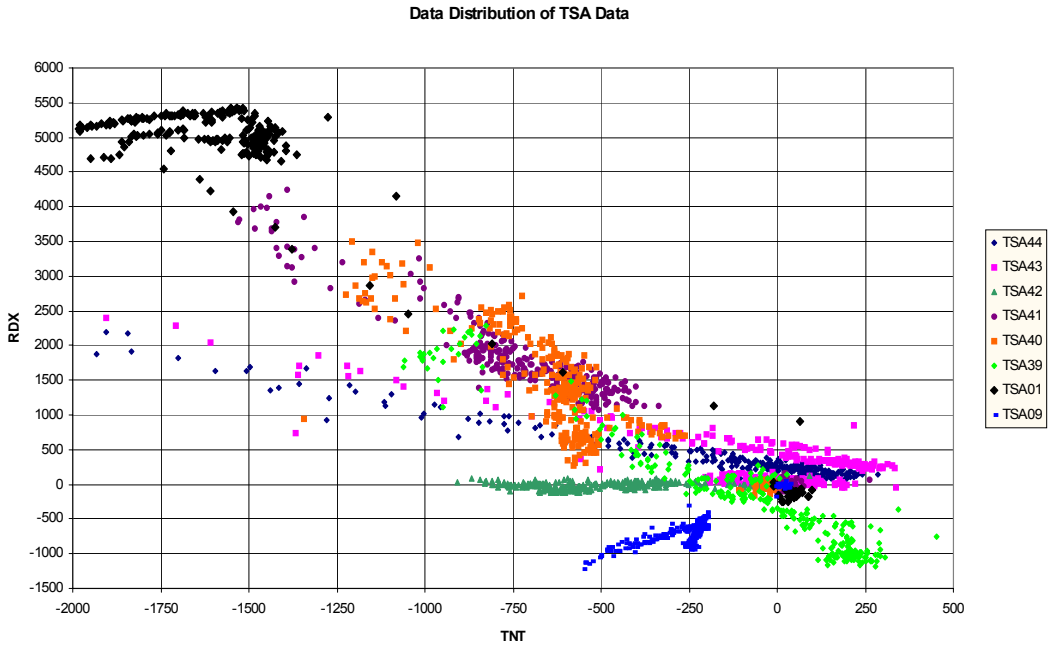

Figure 4.4 Showing Data Clustering of TSA Experiments Described in Table 4.3.

4.3 Cross-Reactivity among Monoclonal Anti-TNT Antibodies

Several studies involving immunoassays or immunosensors have been published suggested cross reactivity among anti-TNT antibodies. Zeck et. al., [64] used the same anti-TNT clone featured in this study to show cross-reactivity of anti-TNT in presence of nitroaromatic compounds. Although his work used an ELISA (Enzyme-linked Immunosorbent Assay) based assay to determine cross-reactivity data, we used it as a road map to compare and contrast data we observed during our analysis of nitrophenol analogs of TNT.

Cross Reactivity Data

Table 2 Cross-reactivities[a, b] and affinity constants K

Analyte	Cross-reactivity [%]	Cross-reactivity [%] (molar)	K ± s [L/mol]
2,4,6-Trinitrotoluene (TNT)	100	100	$(1.3 \pm 0.1) \times 10^9$
2-Bromo-4,6-dinitroaniline	37 ± 6	43 ± 7	$(5.6 \pm 0.9) \times 10^8$
2-Chloro-4,6-dinitroaniline	42 ± 12	40 ± 11	$(5.2 \pm 1.4) \times 10^8$
Tetryl	22 ± 2	28 ± 3	$(3.7 \pm 0.4) \times 10^8$
1,3,5-Trinitrobenzene	17 ± 6	16 ± 6	$(2.1 \pm 1.0) \times 10^8$
2-Amino-4,6-dinitrotoluene	6.4 ± 1.9	5.6 ± 1.6	$(7.3 \pm 2.1) \times 10^7$
2,4-Dinitroaniline	6.3 ± 1.1	5.1 ± 0.9	$(6.7 \pm 1.2) \times 10^7$
2,4-Dinitrotoluene	2.1 ± 0.4	1.7 ± 0.3	$(2.2 \pm 0.4) \times 10^7$
3,5-Dinitroaniline	1.4 ± 0.3	1.1 ± 0.2	$(1.4 \pm 0.3) \times 10^7$
2-Amino-4,6-dinitrobenzoic acid	0.83 ± 0.16	0.83 ± 0.16	$(1.1 \pm 0.3) \times 10^7$
Disperse Blue 79	0.20 ± 0.08	0.56 ± 0.23	$(7.3 \pm 3.0) \times 10^6$
1,3-Dinitrobenzene	0.45 ± 0.11	0.33 ± 0.08	$(4.3 \pm 1.0) \times 10^6$
2,6-Dinitrotoluene	0.18 ± 0.04	0.14 ± 0.03	$(1.8 \pm 0.4) \times 10^6$
4-Amino-2,6-dinitrotoluene	0.10 ± 0.03	0.09 ± 0.03	$(1.1 \pm 0.4) \times 10^6$

[a] 2,4-Dinitrophenol, 2-methyl-5-nitroaniline, 2-methyl-3-nitroaniline, 4-amino-2-nitrotoluene, hexahydro-1,3,5-trinitro-1,3,5-triazine (RDX), 1,3,5,7-tetranitro-1,3,5,7-tetraazocyclooctane (HMX), nitrobenzene, 2-nitrotoluene, 4-nitrotoluene and toluene have cross-reactivities below 0.1% [8]

[b] As the midpoint differs slightly from assay to assay, standards of TNT were included in each plate and all cross-reactivities were determined in relation to this standard curve. Therefore, the cross-reactivities should not be calculated from Table 1

Zeck et.al. Fresenius J. Anal. Chem. (1999) 364:113-120

Figure 4.5 Anti-TNT Cross-Reactivity Data from Zeck et al [64].

4.4 Experiments Conducted at Georgia Tech

Soil Samples containing TNT and several analogous compounds (nitrophenols) obtained through the EPA courtesy of Dr. Bottomley's lab group were examined using our sensing array. The experimental set-up was similar to that shown in Figure 4.1. The chemical structures of these analogs are featured in Table 4.1 along with their published vapor pressure.

Antibody Cross-reactivity: TNT Analogs

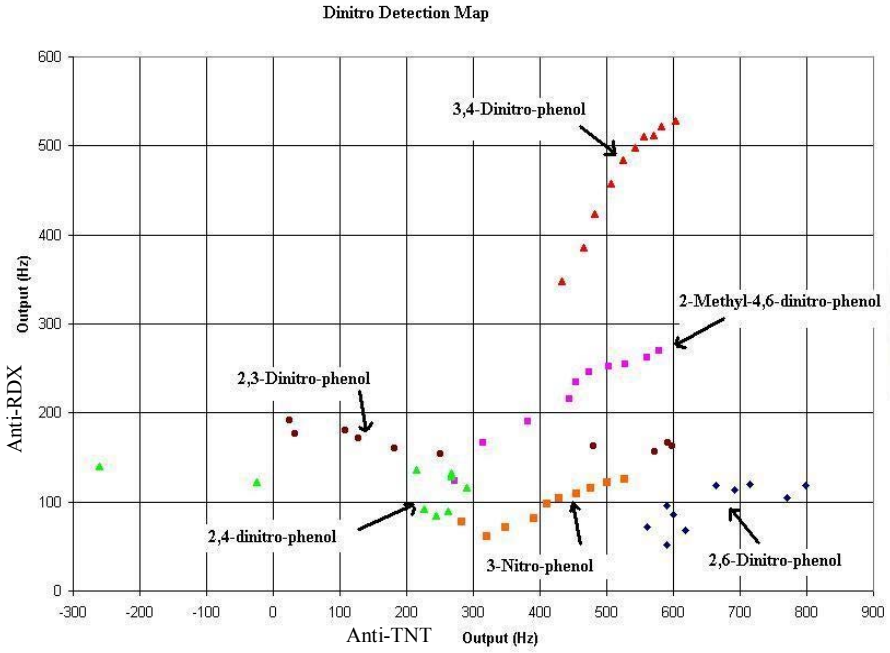

Figure 4.6 Data Clustering Map Created from TSA Experiments

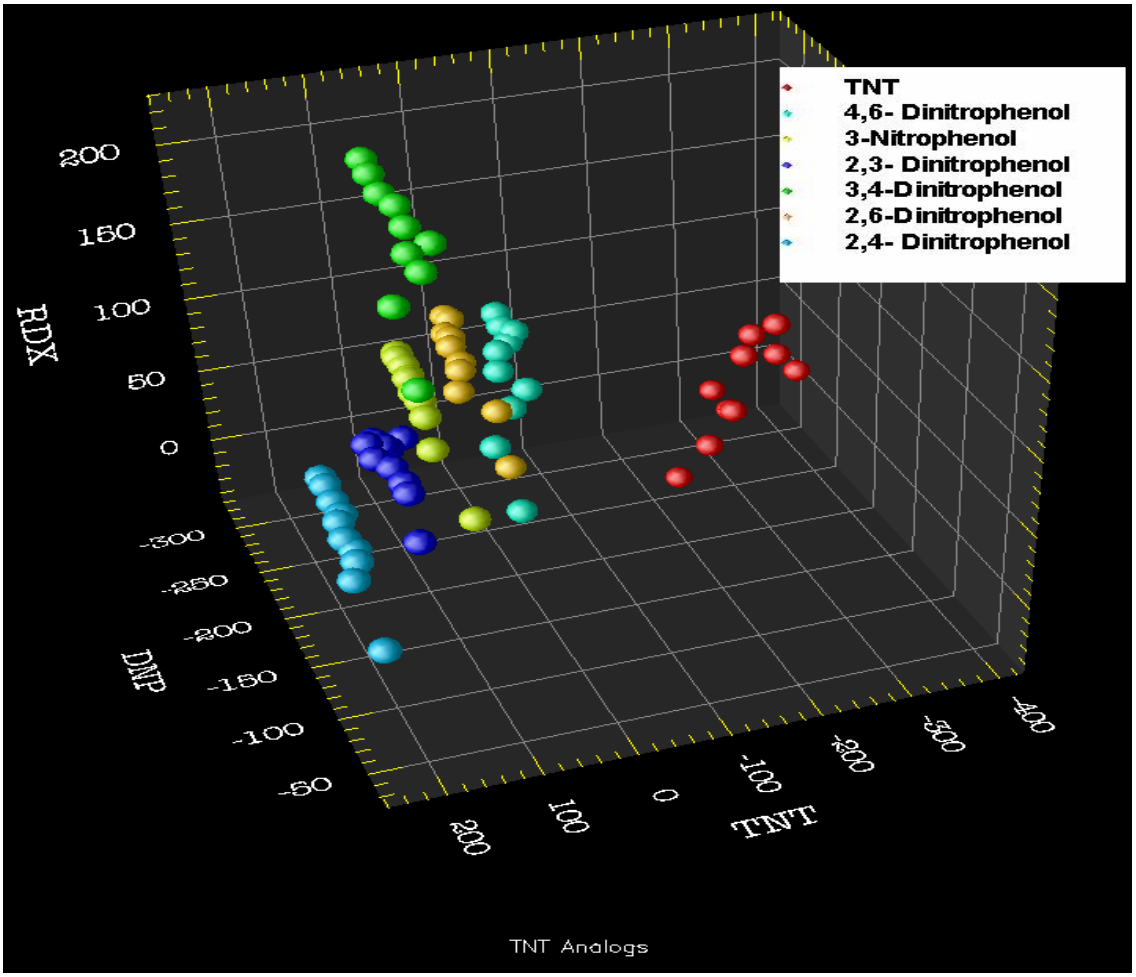

Figure 4.7 Showing the 3-Dimesional Clustering Data from Sampling the headspace of TNT Analogs.

Chapter 5: Effect of Conformational Change on QCM response: A Study of the Conversion of B-DNA to A-DNA

A landmark study done by Ian Wilson [65] revealed that biological interactions such as analyte-receptor binding events are followed by a conformation change in receptor molecule. These conformational changes have been characterized using X-ray crystallography for a series of common biological interactions such as protein-protein, antigen-antibody and DNA-analyte [66-69]. QCM biosensors are becoming an increasingly popular analytical tool for analyzing many these common biological interactions due to its high sensitivity and real-time capability. When used in this capacity, often the sensor response is treated as a measure of mass adsorption to the sensor surface. This mass loading effect occurs when the sensing molecule forms bond with the incoming analyte, and results in a decrease in the shear wave velocity and is defined using Sauerbreys' equation. The equation however, is only applicable if certain conditions are satisfied these include the presence of a uniform, thin and rigid biofilm that vibrates in phase with sensor surface. Unfortunately, the Sauerbrey model describes a static system where the sensing molecules rigidly attached to the surface and does not allow for any molecular conformational change. Molecular displacement within the biofilm can lead to changes in the mechanical stiffness of the film.

5.1 Dynamic Model

Ian Wilson, in another ground breaking study first proposed the induced fit model for antibody-antigen interaction in a 1992 article in Science [70]. Further work by Wilson revealed high order (~10-12Å) of conformational changes [71-74] during specific and non-specific antibody–antigen (specifically small molecules) interactions. In similar experiments involving larger molecules such as proteins there was very little conformational change in the antibody binding regions. The complimentary determining region heavy chain 3 (CDR H3) as part of the six hypervariable loop CDR responsible for molecular recognition, was identified as the loop motif involved in the majority of conformational changes during a binding event, although the other loops did show some changes in the range 1-2 Å. This was discovered by comparing the crystal structures of unliganded antibody structures with that of the ligand bound structure. Wilson concluded that the rotation between heavy and light chains were 15^0 - 20^0, such range of motion eliminates the argument for a lock and key mechanism that requires a more rigid model. It then follows that since biolayer rigidity is the water-mark for mass loading interpretations using Sauerbrey analysis, the antibody based sensor would require considerations of both mass loading and conformational change as part of the device response. In the case of a small molecule, the conformation change would be large when compared to the mass loading effect thus an increase in frequency, as predicted by the perturbation model presented here, would be observed. For proteins, our results suggest that any conformational change during antibody binding is negligible when compared to mass loading effect on the device, which translates, to a large decrease in the fundamental frequency. This is supported by evidence from crystallographic studies which shows

surface interactions between the CDR's of the antibody binding fragment and the surface exposed regions of the protein being the predominant binding and requires minimal antibody structural changes based on the root mean square deviation between unliganded and ligand-bound models.

Thus we hypothesize that a stiffening of the biofilm during and after the molecular molecular recognition event would give rise to an increase in resonant frequency, i.e. a positive f shift.

Hunt equation describing dynamic antibody – analyte reaction.

$$\Delta f = -\frac{f_0^2 h_f}{\pi\sqrt{\rho_q \mu_q}}\left[\Delta\rho - \frac{\Delta\mu}{V_A^2}\right] \qquad (5.1)$$

The transition of B-DNA to A-DNA was first observed by Franklin and Gosling [75]. Since then this transition has been considered as an important target for anti-cancer drugs [76]. Also has been studied by Salazar et. al [77] in relation to the duplex –duplex interactions with RNA which is necessary for transcription and is also an important drug target [78]. When canonical B-form DNA is converted through ethanol dehydration it transitions through 13 distinct conformations. Hydrated form of DNA is the B-form canonical conformation, thus when ethanol is introduced to the environment it "pulls" the water away from the DNA. The crystal structures of each form were published by Cheatham et al [79]. In ethanol solution canonical B-form DNA loses its spine of hydration in the minor groove and there is a 20 degree shift (~4Å displacement) in the

base pairs from the center of the molecule. A-form DNA despite the loss of water is still considered to in a hydrated state stabilized by extensive hydration in the minor groove and by hydrated counterion (Na) association.

The overall structure of DNA (Figure 5.1) reveals a spatial versatility inherent is in its flexible structure. The observed flexibility has lead to the discovery of a reversible structural transition, one of the first documented in a biomolecule. B-DNA the hydrated form of the molecule is characterized by its long, narrow helix with a 10.5 base pair (bp) repeat and a 3.4Å helical rise. The base pairs are stacked at the center of the helix and the molecule is stabilized by a "spine of hydration" in the minor groove. The A-form is characterized by its compact structure consisting of 11bp repeat and 2.8Å helical rise.

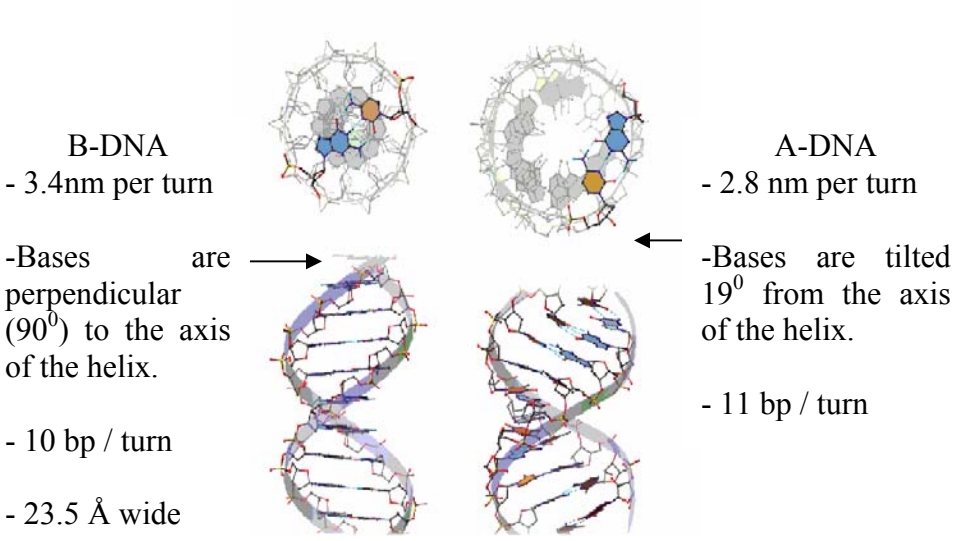

Figure 5.1 Structures of B-form and A-form DNA

5.2 Results

The conformation changes during the transition of B-DNA to A-DNA were measured using quartz crystal devices coated with duplex B-form DNA. Various control sensors were used for the experiments. Control devices were coated with alkanethiol coating, another with single strand DNA and finally a uncoated sensor was used. The controls were used to approximate the wettability of the QCM surface. It was observed that single stranded DNA did not show a consistent, repeatable behavior to the various ethanolic solutions. The uncoated sensor proved too sensitive and its response may have been affected by local cooling on the device caused by rapid evaporation of ethanol on the surface. In addition, a small difference in the response may have been a function of the wetting properties of an uncoated device when compared to the dsDNA coated device. The most consistent control was the SAMs coated device that showed a constant frequency shift (~400 Hz) upon addition of ethanol and a complete return to baseline after flushing the cell with buffer.

The addition of 50% ethanol solution to a flow cell (Figure 5.4) fitted with a SAMs coated QCM and a dsDNA coated crystal resulted in a negative frequency shift ~ -1200 Hz (Figure 5.2) in the fundamental frequency. This is consistent with studies preformed by Fang et al, in which it was shown using AFM technology that large conformation changes in B-DNA occur in ethanol concentrations < 40%. Both devices appeared to recover to baseline in presence of TE buffer which suggests a return of the B-form DNA in the case of the dsDNA coated QCM. The addition of 50% ethanolic solution to the flow cell after incubation with (0.017M) magnesium sulfate resulted in a positive frequency shift (Figure 5.3) which suggests a change in the biolayer stiffness due to

conformation accommodations during the transition from B-DNA to A-DNA. Flushing the flow cell with TE buffer led to a return the baseline frequency suggesting a conversion back to the B-form DNA. Figure 5.4 shows the observed results of a step-wise addition of increasing concentrations of ethanolic solutions to a dsDNA coated QCM. In this experiment there were no attempts to recover the A-form DNA molecule via the addition of TE buffer. Each aliquot of ethanol is allowed to incubate for min with the dsDNA coated device before addition of the next concentration. The results correlate somewhat with that of Cheatham et. al, who first suggested a number of transitional structures during the conversion of B-DNA to A-DNA. The results suggest that it's more likely that we are observing some change in the physical characteristics of the biolayer rather than a measurement of liquid viscosity.

5.2.1 Surface Preparation and DNA Immobilization

The gold surfaces of the QCM crystal were cleaned using Piranha solution (30% H_2O_2 and concentrated H_2SO_4 in 3:7 (v/v) mixture). The crystals were air-dried. 3,3'-Dithiopropionic acid (0.0234g) was dissolved in 100% ethyl alcohol to make a 0.01M alcoholic solution. The solution was applied to the QCM gold electrodes and allowed to incubate overnight. Surface was washed 95% ethanol then aliquots of deionized water before allowing to air dry. 1-Ethyl-3-(3-Dimethylamino-propyl) carbodiimide (EDC) (0.0133mg) was dissolved in 0.1ml of 1x TE buffer. NHS (0.0135g) was dissolved in 0.1ml of buffer and mixed with EDC solution and the resulting mixture was incubated with the QCM surface for 30 min. The surface was washed with deionized water and allowed to dry. Strand 1 and Strand 3 were mixed in 1:1 (v/v) ratio and hybridized by

first heating for 2 min at 95^0C and cooled to 65^0C for 10 min and allowed to incubate at room temperature for 15 min. The QCM devices were then coated with a small dilution factor of the double stranded DNA and allowed to incubate at 4^0C overnight. The crystal was washed with 1 X TE buffer and allowed to dry. The surface was washed with DNase/RNase free deionized water and allowed to air dry.

5.3 Discussion

Quartz crystal microbalance based biosensors rely on molecular recognition between the sensing molecule and the target analyte to produce a unique electronic signature. These signatures are often interpreted using Sauerbreys' equation relating the amount of bound analyte to the frequency shift. This would be sufficient if biological interactions were static, however, it is well documented that these interactions are usually dynamic in nature and require some sort of molecular conformational change in the sensing molecule. During a binding event the mechanical stiffness of the biofilm may increase and result a net frequency shift that is negative or decrease resulting in a positive net frequency shift solely due to molecular conformational changes in the biofilm. Here, we monitor a biological reaction that did not involve a mass change; that is, the conversion of B-form DNA to the A-form. This reaction is characterized by a 20^0 shift of the base pairs and an overall 4Å displacement of the DNA molecule normal to plane of the QCM surface. The data we present suggests that this conformational change lead to a decrease in the mechanical stiffness resulting in a negative net frequency shift. By designing a two-sensor system we were able to provide an adequate reference device to subtract out the affects of changes in viscosity, temperature and pressure.

The experiment describes a reversible reaction however the frequency never recovered completely to baseline, this begs the question; are we actually monitoring the B-DNA to A-DNA conversion? To address this we used magnesium salt solution a known inhibitor of this reaction and the results yielded a net frequency increase.

Magnesium counterions coordinate water with the negatively charged phosphate backbone of the DNA molecules rendering them less susceptible to dehydration by ethanolic solutions. This may result in a slight increase in the mechanical stiffness of the film. As for the fact that the device never recovers all the way to baseline, the obvious reason could that some of the DNA molecules may have become too denatured to regain its B-form conformation. Changes in mass as well stiffness account for the net frequency change. Our results suggest that conformational changes during biomolecular interactions involving receptor-ligand binding, can be significant when examining the overall QCM response and should be addressed when interpreting sensing data.

5.4 Experimental

Mixtures 20%, 30%, 40% and 50% (v/v) of 95.5% ethanol (reagent) in 1 X TE buffer were made to facilitate the conversion of B-form DNA to A-form DNA. The flow cell was fitted over two QCM devices, a reference device and a device coated with double stranded DNA. The mixtures were delivered to the flow cell via a Harvard syringe pump system. The ethanol solutions were allowed to incubate for 5min and the frequency was monitored in real-time using a Maxtek film depositing frequency monitor and the data was analyzed using an “in-house” Labview® program. The ethanol concentrations used

in this experiment were carefully chosen based on the volume of available data found previously cited works.

DNA sequence

Strand 1
5'amino- GGG CAG TCA GTG GAT CCC AGT CAG TCC CGG GCA GTC AGT GAA TTC CAG TCA GGC GGC CGC-3'

Strand 3
5' fluorescein - GCG GCC GCC TGA CTG GAA TTC ACT GAC TGC CCG GGA CTG ACT GGG ATC CAC TGA CTG CCC-3'

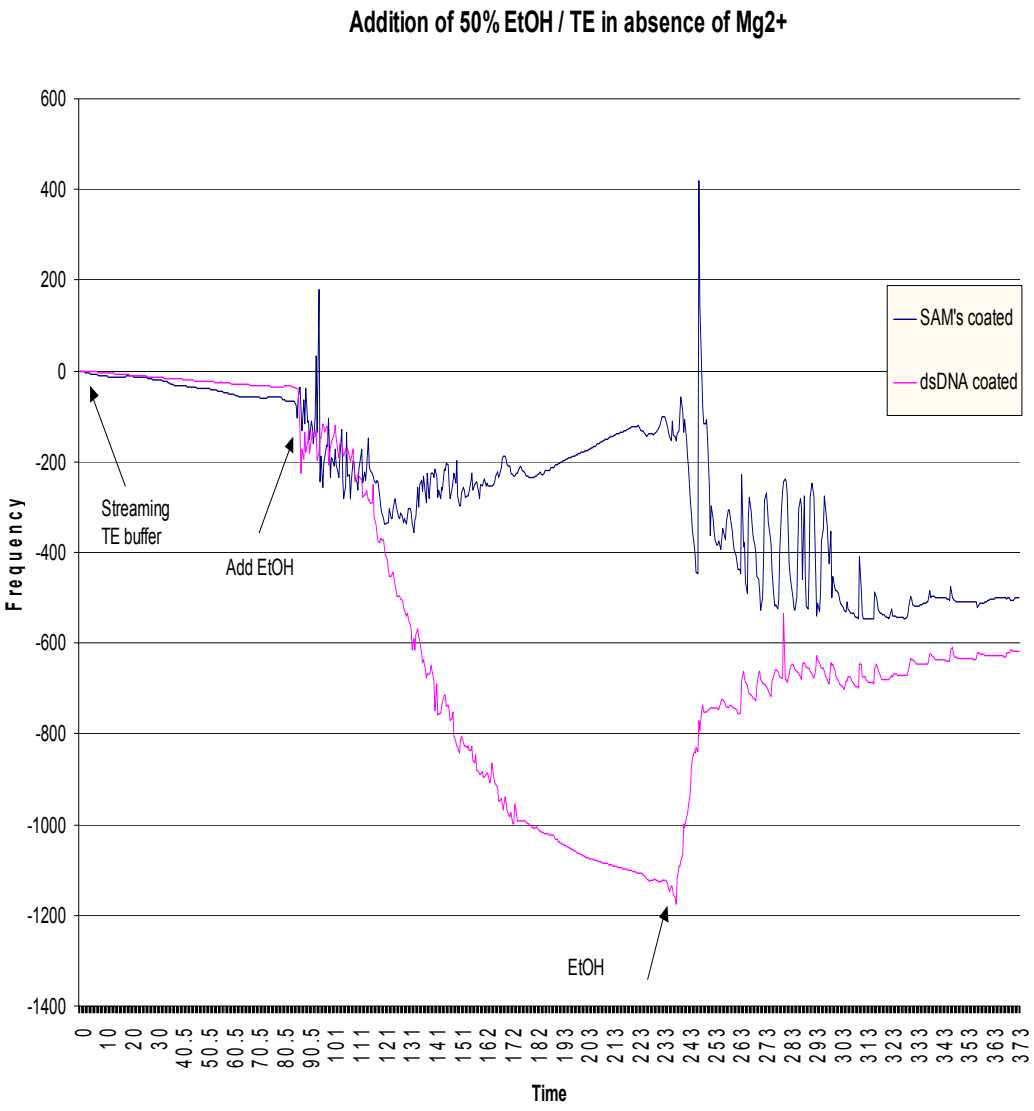

Figure 5.2 Plot Showing B-DNA –A-DNA Conversion.

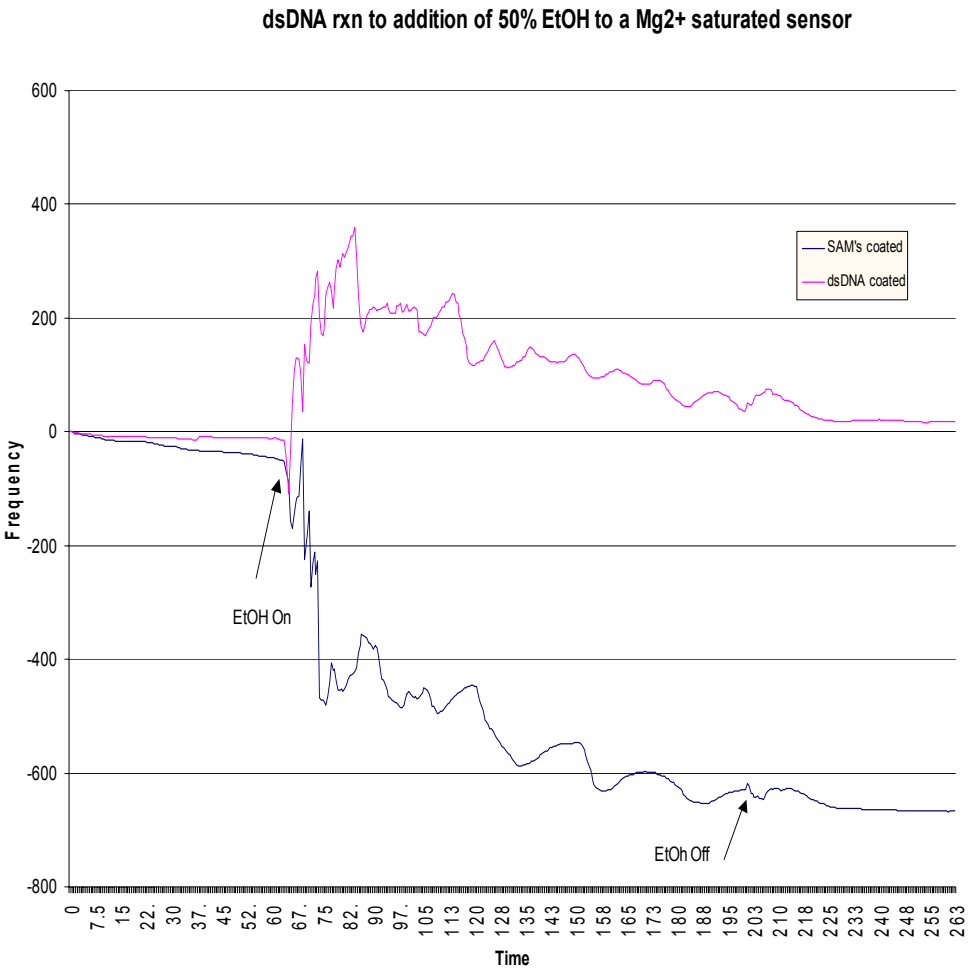

Figure 5.3 Showing Magnesium counterions Effect on B-DNA –A-DNA Conversion.

Figure 5.4 Showing Response to an Increasing Concentration of Ethanolic Solutions

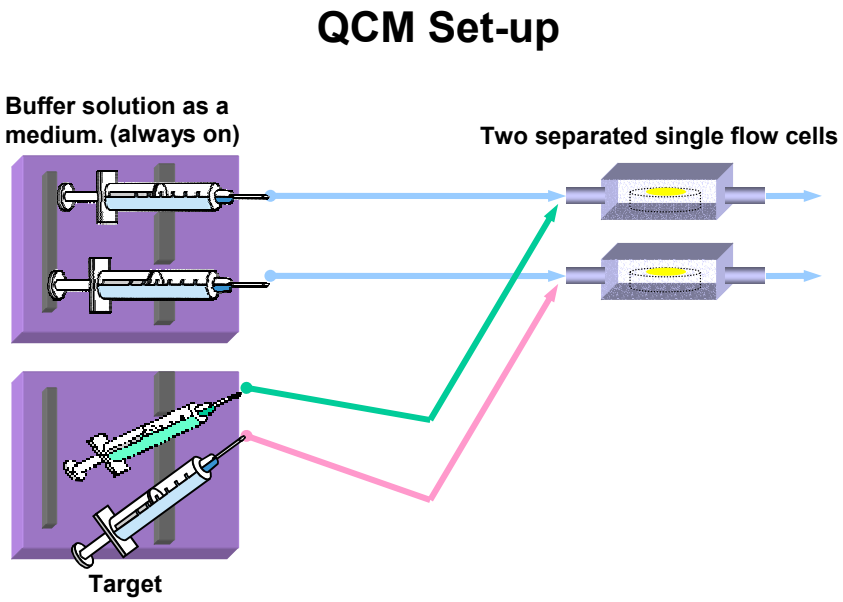

Figure 5.5 QCM Experimental Set-up

5.5 Stiffness Calculations

The following is an attempt to quantify the amount of stiffness change during the transition of B-DNA to A-DNA using stiffness complexes involved in crystallographic structures. The model is inherently flawed based on the vast differences between biomolecules and crystal lattices; however it does provide valuable insight relevant to changes in molecular structure affecting its intrinsic stiffness modulus. Consider the example of silicon and gallium arsenide, silicon has a unit cell dimension of 5.43Å and a stiffness constant (C_{44}) of 7.956 x10^{10} N/m^2, gallium arsenide has a unit cell dimension of 5.65Å and a stiffness constant (C_{44}) of 5.94 x10^{10} N/m^2 [3]. Despite the fact that the net displacement between molecules is only 0.22Å the overall stress change is ~2 N/m^2. This maybe significant since the current data measuring molecular displacement during biomolecular interactions are reported to be between ~4Å and 6Å may result in a 20-fold increase in mechanical stress. Changes in the films mechanical stress can lead to perturbation of the shear wave particle displacement resulting in a frequency shift. Recently we published a more dynamic model that accounts for the inherent flexibility of biomolecules and the conformational changes they undergo during biological interactions. The Hunt model uses a modified Sauerbrey equation to describe the affect of changes in the mechanical stiffness in the biofilm during a molecular recognition event.

Using a stiffness constant (C_{44}) of 7.82 x10^{10} N/m^2 based on a shifted resonance frequency for a coated QCM, we were able to estimate the expected amount of frequency change per Newton-area. For our sensor a stiffness sensitivity of 1.28 x 10^{-5} Hz-cm^2/N allows us to calculate an expected frequency shift assuming 100% DNA coverage of 11,674 Hz decrease. The frequency change observed when B-DNA is converted to A-

DNA was approximately 10 fold less than that of the calculated value can be easily explained when considering the fact that it is impossible to achieve 100% surface coverage of DNA molecules. This mainly due to the structural characteristics of the molecule, that is, the negatively charge phosphate backbone of the helical molecule dictates a spatial requirement due to charge-charge repulsion.

Table 5.1 Showing stiffness calculation for DNA coated QCM

C_{44} for coated QCM	7.82×10^{10} N/m^2
Area of QCM electrode	2.28×10^{-5} m^2
Amount of DNA molecules immobilized (assuming 100% coverage)	2.28×10^{12}
Estimate of stiffness change per molecule based on a 4Å displacement	40 N/ m^2

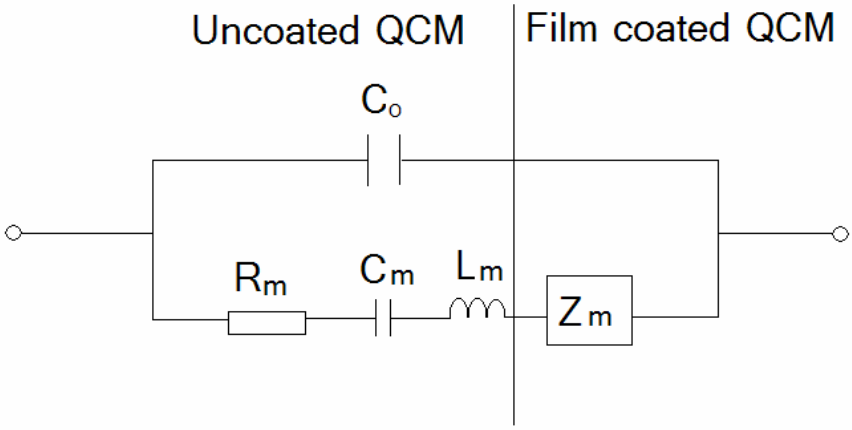

where: Z_m motional impedance
C motional capacitance
L motional inductance

Motional impedance at resonance frequency approximates 0

$$Z_m = \mathrm{Re} + \frac{1}{j\omega C} + j\omega L \qquad (5.2)$$

$$Z_m = \frac{1}{j\omega C} + j\omega L = 0 \qquad (5.3)$$

$$\omega = 2\pi f_0 \qquad (5.4)$$

$$f_0 = \frac{1}{2\pi (L \bullet C)^{1/2}} \qquad (5.5)$$

When a mass layer is applied to one side of a thickness shear mode resonator such as a QCM, the electrical characteristics are changed. Figures 5.4 & 5.5 shows the effect of mass loading on QCM impedance operated near resonance. It is apparent that the major effect of the mass layer is to translate the impedance curves toward a lower frequency without affecting the impedance magnitude. This behavior holds true as long the mass

layer/film is firmly attached to the device surface such that it moves synchronously with the resonator surface. Thus for the linear frequency-to-mass relationship established in the Sauerbrey equation to be valid, there must be a thin, homogeneous, rigid film attached to the sensor surface, otherwise viscoelastic changes will occur and contribute to the frequency shift leading to erroneous interpretation of the mass.

An impedance analysis of a coated QCM resonator can elucidate the dynamic behavior of the film's shear displacement versus the position across the film thickness by measuring the acoustic phase (impedance) Φ across the film [80-84]. If the film is sufficiently thin and/or rigid so that $\Phi << \pi/2$, then the entire film tends to move synchronously with the resonator surface. In this case particle displacement (surface motion) is uniform across the thickness of the film and a negligible strain occurs in the film. This because elastic energy stored in the film and the power dissipated remain negligible when $\Phi << \pi/2$. This is referred to as the microbalance regime of operation, where changes in resonant frequency can be monitored to indicate accumulated mass/area on the QCM surface.

If the film coating is compliant, resulting in an appreciable phase shift Φ through the thickness of the film, the upper regions of the film tend to lag behind the driven resonator/film interface. Significant shear deformation is induced in the film causing elastic energy to be stored and dissipated. In this regime, the film displacement is not synchronous with the driving resonator surface, but varies across the film thickness. In this case the resonator no longer functions as a simple microbalance, but the resonant frequency and damping depend upon film thickness, density, and shear elastic properties.

For $\Phi < \pi/2$, displacement at the upper surface of the film exceeds that at the resonator surface (i.e. overshoots occurs), but remains essentially in-phase with the driving surface displacement. In this case, the frequency is lower than for the uncoated sensor. For Φ near $\pi/2$, film resonance occurs and the interaction between the resonator and film exhibits characteristics of coupled resonant systems, displacement in the film-resonator system exhibits in-phase and out-of-phase modes, with a concurrent splitting of resonant frequency into two corresponding branches [84-87]. For $\Phi = \pi/2$, the upper film surface is 180^0 out of phase and frequency is higher than for the uncoated device. In addition, the system is highly damped in the vicinity of resonance making sensor operation more difficult.

The modified lumped-element (Butterworth-Van Dyke or BVD) electrical equivalent circuit consists of a static capacitance in parallel with a motional branch. The static capacitance results from the physical capacitance of parallel electrodes on both faces of the quartz crystal and parasitic capacitances arising from the connectors at 10 MHz. The motional branch consists of a series RLC circuit where C represents the quartz compliance, L and R are the sum of the respective inductance and resistance due to the bare quartz and the visco-elastic load (film and liquid overlayer). The motional resistance in the BVD electrical equivalent model measures the viscous losses arising from the damping of the acoustic wave as it penetrates through the biolayer [88].

The contribution of acoustic impedance of the film to the overall quartz impedance is given by $Z_f = R_f + X_{Lf}$ where R_f represents the power dissipation and $X_{Lf} = j\omega L_f$ represents the kinetic energy storage in the viscoelastic load with $\omega = 2\pi f_s$ [3].

If the quartz impedance is much larger than the surface impedance , Z_s , due to the viscoelastic film and the liquid overlayer, $Z_Q >> Z_s$, a lumped – element BVD equivalent circuit can be used as a valid approximation to describe the QCM behavior near resonance, and both the quartz crystal and the surface impedance can be regarded as additive.

The properties of a viscoelastic film subject to a sinusoidal perturbation in the acoustic frequencies can be described by its shear modulus [3]:

$G = G' + jG''$ (5.6)

Where the real part, G' is the shear storage modulus that describes the energy stored in each sinusoidal cycle and the imaginary component, G", describes the energy losses in the viscous medium.

Granstaff and Martin were first to publish relating the quartz crystal impedance components R_f and X_{Lf} to the viscoelastic modulus, density and thickness of the surface film:

$$Z_s = \frac{2\omega L_Q}{\pi(\mu_Q \rho_Q)^{1/2}} \frac{Z_f^* \tanh(k_f d_f) + Z_1^* \tanh(k_1 d_1)}{1 + \frac{Z_1^*}{Z_f^*} \tanh(k_f d_f) \tanh(k_1 d_1)} \qquad (5.7)$$

where $\mu_Q = 2.957 \times 10^{10}$ Nm^{-2} is the elastic constant for piezoelectrically stiffened quartz, ρ_Q = 2650 Kg m^{-3} is the density of the quartz and $L_Q \sim 7.5mH$ is the equivalent inductance of the bare quartz crystal. The characteristic impedance of each layer is Z^* =

$(\rho G)^{1/2}$, $k = j\omega (\rho/G)^{1/2}$ is the wave propagation constant and d is the thickness of the layer of density, ρ . Subscripts l and f stands for liquid and film respectively.

An ideal mass layer is assumed to have an infinitesimal thickness yet contribute a finite areal mass density to the device surface. Earlier it was noted that this criterion holds as long as the acoustic phase shift across the film, Φ is small compared with π. The equivalent circuit model for the mass-loaded resonator can be determined from the surface mechanical impedance Z_s contributed by a surface perturbation The surface stress required to sinusoidally accelerate a mass layer is

$$T_{xy} = \rho_s \upsilon_{x0} = j\omega \rho_s \upsilon_{x0} \qquad (5.8)$$

ρ_s is the areal mass density ($\rho_s = \rho h$ where ρ and h are film density and thickness) contributed by the mass layer, and υ_{x0} is the surface particle velocity.

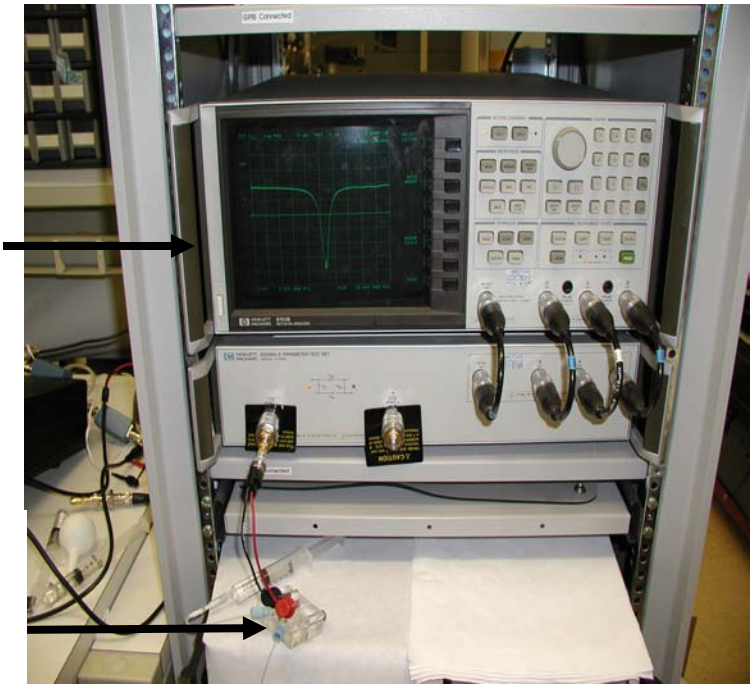

Figure 5.6 Experimental Set-up for Impedance Investigation

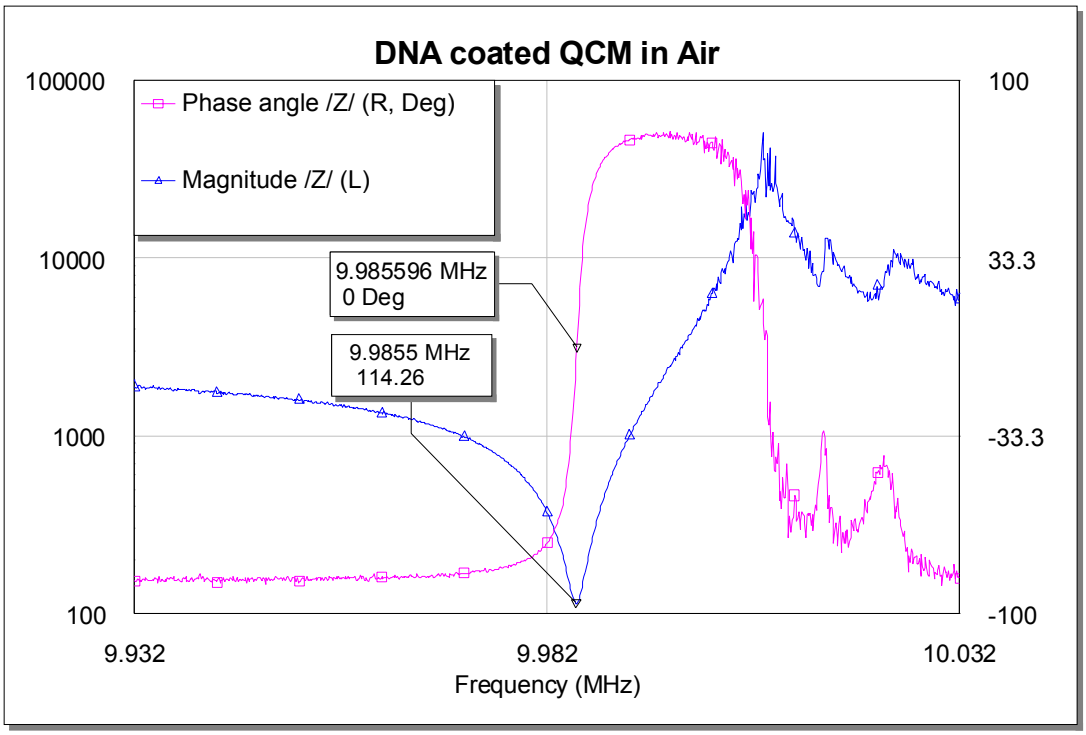

Figure 5.7 Showing Impedance Plot of DNA coated QCM

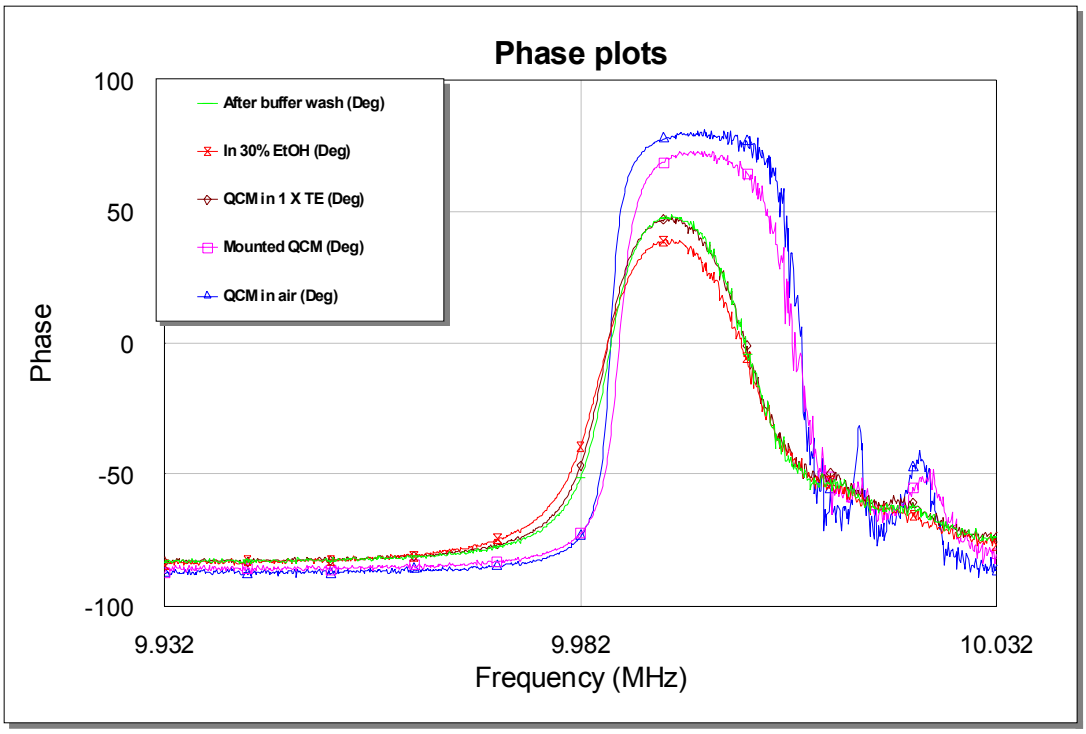

Figure 5.8 Plot of Impedance Phase during DNA Experiment

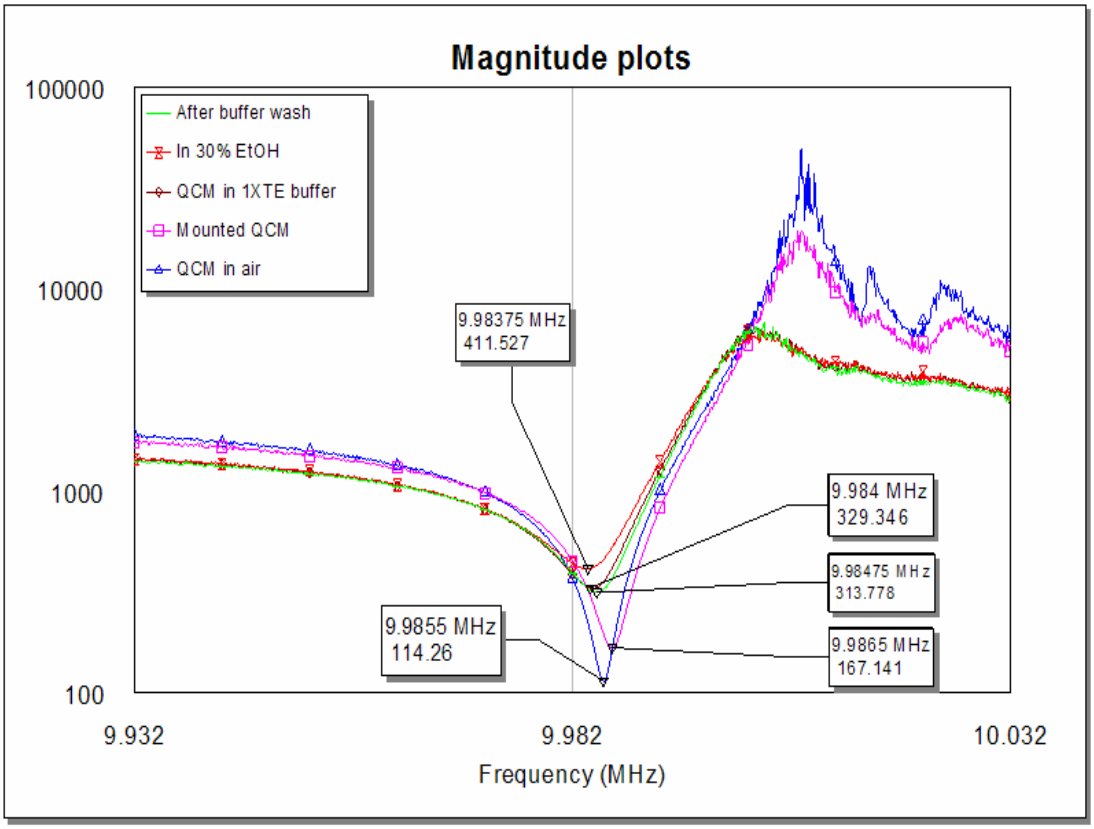

Figure 5.9 Plot of Impedance Magnitude during DNA Conversion Experiment.

Appendix A

The Role of Sensing Technology in Homeland Defense : A Policy Study Conducted under the Supervision of the Sam Nunn Fellowship Program

By Desmond D. Stubbs

Presented at the Sam Nunn Policy Forum

Georgia Institute of Technology Hotel

Atlanta, GA

April, 2005

Introduction

Since the end of the Cold War the United States has emerged as the world's only remaining Superpower. The events on September 11th 2001 define the new security challenges Americans face in the 21st century, that is, the threat of terrorism. The unconventional nature of this type of threat has revealed a critical deficiency in our security infrastructure that is being exploited by the terrorists. This vulnerability stems from the lack of effective countermeasures technology. History supports the fact that a vast infusion of technology during times of conflict usually yields the preferred result, a swift and less costly (in lives and money) end to that conflict. In this paper, we present our policy recommendations that call for a vast infusion of new technology to embolden our countermeasures efforts both home and abroad.

Providing adequate security for the homeland is a complex and massive task by any measure. Contributing to the complexity of this issue was the fact that, prior to the signing of the Homeland Security Act (2002), the functions that are considered under the banner of "homeland security" were spread throughout the federal government. To bring all of these related agencies (twenty-two in all) under one command, the Bush Administration established the Department of Homeland Security (DHS). This was a major accomplishment in the effort to make America safer. To ease the transition, many of the functions of those agencies remained the same; however, the homeland security aspects of their mission became top priority. The general mission of DHS is to prevent and deter terrorist attacks. Its' mandate aimed to harness the nation's scientific and technological resources to provide Federal, state, and local officials with the technology and capabilities to protect the homeland [89,90].

An important area of focus for the Department is catastrophic terrorism; threats to the security of our homeland that could result in large-scale loss of life and major economic impact. To address this issue the Department has made substantial investments in research designed to counter threats to the homeland, both by evolutionary improvements to current capabilities and by technology innovation [91].

In November 2004, the Bush administration announced the budget for the Department of Homeland Security FY2005 of $40.2 billion. The budget earmarked $5.3 billion for the Transportation Security Administration (TSA) to improve the quality and efficiency of screening operations. The TSA budget included a $900 million allotment for Science and Technology. These funds were designated for research, development and deployment of innovative technologies including those proposed by universities, national labs, not-for-profit organizations and private companies:

- $484 million for development of nuclear, chemical, biological, and high explosives countermeasures [92];
- $80 million for the rapid development and prototyping of homeland security technologies;
- $60 million for research, development and testing of antimissile devices for commercial aircraft;
- $40 million to deploy sensors to detect aerosolized bio-threats in large metropolitan areas; and
- $35 million for university-based centers of excellence.

Our efforts to secure the homeland are not as isolated as it may appear on the surface. The Honorable Cresencio Arcos wrote "No one country can be truly safe without the cooperation and like-minded commitment of others. We understand that we have to take actions far away from our shores and borders in order to ensure that the systems that connect us with the rest of the globe cannot be used by terrorists to travel to the United States or to transport the instruments of terrorism. The interconnectedness of the world today spans many sectors--political, military, economic, educational, and even homeland security" (-*The Role of the Department of Homeland Security Overseas*).

Current Detection Technology

I. Congressional Mandate

In an attempt to address airport security concerns stemming from the events on 9-11, Congress hastily directed the Federal government to screen all checked baggage for explosives prior to being loaded on to a commercial passenger aircraft by December 31, 2002. Four years later only a handful of airports are in full compliance with the mandate, with others citing lack of funding and unrealistic compliance dates as reasons for non-compliance. Many have taken advantage of a loop-hole known as LOI (letter of intent) to circumvent the law. A letter of Intent (LOI) is a promissory note negotiated between the TSA and airport executives. These notes allowed airports to meet the mandated security requirements with the promise of reimbursement from the federal government. Congress's mandate has been extremely ineffective because it never considered the

availability of these detection systems, the cost for installation, or even the compatibility with current airport systems.

In an effort to meet the explosive detection deadline, the Transportation Security Administration (TSA) deployed 1,390 Explosive Detection Systems (EDS) and 7601 Explosive Trace Detection Systems (ETD) to the check-in areas of 449 commercial service airports across the country. Critics, both inside and outside of Washington, contend that these machines have crowded airport lobbies and created safety and security concerns, decreased system efficiency, and unnecessarily increased TSA staffing requirements [93].

II. Explosives Detection Systems

TSA uses two types of devices to screen checked baggage for explosives: explosive trace detection machines (ETD) and explosive detection systems (EDS). Both types of technologies have limitations that create operational inefficiency and require additional backup screening methods.

ETD machines are roughly the same size as a common laser printer and cost only a few thousand dollars. ETD machines can detect minute traces of explosive residue, which may have been transferred to baggage surfaces through direct or indirect contact. While the ETD machines themselves have extremely high detection rates and very low false-positive rates, the process for collecting trace samples is slow, very labor intensive, and highly susceptible to human error. ETD machines work best as a primary means of explosive detection at low-throughput airports. However, to meet the baggage screening deadline, TSA deployed ETD machines extensively.

In contrast, EDS machines can be as large as a family minivan, weigh up to 17,000 pounds and cost over $1 million each. EDS machines can be highly automated and networked and can scan several hundred bags an hrs. They use computer tomography (CT) to scan objects and compare their density to the density of known explosives. Unfortunately, many common objects have densities similar to commercial and military grade explosives, which result in a high number of false alarms. EDS machines can also have higher false-negative rates since they require the presence of a sufficiently large mass of explosive to function correctly.

To accommodate the size and weight of the EDS machines, most airport terminals require significant modification prior to installation. There are currently only two certified manufacturers of EDS machines that have received Federal Aviation Administration (FAA) and TSA certification-- L-3 Communications Corporation and InVision Technology, Inc. To date, TSA has purchased 909 InVision CTX machines and 507 L-3 eXaminer EDX 6000 machines. Recently TSA announced the certification of a third vendor, Reveal CT-80 a promising new EDS that is being tested in a few airports.

Detection dogs

The highly specific and complex nature of olfactory sensing systems has lead to the emergence of the electronic nose. These devices are currently being used in biotechnology, food industry, medicine, environment and most recently law enforcement. Efforts continue in the search for technologies that can provide an alternative to dogs as detectors of narcotics and explosives. Among these reasons are the expenses of training and care for the dogs and handlers. Further, it is still unclear as to what the dogs are

actually detecting and this may vary from dog to dog Consequently, all dogs do not respond to the same explosives sample. That is, there is an inherent false positive rate (Institute of Biological Detection Systems, Auburn University) due to odors that have similar aromas, which could have some legal implication in the area of legal searches by law enforcement officials. Although, the dogs have proved to be a highly useful tool in detecting illicit materials, as a tool for analytical chemistry they leave one wanting. One would never accept data from an instrument without having a solid idea of the physical mechanism behind the detection event.

Integrate Inline EDS

The airport community has lobbied TSA to move the EDS equipment out of airport lobbies and integrate them into the airports' automated baggage systems. Both InVision and L3 produce versions of their EDS machines that can be integrated inline and can be configured to have higher explosive detection capabilities, on-screen alarm resolution, better false-positive rates, fewer staffing requirements, lower maintenance costs, and less out-of-service time.

To date, eight airports (Boston, Boise, Manchester, Jacksonville, Lexington (KY), Orange County, Tulsa and Tampa) have converted to full in-line EDS systems. San Francisco has partially converted its system and has received funding to complete the remainder of the airport. Eight airports (Denver, Dallas Fort Worth, Las Vegas, Los Angeles/Ontario, Seattle-Tacoma, Atlanta and Phoenix) have signed letters of intent with TSA to fund inline installation and have facility modifications underway. Twelve more

(Orlando, Houston, O'Hare, Ft. Myers, Spokane, Baltimore, Harrisburg, Philadelphia, Pittsburgh, Okaloosa (FL), El Paso and Miami) have approved plans and are awaiting Federal funding.

Letters of Intent, LOIs

Initially, Congress intended for TSA to use the LOI program to leverage limited Federal funds by stretching out debt payments to 5 to 10 years. However, to date, the Administration has chosen to treat the LOI program as grant-reimbursement program, reimbursing airports for expenses as they are incurred. Thus the program is currently being used as a loophole by the Airport executives to avoid the mandate passed by Congress in 2002.

A report from the Subcommittee on Aviation on Inline Explosive Detection Systems [93] revealed that eight airports currently have in-line EDS, and the TSA has issued an additional eight letters of intent (LOIs) to cover the costs of installing nine more systems. In total, there will be approximately seventeen in-line systems by 2006. TSA does not plan to issue any new LOIs or install any additional in-line systems under its fiscal year 2005 requested level of funding. This could prove problematic as early estimates indicate that as many as 60 airports are or will be seeking LOIs. TSA estimates that it will require more than $2 billion for inline EDS installation at the top 20 airports, and more than $4 billion for all airports. The report concludes that if Congress does not provide additional funding for inline EDS installation, TSA will not sign off on any additional LOIs, leaving a significant number of airports across the country without a long-term EDS solution.

Of the eight airports with full inline systems, only Jacksonville received any Federal funding for construction. San Francisco funded the majority of its system with airport revenue, and Boston Logan has signed an agreement with TSA to be reimbursed for their inline EDS expenditures.

To this point, TSA has issued the following LOIs, which will be paid over several years subject to the availability of funding:

Table 6.1 Showing reported letters of Intent LOI's [93]

Airport	LOI Total Cost
Denver International	$95 million
Dallas/Fort Worth	$140 million
Los Angeles/Ontario	$342 million
Boston Logan	$116 million
Las Vegas McCarren	$125 million
Atlanta	$125 million
Seattle/Tacoma	$212 million
Phoenix	$122 million
Total (8 airports):	$1.277 billion

Dog-on-a Chip : Surface Acoustic Wave Resonators as an Explosives Sensor

The two main features of a functional vapor-sensing device are sensitivity, prescribed by device design and specificity, which is the ability to differentiate the target analyte from other molecules. Here, we used anti-TNT antibodies as our sensing biolayer for the detection of TNT molecules contained in a vapor stream. Researchers have analyzed the headspace vapor of various explosive samples and have found it to contain fixed amounts of the molecule under conditions prescribed by the vapor pressure, temperature and concentration of the sample.

Surface Acoustic Wave (SAW) devices typically have gratings with metal fingers spaced at equal widths [106]. The metal fingers convert the applied voltage to an acoustic wave. Between the gratings lie interdigital transducers (IDTs), which act as the input and output for Rayleigh acoustic waves. An ST-X quartz substrate is used because this cut provides high temperature stability near room temperature. The antibodies were immobilized using Protein A as the cross-linker, and a 3-μm-thin layer of hydrogel kept the antibodies in their proper conformation and minimized humidity effects.

In the SAW quartz device, when the antigen binds to the antibody, the researchers measure and compare the shift in the oscillator frequency caused by the alteration in the acoustic velocity. Other molecules will not interact in quite the same way with the antibody, and the difference can be detected electronically. The Sauerbrey Equation is an

extremely useful mode of describing the relationship between the mechanical vibration on the quartz surface and the immunological interactions at the interface.

To simulate 2,4,6-trinitrotoluene (TNT) in the atmosphere, a vapor generator delivered 50 pico grams of TNT vapor as 0.3s pulses in an air stream to a flow cell containing four SAW resonators. Because the flow-rate, temperature, and pressure remained constant with the addition of the pulse, the researchers concluded that the observed frequency shifts were the result of TNT molecules perturbing the surface of the chip. Compared with uncoated devices and anti-FITC coated devices, which were used as negative controls, the sensor showed a positive response to TNT. A newer version of the device has three sensors on each chip, one to detect explosives, one to detect cocaine, and one to detect heroin.

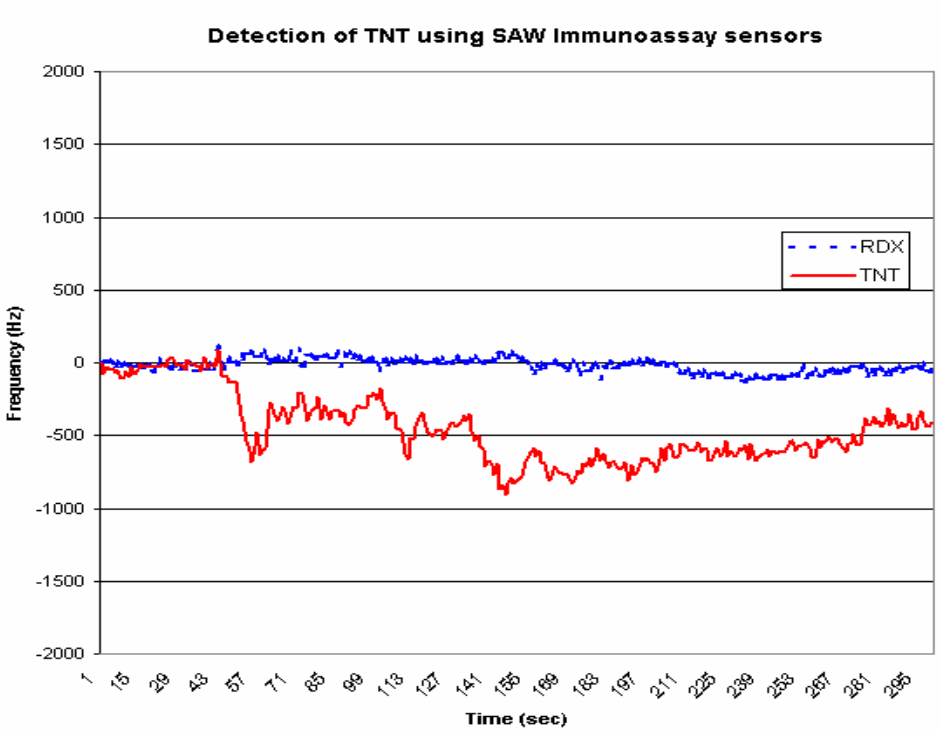

Figure 6.1 Responses of a device coated with anti-TNT antibody and a protective hydrogel (dotted line). A negative control device coated with anti-RDX (Royal Demolition eXplosives) forms the sensing array that is presented with two pulses of TNT vapor from a vapor generator.

The ability to detect and identify small molecules with low vapor pressure (a.k.a. non-volatile) based on its electronic vapor signature may have far reaching implications both locally and globally. The technology has implications for the war on terrorism in the detection of explosives and chemical warfare agents. The relative low cost of our technology offers the prospect of ubiquitous sensing in airports, public spaces and ports of entry.

Policy Recommendations

Unfortunately, at most airports, installation of an inline EDS system would require extensive terminal modifications--such as reinforced flooring, IT networking, electrical upgrades, new conveyer systems, new facilities, etc. Airport officials estimate the total cost for inline integration of EDS nationwide to be $5 billion. Thus the need for better technology through innovation. Electronic nose technology is a promising countermeasure tool for providing an effective explosives detection screening system.

Transportation Security Administration (TSA)

Currently the Transportation Security Administration is responsible for certifying, purchasing and implementing explosives detection systems. As a result of their proximity to issue of screening and detection this organization is best prepared to assess the technological needs. We recommend that the TSA control the distribution of research funding as it relate to explosive detection technology.

The office of Science and Technology Directorate formed in 2002 under Title III of the Homeland Security act is responsible for developing, testing, evaluating and conducting

research on new technology geared towards the strengthening the United States' ability to respond to nuclear, biological and chemical attacks. However, in its May 2004 report to the Subcommittee on Emerging Threats and Capabilities, the GAO (General Accounting office) criticized the DHS for not completing a strategic plan to identify its research priorities for the R&D of homeland security technologies. Instead, to fund projects, the GAO found that DHS has relied upon its managers to set priorities based upon their knowledge of current threats and capabilities [96]. In addition, gaps remain in DHS's efforts to coordinate with other federal agencies conducting homeland security R&D. Lack of coordination could increase the potential for duplication of research efforts and limit DHS's ability to leverage resources with other federal R&D activities. The report revealed that the department spent an exorbitant amount of time on organizing, developing policies and procedures and hiring the necessary staff.

We believe that due to the imminent nature of the threat, our nation would be best served if TSA were allowed to control research and funding as it pertains to explosives detection.

TSA's Explosives detection Canine Program has existed for over 30 years with an operating cost of ~ 15 million (Congressional Record Weekly Update (2004)). We believe that detection schemes that are scientifically based tend to be more consistent, unfortunately in the case of canines, to date, we are unaware of any scientific data detailing detection limits, detection probability or even how they work. Thus, we propose the elimination of the canine detection program based on the aforementioned criteria for a

standard analytical tool. This will free up additional funds for explosive detection research [102,103].

Congressional Intervention

One of the main impedance to the rapid development and introduction of more innovative explosive detection technology is the TSA certification process. This process has been known bottleneck sometimes taking up to two years for a decision. We see this as an opportunity for Congress to intervene by set a sunset clause establishes a deadline for the certification process within the next TSA appropriation Bill. The limits would be based on recommendations from a panel of independent experts in the field appointed by Congress. This group would be responsible for initially reviewing the current certification process and finally recommending reasonable time allowances for laboratory and field-testing based on their findings.

As a lateral approach, Congress can commission other agencies to develop their own explosives detection certification process. An agency such as the Department of Energy (DOE) has been suggested by many who have studied these issue as a viable alternative to the TSA.

Congress Budget Constraints

The failure of Congress's mandate that all airports be fully equipped with explosives detection systems by December 31, 2002 has lead to some changes on how constraints should the legislators place on future funding. More recently, Congress has largely

refrained from adding money to DHS's R&D budget for special projects allowing DHS to set its own research priorities. For fiscal 2006 (Figure 2), these priorities include $362 million for biological countermeasures, $102 million for radiological and nuclear countermeasures, as well as nearly $15 million for explosive countermeasures. In a recent senate committee hearing DHS Asst. Secretary for Science & Technology, Penrose Albright said the explosives countermeasure effort will launch a long-range R&D program, at about $40 million to $50 million per year, to develop and deploy standoff detection for vehicle-borne improvised explosive devices [102,103,104].

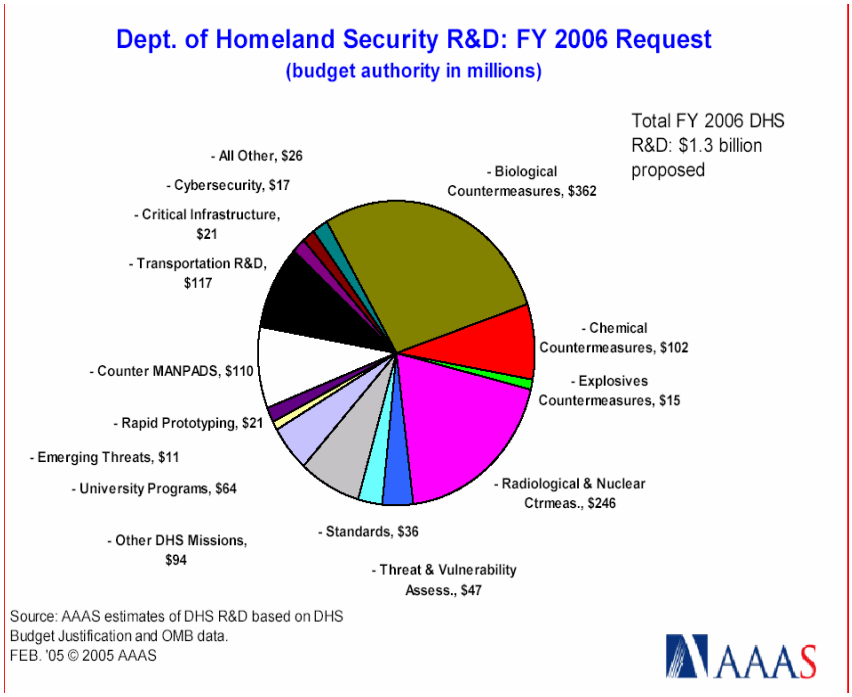

Figure 6.2 Showing DHS FY 2006 Budget Request.

Airport Security Proposal

To alleviate much of the problems caused by EDS and ETDS systems (discussed earlier) we join with other prominent scholars calling for a security scheme that consists of a Multi-tier system similar to the strategies adopted by the Europeans (eg. Heathrow, Copenhagen, Dusseldorf, Frankfurt, Hamburg, Naples, Rome, Turin, Vienna) [98]. This system will possess well-defined layers of security that deploy the necessary technology based on the risk assessment [98]. This will alleviate the need to have EDS/ ETD systems completely integrated (inline systems) in the airport terminal a very costly requirement. For example Heathrow airport in London employs automated X-ray machines as the primary screening technology in Tier I. Flagged baggage from tier I are passed to tier II where the screening technology consists of high-end X-ray machines complete with visual analysis capabilities. Heathrow's tier III is outfitted with in-line EDS/ETD systems for the highest degree of scrutiny [98]. Upon implementation such a security system would allow for better accountability for security operations at each layer. The first Tier of security technology should be the most efficient and adaptable, that is, requiring limited terminal modifications for installation. Sensing technologies like the electronic noses can be easily integrated into an airport system [97,98,99].

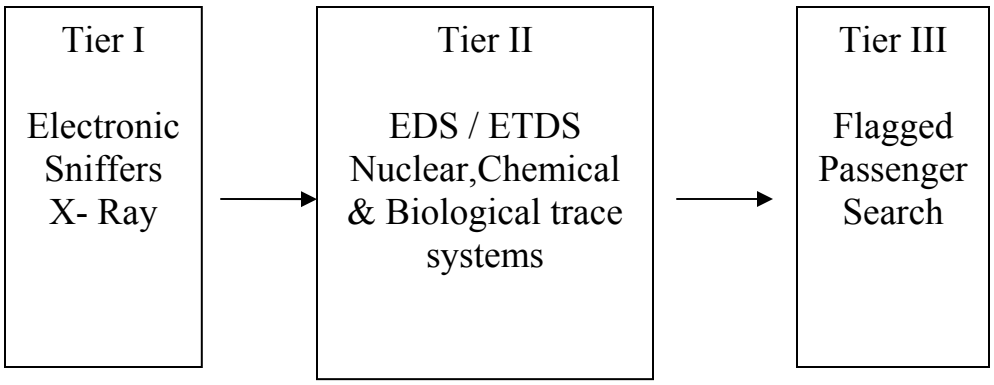

Figure 6.3 Showing Proposed Airport Security Tier System.

Appendix B

Publications

Corso, C.D., Stubbs, D.D., Goggins, M., Hruban, R.H., Hunt, W.D. *Cancer Detection and Prevention,* "Early Detection of a Pancreatic Cancer Biomarker in cell line supernatants by a QCM based Immunosensor". Accepted for publication.

Lee, S., Stubbs, D.D., Hunt, W.D., *IEEE Sensors Journal* "Rapid Detection of Bacterial Spores Using A Quartz Crystal Microbalance (QCM) immunoassay", vol.5, no.4, (2005) Pg. 737-743.

Stubbs, D.D., Lee, S., Hunt, W.D., *"IEEE Sensors Journal"*, "Vapor Phase Detection of a Narcotic Using Surface Acoustic Wave Immunoassay Sensors", Vol. 5, no. 3, (2005), Pg. 335-339.

Sommers, D.R., Stubbs, D.D., Hunt, W.D., *IEEE Sensors Journal* "A PDA-Based Wireless Biosensor Using Standard Components", Vol. 4, No. 5, (2004), Pg. 551-558.

Stubbs, D.D., Lee, S., Hunt, W.D., *J. Anal. Chem*. (*Research Profile)*, "SAW Chip Sniffs out Cocaine", Vol. 75, Iss.23, (2003) Pg. 492A.

Stubbs, D.D., Lee, S., Hunt, W.D., *J. Anal. Chem*. "Investigation of a Cocaine Plume Using Surface Acoustic Wave Immunoassay Sensors", Vol. 75, Iss.22, (2003), Pg. 6231-6235.

Stubbs, D.D., Lee, S., Hunt, W.D., *Proceedings of the IEEE* "Time-dependent signatures of Acoustic Wave Biosensors", Vol. 91, Issue: 6, (2003), Pg. 890-901.

Stubbs, D.D., Lee, S., Hunt, W.D., Cairney, J., *Proceedings of IEEE Sensors*, "Real-Time Detection of Bacteria Spores Using A QCM Based Immunosensor", (2003), Pg. 1194-1198.

Stubbs, D.D., Lee, S., Hunt, W.D., Doyle**,** D.F., *Biosensors and Bioelectronics "*Gas phase activity of anti-FITC antibodies immobilized on a surface acoustic wave resonator device", 17 (2002) Pg. 471-477.

Stubbs, D.D., Lee, S., Hunt, W.D., *IEEE Sensors Journal* "Molecular Recognition for Electronic Noses Using Surface Acoustic Wave Immunoassay Sensors", Vol. 2, No.4, (2002), Pg. 294-300.

Stubbs, D.D., Lee, S., Hunt, W.D., *Proceedings of IEEE International Frequency Control Symposium,* "Cocaine Detection Using Surface Acoustic Wave Immunoassay Sensors" (2002), Pg 289-293.

Stubbs, D.D., Lee, S., Hunt, W.D., *Proceedings of IEEE Sensors,* "Investigation of SPR Technology Using Texas Instruments : Spreeta™ Sensor", (2002), Pg. 1244-1249

Stubbs, D.D., Lee, S., Hunt, W.D., *Proceedings of IEEE SENSORS 2002,* "Vapor Phase SAW Immunoassay Sensors", (2002), Pg. 335-338.

Stubbs, D.D., Lee, S.H., Doyle, D.F., Hunt, W.D., *Proceedings IEEE Ultrasonics Symposium,* "Vapor Phase SAW Immunoassay Sensors", (2001) Pg. 357-360.

Patents

W.D. Hunt and D.D. Stubbs, "Surface Acoustic Wave Immunosensor for Detection of Bacteria Spores in Air", GTRC ID No. 3271, filed with USPTO, September 24, 2004.

W.D. Hunt, D.D. Stubbs, Sang-Hun Lee, P. Edmonson, U.S. Patent Application # 11/088809 "Differentiation and Identification of Analogous Chemical or Biological Substances with Biosensors.

References

[1] Stubbs, D.D., Lee, S., Hunt, W.D., *Proceedings of the IEEE,* Vol. 91, Issue: 6, (2003), Pg. 890-901.

[2] Kohler, G. and Milstein, C., *Nature*, (1975), Pg. 495-497.

[3] Ballantine, D.S., White, R.M., Martin, S.J., Ricco, A.J., Zellers, E.T., Frye, G.C., Wohltjen, H., *Acoustic Wave Sensors*, Academic Press, (1997).

[4] Barger, W.R., Wohltjen, H., Snow, A.W., Lint, J., Jarvis, N.L., *Fundamentals and Applications of Chemical Sensors*: ACS Symp. Series #309, Schuetzle, D., Hamerle, R., EDS, Amer. Chem. Soc. Washington D.C., (1986), Pg. 155-165.

[5] Thomas, R.C., Sun L., Crooks, R.M., Ricco, A.J., *Langmuir*, 7, (1991), Pg. 620.

[6] McCaffrey, R.R., Bruckenstein, S., Prasad, P.N. *Langmuir,* 2, (1986), Pg. 28.

[7] Bruckenstein, S; Shay, M. *Electrochim*. *Acta.* 30, (1985), Pg. 1295.

[8] Heising, R. A. *Quartz Crystals for Electric Circuits*. Vab Nostrand: New York (1946).

[9] Lin, Z.; Yip, C.M.; Joseph, I.S.; Ward, M. D. *Anal. Chem*. 65, (1993), Pg. 1546.

[10] O'Toole, R.P.; Burns, S.G.; Bastianns, G.J.; Porter, M.D. *Anal Chem*. 64, (1992), Pg. 1289.

[11] Ricco, A.J. and Martin, S.J. *Thin Solid Films* 206, (1992), Pg. 94.

[12] Li, Y., Huang, J., McIver, R.T., Hemminger, JC, *J. Am. Chem. Soc*., 114, (1992) Pg. 2428-2432.

[13] Bain, C.D., Whitesides, G.M., *Science* 240, (1988), Pg. 62-63 .

[14] Bain, C.D., Whitesides, G.M., *J. Am Chem. Soc.* 110, (1988), Pg. 6560-6561.

[15] J. Justin Gooding and D. Brynn Hibbert, *Trends in analytical Chemistry,* vol.18, no.8, (1999), Pg. 525.

[16] Everett, W.R., Welch, T.L., Reed, L., Furtsch, I*., Anal. Chem.* 67, (1995), Pg. 292.

[17] Gersten, D. and Marchalonis, J., *J. of Immunol Methods* , 127, (1990) Pg. 215-219.

[18] Johnson C.P., Jensen, I.E., Prakasam, A., Vijayebdran, R., Leckband, D., *Bioconjugate Chem.,* 14, (2003), Pg. 974-978.

[19] Lu, B., Smyth, M.R., Kennedy, R.O., *Analyst*, 121, (1996), Pg. 29R-32R.

[20] Stefan Dübel, *The Recombinant Antibody Pages,* (http://rzv054.rz.tu-bs.de/Biotech/SD/SDscFVSite.html).

[21] Westhoff, E., *Ann. Rev. Biophys. Biophysical Chem*., 17, (1998), Pg. 125-144.

[22] Nagerdra, H.G., Sukuma, N., Vywjan, M., *Ann. Rev. Biophys. Biophysical Chem*.,32, (1998), Pg. 229-240.

[23] Stubbs, D.D., Lee, S., Hunt, W.D., *IEEE Sensors Journal,* Vol. 2 No.4, (2002), Pg. 294-300

[24] Ogston, A.G., Preston, B.N, Wells, J.D., *Proc. R. Soc. Lond. A.,* 333, (1973), Pg. 297-316.

[25] Brinkman, H.C., Appl. Sci. Res. A., 1, (1947), Pg. 27-34.

[26] Renkin, E.M., J. Gen. Physiol., 38, (1954), Pg. 225-243.

[27] Pluen, A., Netti, P.A., Jain, R.K., Berk, D.A., *Biophys. J.,* 77, (1999), Pg. 542-552.

[28] Martin, S.J., Frye, G.C., Ricco, A.J., Senturia, S.D., *Anal. Chem*., 65, (1993), Pg. 2910-2922.

[29] Sauerbrey, G.Z., *Phys.* 155, (1959), Pg. 206-222.

[30] Kanazawa, K.K., and Gordon, II, J.G., *Anal. Chem*., 57, (1985), Pg. 1770-1771.

[31] Stubbs, D.D., Lee, S., Hunt, W.D., Cairney, J., *Proceedings of IEEE Sensors*, 2003, Pg. 1194-1198.

[32] Grate, J.W.; Martin, S.J.; White, R.M., *Anal. Chem*., 65, (1993) Part I: 940A – 948A; Part II: 987A – 996A

[33] Miller R.L., Nothnick, C.E., Bailey, D.S., *Acoustic Charge Transport: Device Technology and Applications*, Artech House, Boston (1992).

[34] Collins S., and Janata, J., *Analytica Chimica Acta,* (1982), Pg. 93-99.

[35] Persaud, D.R., Haunerland, N.H., *J. Insect Sci*., 4, (2004), Pg. 1-10.

[36] Skladal, P., Minunni, M., Mascini, M., Kolar, V., Franek, M., *J. Imm. Meth.,* 176 (1994), Pg. 117-125.

[37] Guilbault, G.G., *Anal. Chem*., 55, (1983), Pg. 1682-1684.

[38] Ngeh-Ngwainbi, J., Foley, P.H., Kuan, S.S., Guibault, G.G., *J.Am Chem. Soc*, 108, (1986), Pg. 5444-5447.

[39] Guibault, G.G., and Luong, J.H., *J. Biotech*., 9, (1988), Pg. 1-10.

[40] Rajakovic, L., Ghaemmaghami, V., and Thompson, M., Anal. Chem. Acta., 217, (1989), Pg. 111.

[41] Lam, C.S., Holt, D.E*., IEEE Ultrasonics Symp. Proc*. (1988) Pg. 273-277.

[42] Campbell, S., *Science and Engineering of Microelectronic Fabrication*, Oxford University Press, NY, New York, 2001.

[43] Stubbs, D.D., Hunt, W.D., Lee, S., Doyle**,** D.F., *Biosensors and Bioelectronics*, 17, (2002), Pg. 471-477.

[44] Stubbs, D.D., Lee, S., Hunt, W.D., *Proceedings of IEEE International Frequency Control Symposium* (2002), Pg 289-293.

[45] Stubbs, D.D., Lee, Sang-Hun Doyle, D.F., Hunt, W.D., *Proceedings IEEE Ultrasonics Symposium,* (2001) Pg. 357-360.

[46] Waggoner, L.P., Jones M., Williams, M., Edge, C., Johnston, J.M., Petrousky, J.A, *Effect of Extraneous Odors on Canine Detection,* Institute for Biological Detection Systems, Auburn University. Office of Special Technology Fort Washington, MD.

[47] Cain, W. S. and Drexler M., *Annals of the New York Academy of Science, 237*, (1974) 427-439.

[48] Laing, D. G., Panhuber, H., and B. M. Slotinick. *Physiology and Behavior, 45*, (1989), Pg. 689-694.

[49] J. M. Johnston, L. P. Waggoner, M. Williams, J. Jackson, M. Jones, L. Myers, S. F. Hallowell, and J. A. Petrousky, *Proceedings of the 5th International Symposium on the Analysis and Detection of Explosives,* (1996).

[50] Garner, K., Busby, L., Cornell, P., Johnston, J., Mullins, K., Edmonds, J., Radar, K., Williams, J., *Duty Cycle of a Detection Dog: A Baseline Study*, Institute for Biological Detection Systems, Auburn University, (2001).

[51] M. G. Hartell, C. C. Edge, M. Q. Pierce, S. F. Hallowell, and J. A. Petrousky, "Overview of current olfactometer performance across different odorant systems",

In P. Pilon and S. Burmeister, eds. *Chemistry and Biology Based Technologies for Contraband Detection,* Bellingham, WA, SPIE: 29371996.

[52] Lawrence, A.H., Elias, L., Anal. Chem., 69, (1985), Pg. 4283-4285.

[53] Stubbs, D.D., Lee, S., Hunt, W.D., *Anal. Chem.,* 75, (2003), Pg. 6231-6237.

[54] Behring, E., Kitasato S.*, Dtsch. Med. Wschr*., 16, (1890), Pg. 1113-1114.

[55] Landsteiner, K., Wiener, A.S., *Proc Soc Exp Biol Med*, 43, (1940), Pg. 223-224.

[56] Cameron, D.J. and Erlanger, B.F. *Nature* 268: (1977), Pg. 763–765.

[57] James, L.C., Tawfik, D.S., *Protein Science*, 12, (2003), Pg. 2183-2193

[58] Avraham, B., and Mathies, R.A., *Anal. Chem.,* 75, (2003), Pg. 1188-1195.

[59] Matz, L.M., Tornatore, P.S., Hill, H.H., *Talanta*, 54, (2001), Pg. 171-179.

[60] Hable, M., Stern C., Asowata C., Williams, K., *J Chromatogr. Sci.,* 29, (1991), Pg.131–135.

[61] Richard, J.J., Junk G.A., *Anal Chem*., 58, (1986), Pg. 723–725.

[62] Bruns-Nagel, D., Breitung J., von Löw, E., Steinbach, K., Gorontzy T., Kahl, M., Blotevogel, K.H., Gemsa, D., *Appl Environ Microbiol,* 62, (1996), Pg. 2651–2656.

[63] Keuchel, C., Weil, L., Niessner, R., *Anal Sci*., 8, (1992), Pg. 9–12.

[64] Anne Zeck, Michael G. Weller, Reinhard Niessner, *Fres. J. Anal. Chem*.,364, (1999) Pg. 113-120.

[65] Stansfield, R.L., Fieser, T.M., Wilson, I.A., *Science*, 248, (1990), Pg. 712.

[66] Wilmot, C.M., Thornton, J.M., *Protein Eng*., 3, (1990), Pg. 479.

[67] Yeats, T.O., Rees, D.C., *J. Appl. Crystallogr*. 11, (1988), Pg. 925.

[68] Fitzgerald, P.M.D., *J. Appl. Crystallogr*. 21, (1988), Pg. 273.

[69] Harrison, S.C., *J. Appl. Crystallogr*., 1, (1968), Pg. 84.

[70] Rini, J.M., Schulze-Gahmen, U., Wilson, I.A., *Science,* (1992), Pg. 959-965.

[71] Stanfield, R.L. and Wilson, I.A., *Curr. Opin. Struc. Biol*. 4, (1994), Pg. 857-867.

[72] Webster, D.M., Henry, A.H., Rees, A.R., *Curr. Opin. Struc. Biol*., 4, (1994), Pg. 123-129.

[73] Freund, C., Ross, A., Pluckthun, A., Hotak, T.A., Biochemistry, 33, (1994), Pg. 3296-3303.

[74] Padlan, E.A., Mol. Immunol. 31, (1994), Pg. 169-217.

[75] Franklin and Gosling, *Nature,* 173, (1953), Pg. 740-741.

[76] Takahara P.M., Rosenzweig, A.C., Frederick, G.A., Lippard, S.J., *Nature*, 377, (1995), Pg. 649-652.

[77] Salazar, M., Champoux, J.J., Reid, B.R., *Biochemistry*, Vol. 32, (1993), Pg. 739-744.

[78] Horton, N.C., Finzel, B.C., *J. Mol. Biol.,* 264, (1996), Pg. 521-533.

[80] Cheatham, T.E., Crowley, M.F., Fox, T., Kollman, P.A., *PNAS*, 94, (1997), Pg. 9626-9630.

[81] Fang, Y., Thomas, S.S., and Hoh, J., *Nucleic Acids Research*, 27, No.8, (1999), Pg. 1943-1949.

[82] Kim, G., Rand, A.G., Letcher, S.V., *Biosens. Bioelec.,* 18, (2003) Pg. 83-89.

[83] Hayward, G.L., Thompson, M., *J. Appl. Phys.* 83, (1998), Pg. 2194-2201.

[84] Nwanko, E., Durning, C.J., 69, (1998), Pg. 2375-2384.

[85] O'Sullivan, C.k., Vaughan, R.D., Guibault, G.G., Anal. Let., 32, (1999) 2353-2377.

[86] White, R.M., *Proc. IEEE*, 58, (1970), Pg. 1238-1276.

[87] Datta, S., *Surface acoustic Wave Devices*; Prentice-Hall: Englewood Cliffs, NJ (1986)

[88] Morgan, D.P., *Surface-Wave Devices for Signal Processing;* Elsevier: New York (1985).

[89] Frederick, D.K., Carlson, A.B., *Linear Systems in Communication and Control*, Wiley, New York (1971).

[90] Clavo, E.J*., Electrochemistry Communications,* 1, (1999), Pg. 167-170.

[91] Veronique de Rugy, "What does Homeland Security Spending Buy?", American Enterprise Institute for Public Policy, October 29th 2004.

[92] Kevin Coleman, "Technology and Homeland Security", Directions Magazine, March 6, 2003.

[93] Jack Spencer, Ha –Nguyen , "Are we safer today than before 9-11" Heritage Foundation, September 10, 2003.

[94] Homeland Security Funding 2004 www.homelanddefensestocks.com/

[95] Subcommittee on Aviation: Hearing on In-line Explosive Detection Systems: Financing and Deployment, July 14th 2004.

[96] Michael Fickes "Paying the Airport Share of Explosives Detection", Access Control and Security Systems, March 1, 2003.

[97] Paul Rothman, "The Long Road to TSA Certification", Access Control and Security Systems, Nov. 1, 2002.

[98] United States Government Accounting Office, "Homeland Security: DHS needs a Strategy to use DOE's Laboratories for Research on Nuclear, Chemical and Biological Detection and Response Technologies" May 2004, GAO-04-653.

[99] Heritage Foundation: Policy Research and Analysis www.heritage.org/

[100] Butler, V., Poole R.W., "Rethinking Checked-Baggage Screening" Reason Public Policy Institute www.rppi.org/ , July 2002.

[101] Lois R. Ember, "Parceling Homeland Security R&D Funding", Chemical & Engineering News , March 21, 2005

[102] Jim Harper (Director of Information Policy Studies) Cato Institute: Public Policy and Analysis www.cato.org/

[103] Congressional House Site : http://www.house.gov/transportation/aviation/07-14-04/07-14-04memo.html

[104] Transportation Security Administration, www.TSA.gov/

[105] Department Homeland Security, www.DHS.gov/

[106] Lois Ember "Parceling Homeland Security R&D Funding", C&EN, March 2005.

[107] Stubbs, D.D., Lee, S., Hunt,W.D., *J. Anal. Chem*. (*Research Profile)*, Vol. 75, Iss.23, (2003) Page 492A.

Vita

Desmond Dion Stubbs received a B.S. degree in Chemistry from Morris Brown College, Atlanta Ga in 1997. He later received his M.S. in Chemistry from Georgia Tech in 1999. After working in Georgia Tech's School of Chemistry as a Demonstration's Teacher for two years he later return to Georgia Tech as a full-time doctoral student. One of the highlights of his graduate career was a publication in Analytical Chemistry entitled "Investigation of a Cocaine Plume Using Surface Acoustic Wave Immunoassay Sensors". The paper was then flagged by the American Chemical Society interest and later featured as a press release on their website. The story led to numerous media interviews including an appearance on Fox News (cable service) and a feature in Time Magazine's new series Innovators.